THE PETROCHEMISTRY AND ORIGIN OF THE BOURNE COMPLEX, NORTHWESTERN ELLESMERE ISLAND, CANADA

Andrew S. Henry

Submitted in Partial Fulfillment of the Requirements
for the Degree of Bachelor of Science, Honours
Dalhousie University, Halifax, Nova Scotia
March 1991

Dalhousie University

Department of Geology
Halifax, Nova Scotia
Canada B3H 3J5
(902) 494-2358

DATE April 12, 1991

AUTHOR Andrew S. Henry

TITLE The Petrochemistry and Origin of the Bourne Complex, Northwestern Ellesmere Island, Canada

Degree BSc. Hons. Convocation Spring Year 1991

Permission is herewith granted to Dalhousie University to circulate and to have copied for non-commercial purposes, at its discretion, the above title upon the request of individuals or institutions.

Distribution License

DalSpace requires agreement to this non-exclusive distribution license before your item can appear on DalSpace.

NON-EXCLUSIVE DISTRIBUTION LICENSE

You (the author(s) or copyright owner) grant to Dalhousie University the non-exclusive right to reproduce and distribute your submission worldwide in any medium.

You agree that Dalhousie University may, without changing the content, reformat the submission for the purpose of preservation.

You also agree that Dalhousie University may keep more than one copy of this submission for purposes of security, back-up and preservation.

You agree that the submission is your original work, and that you have the right to grant the rights contained in this license. You also agree that your submission does not, to the best of your knowledge, infringe upon anyone's copyright.

If the submission contains material for which you do not hold copyright, you agree that you have obtained the unrestricted permission of the copyright owner to grant Dalhousie University the rights required by this license, and that such third-party owned material is clearly identified and acknowledged within the text or content of the submission.

If the submission is based upon work that has been sponsored or supported by an agency or organization other than Dalhousie University, you assert that you have fulfilled any right of review or other obligations required by such contract or agreement.

Dalhousie University will clearly identify your name(s) as the author(s) or owner(s) of the submission, and will not make any alteration to the content of the files that you have submitted.

If you have questions regarding this license please contact the repository manager at dalspace@dal.ca.

Grant the distribution license by signing and dating below.

_____ _____

Name of signatory Date

Abstract -- New petrological and petrochemical analyses provide insight into the origin of the hypabyssal and volcanic rocks of the Bourne Complex, northwestern Ellesmere Island, Canada. Field relationships and petrographic characteristics reveal three groups of igneous rocks within the Complex: 1) Porphyritic Andesite (PA), 2) Plagioclase Porphyry dykes (PD), and 3) North-trending dykes (ND). Immobile trace element, and minor element ratios define the tectonomagmatic character of the Complex. Cluster analysis, using ratios of Y, Nb, Zr, TiO_2, and P_2O_5, confirms the petrographic classification. An Nb/Y - Zr/Ti discrimination diagram indicates that the PA are andesitic, that the PD have subalkaline basalt compositions, and that the ND are alkali basalt transitional to basanite. Ti-Y-Zr and Hf-Ta-Th tectonic discriminator diagrams indicate that the PA belong to a destructive plate margin setting, that the PD indicate a destructive plate margin transitional to backarc basin setting and that the ND show a within plate setting. $^{40}Ar/^{39}Ar$ isotope dating of primary hornblende from the PA yields an age of 380 +/- 10 mya. The PA may relate to magmatism resulting from the transpressive accretion of the Pearya terrane, ca. 390 mya., whereas the PD likely relate to backarc magmatism resulting from the Ellesmerian Orogeny, ca. 360 mya. Calcalkaline magmatism associated with the docking of Pearya may have been much more widespread than previously suspected.

Keywords -- Ellesmere Island - Bourne Complex - Igneous petrology
Calcalkaline magmatism - Trace element geochemistry
Tectonomagmatic discrimination - $^{40}Ar/^{39}Ar$ dating

ACKNOWLEDGEMENTS

I would like to thank my supervisor, Dr. Gunter Muecke for his patient guidance, generous loans of equipment, and for introducing me to his Arctic. Dr. Barrie Clarke tirelessly offered his editorial expertise. Dr. Peter Reynolds reviewed Chapter 5 and made many helpful comments. While completing this work I had many stimulating and fruitful conversations with Doug Merrett and Melanie Haggart. David Ritcey assisted with sample preparation and analysis. Robbie Hicks and Davis Bennett were extremely helpful towards the end. Finally, I wish to thank Carolyn for her patience and love.

TABLE OF CONTENTS

List of Figures.....i
List of Tables.....iii

CHAPTER 1: Introduction.....1
1.1 Introduction.....1
1.2 Location.....4
1.3 Regional Geological Setting.....4
1.4 Previous Work.....8
1.5 Statement of Purpose.....9

CHAPTER 2: Geological Setting.....11
2.1 Introduction.....11
2.2 Canadian Shield and Arctic Platform.....13
2.3 Innuitian Tectonic Province.....14
  2.3.1 Franklinian Mobile Belt.....14
    2.3.1.1 Franklinian Shelf.....15
    2.3.1.2 Deep Water Basin.....15
  2.3.2 Pearya.....18
  2.3.3 Sverdrup Basin.....20
2.4 Discussion.....22
2.5 Summary.....23

CHAPTER 3: Field Relations and Petrology.....24
3.1 Introduction.....24
3.2 Field Relations.....24
3.3 Petrography.....27
  3.3.1 Mineralogy.....28
  3.3.2 Texture.....40
3.4 Mineral Chemistry.....46

CHAPTER 4: Geochemistry.....51
4.1 Introduction.....51
4.2 Methods.....51
4.3 Results.....52
4.4 Chemical Classification.....56
4.5 Tectonomagmatic Discrimination.....67
4.6 Summary.....71

CHAPTER 5: 40Ar/39Ar Dating.....74
5.1 Introduction.....74
5.2 The 40Ar/39Ar Method.....74
5.3 Results.....77
5.4 Interpretation.....77

CHAPTER 6: Summary and Conclusions.....83
6.1 Summary.....83
6.2 Conclusions.....85
Appendix A.....87
Appendix B.....99
Appendix C.....103
Appendix D.....111
References.....118

LIST OF FIGURES

Figure		Page
1.1	Location map of the Canadian Arctic Archipelago	2
1.2	Location of the Sverdrup Rim and Sverdrup Basin	3
1.3	Location of the Bourne Complex	5
1.4	Regional geologic setting	6
2.1	Geological provinces of the Arctic Islands	12
2.2	Geological subprovinces of Ellesmere Island	17
2.3	Major successions of Pearya terrane	19
3.1	Sample location map of study area	26
3.2	Photomicrograph: porphyritic andesite	29
3.3	Photomicrograph: porphyritic andesite	30
3.4	Photomicrograph: plagioclase porphyry dyke	31
3.5	Photomicrograph: plagioclase porphyry dyke	33
3.6	Photomicrograph: porphyritic andesite	34
3.7	Photomicrograph: North-trending dyke	35
3.8	Photomicrograph: porphyritic andesite	36
3.9	Photomicrograph: porphyritic andesite	38
3.10	Photomicrograph: plagioclase porphyry dyke	39
3.11	Photomicrograph: plagioclase porphyry dyke	41
3.12	Photomicrograph: porphyritic andesite	43
3.13	Photomicrograph: porphyritic andesite	44
3.14	Photomicrograph: porphyritic andesite	45
3.15	Classification of clinopyroxene	47
3.16	Classification of amphibole	48
3.17	Classification of amphibole	49

4.1 P-Zr binary plot.....58
4.2 Na+K - Zr binary plot.....59
4.3 Y, Nb, Ti, P immobile element binary plots.....61
4.4 Cluster analysis tree diagram.....64
4.5 Zr/Ti - Nb/Y chemical classification diagram.....66
4.6 Ti-Y-Zr tectonomagmatic discrimination diagram.....68
4.7 Hf-Ta-Th tectonomagmatic discrimination diagram.....70
4.8 F1 - F2 tectonomagmatic discrimination diagram.....72
5.1 Inverse isochron plot for sample FJ87-136.....78
5.2 Inverse isochron plot for sample FJ87-138.....79
5.3 Inverse isochron plot for sample FJ87-146.....80

LIST OF TABLES

Table Page

4a Synthesis of porphyritic andesite compositions.....53

4b Synthesis of plagioclase porphyry dyke compositions.....54

4c Synthesis of north-trending dyke compositions.....55

4d Pearson correlation matrices.....60

B1 Mean clinopyroxene analyses.....99

B2 Mean amphibole analyses.....101

C1 Whole rock geochemistry.....103

CHAPTER 1: INTRODUCTION

1.1 Introduction

Ellesmere Island is the most northerly of the Queen Elizabeth Islands, a group of islands that forms the northernmost region of the Canadian Arctic Archipelago (Fig. 1.1). The Sverdrup Basin (Fig. 1.2) extends across much of the western and southwestern portion of the Queen Elizabeth Islands. This large extensional basin contains a nearly complete sequence of Early Carboniferous to Early Tertiary sedimentary and volcanic rocks (Williamson 1988). The basin originated during a Carboniferous-Early Permian rifting event, the cause of which is unknown (Trettin 1989).

A horst, known as the Sverdrup Rim (Fig. 1.2), separates the Sverdrup Basin from the Canada Basin to the north. In places along the rim, rock that underlies the Sverdrup Basin is exposed through uplift, block faulting, and erosion. The Bourne Complex (Fig. 1.3) crops out on the northwestern coast of Ellesmere Island, within the Sverdrup Rim. The complex is characterized by the presence of plagioclase-porphyritic dykes or sills, which intrude mildly-metamorphosed volcanic and sedimentary rocks. If the Bourne Complex represents part of the underlying rock of the Sverdrup Basin, then an excellent opportunity exists to study the magmatism that was occurring in the region prior to the initiation of rifting in the basin.

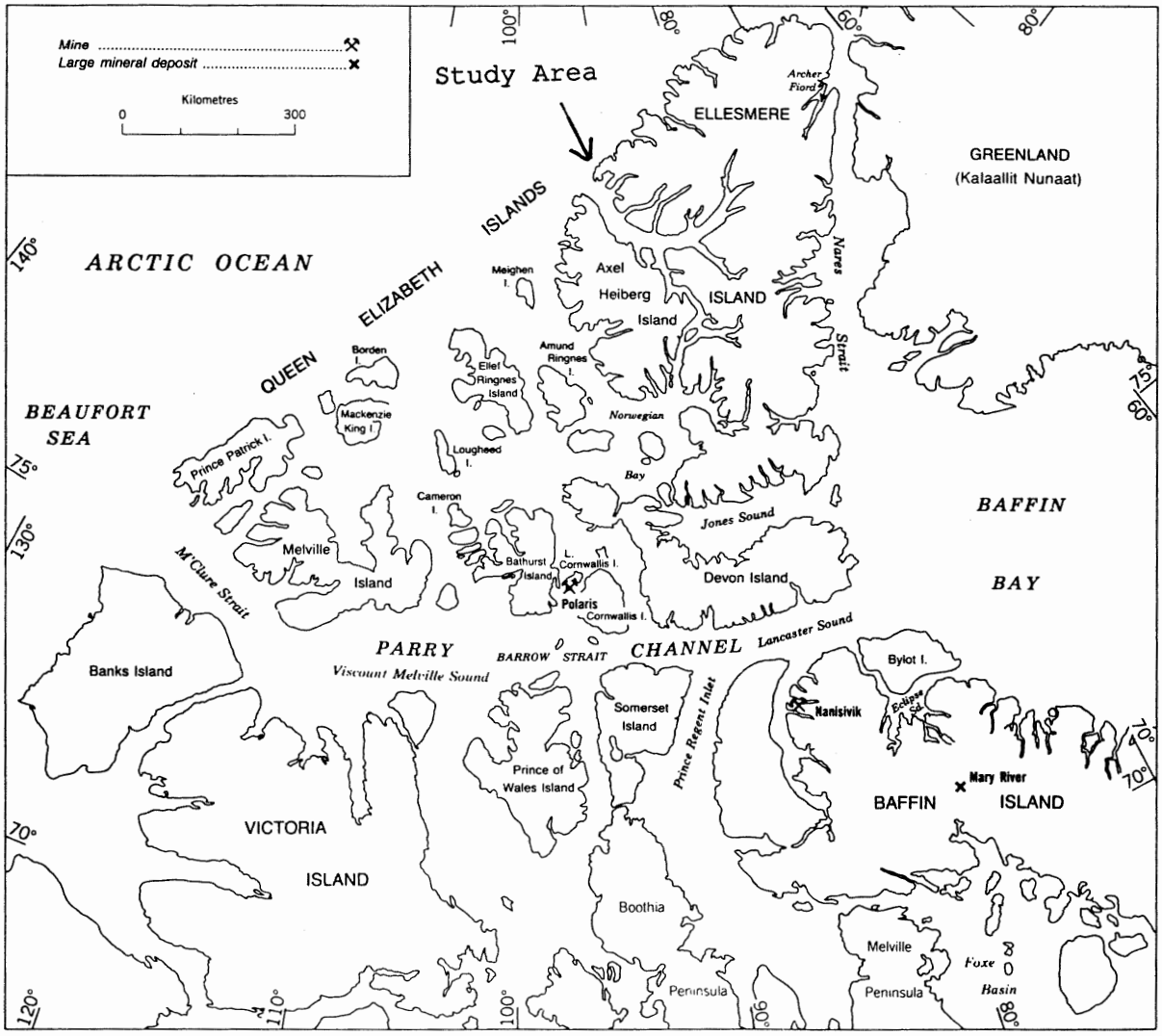

Figure 1.1 Location map of the Canadian Arctic Archipelago showing Ellesmere Island, the Queen Elizabeth Islands, and the Bourne Complex study area (from Plate 9, Trettin 1989).

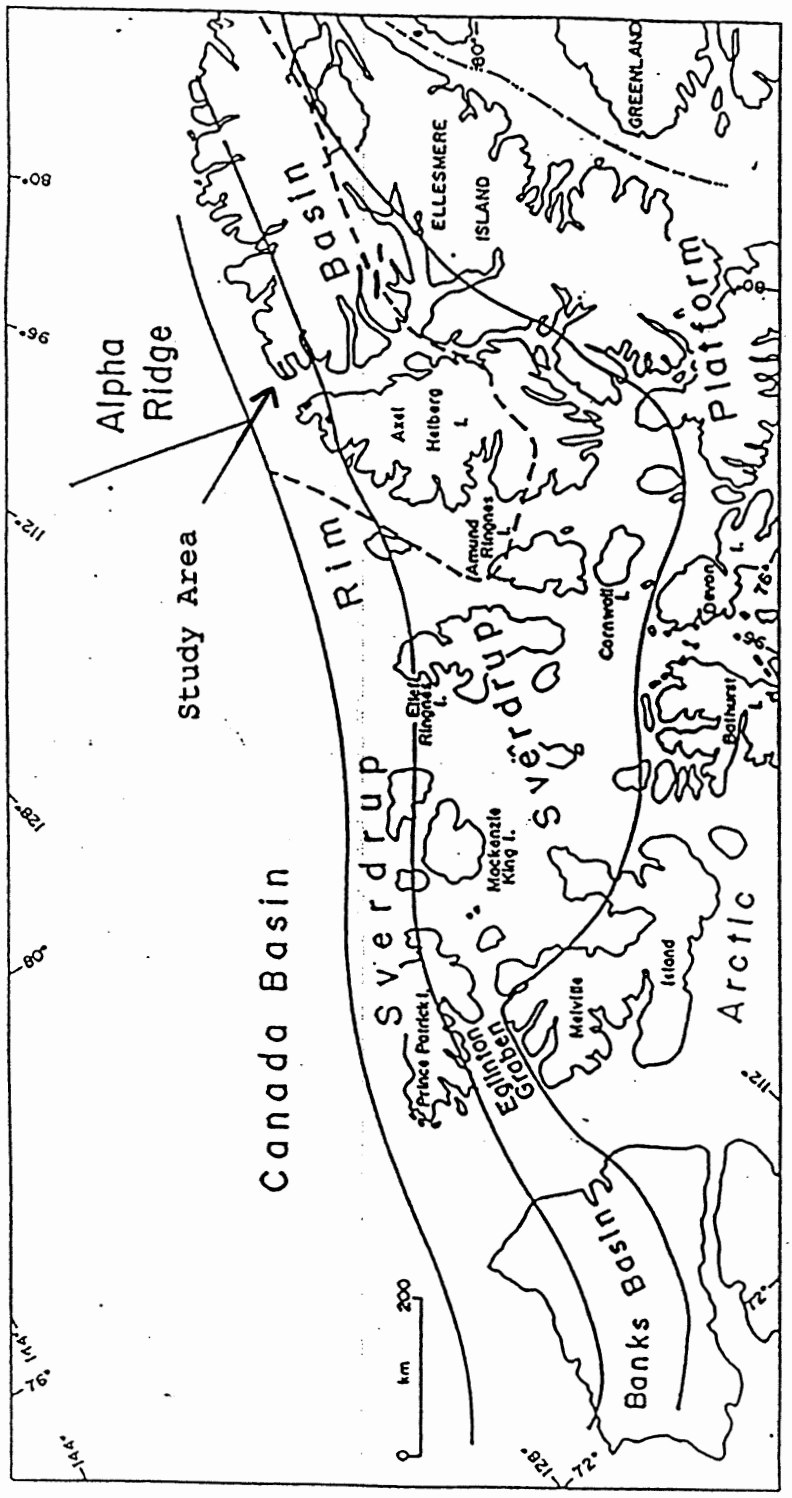

Figure 1.2 Location of the Sverdrup Rim, Sverdrup Basin, and the Bourne Complex study area (after Embry and Osadetz 1988).

1.2 Location

The Bourne Complex (Fig. 1.3) crops out along the northwestern coast of Ellesmere Island, on the Kleybolte Peninsula, between Cape Bourne to the north and the mouth of Auhdhild Bay to the south. The Arctic Ocean forms the western boundary of the complex. Exposures of Late Ordovician-Early Silurian Imina Formation form the eastern, fault contact, boundary. Fjeldholmen Island is the southern limit of Bourne Complex exposure where the complex is in fault contact with the Carboniferous Nansen Formation. Krueger Island lies four kilometres north of Fjeldholmen Island. This study focuses on the volcanic rocks of the Bourne Complex exposed on Fjeldholmen and Krueger Islands.

1.3 Regional Geological Setting

This brief summary of the regional geology of the Canadian Arctic Archipelago serves as an introduction to the complex geological history of the region. Chapter 2 contains a more comprehensive treatment.

The Canadian Arctic Archipelago includes several geological provinces and sub-provinces (Fig. 1.4). In the southern and eastern portions of the region the Precambrian Canadian Shield is widely exposed. During the Late Precambrian and Early Palaeozoic, shelf and deep-water basin sediments that now form the Arctic Platform and the Franklinian mobile belt (FMB) covered

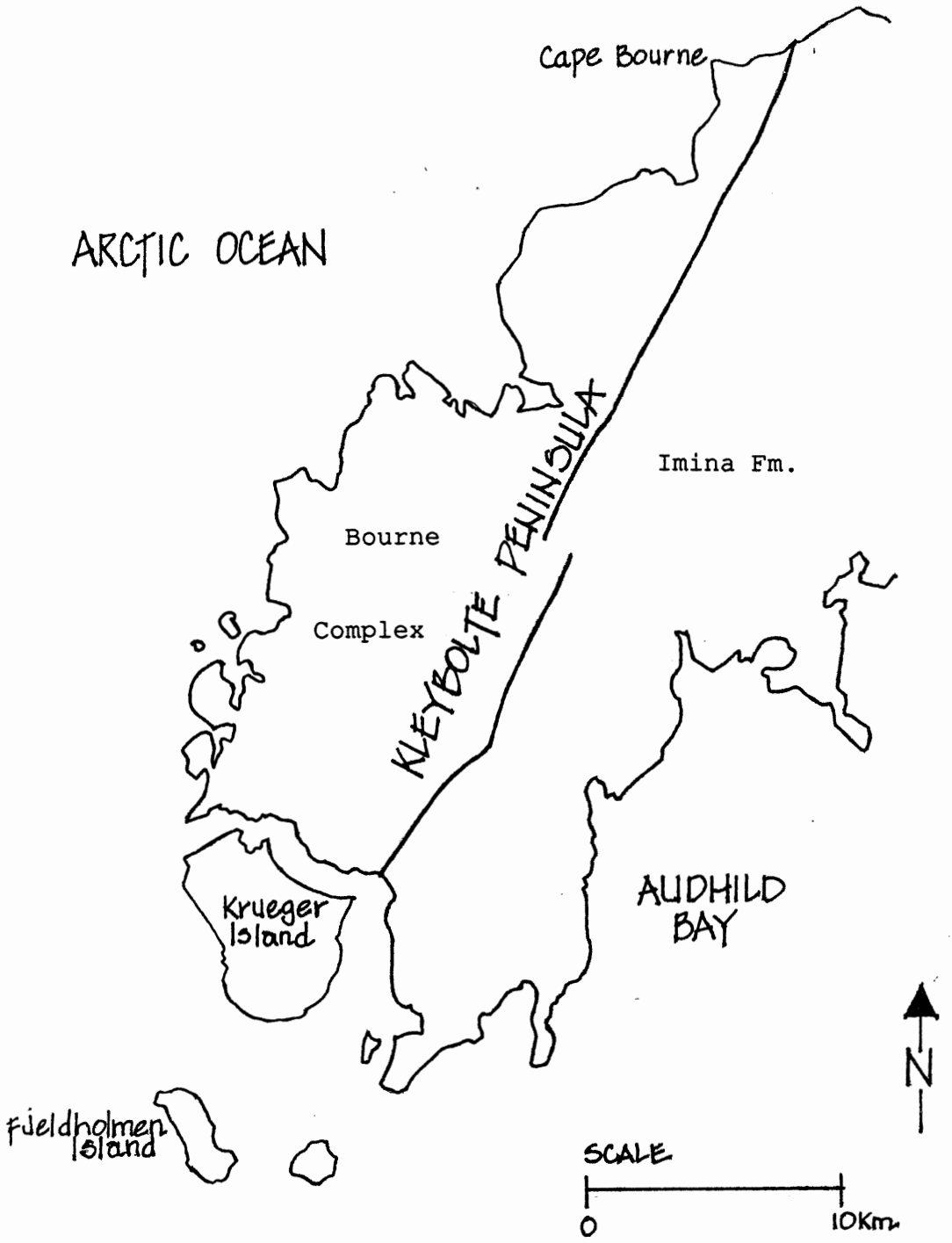

Figure 1.3 Location of the Bourne Complex on Kleybolte Penninsula, showing Krueger and Fjeldholmen Islands (from Trettin 1969).

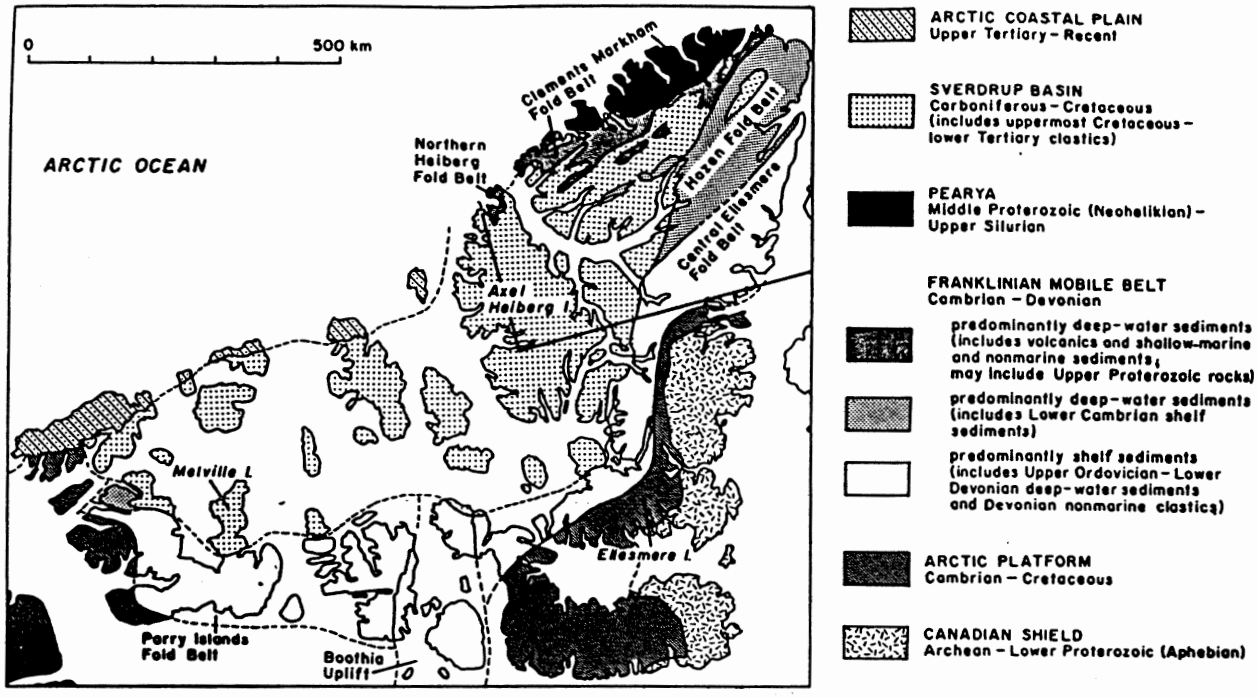

Figure 1.4 Regional geologic setting, illustrating geologic provinces and subprovinces of the Arctic Islands (from Trettin 1989).

the northwestern flank of this ancient craton. During the Middle to Late Palaeozoic, the continental Siberian plate converged toward the northern margin of the region. The resulting closure of the intervening Proto-Arctic ocean may have occurred along a southward-dipping subduction zone (Ziegler 1988). The presence of a subduction zone in this region has some very important implications with respect to the origin of the Bourne Complex.

Several orogenic events deformed the strata of the FMB. One of these events resulted in the accretion of Pearya, a composite terrane. Pearya accreted by sinistral strike-slip as a series of fault slices against the Clements Markam fold belt (CMFB) of northern Ellesmere Island. The Late Devonian-Early Carboniferous Ellesmerian Orogeny affected the entire FMB and, in particular, northern Ellesmere Island where Pearya and the CMFB experienced deep-seated basement deformation.

The Sverdrup Basin developed during the Early to Late Mississippian on the deformed and eroded strata of the FMB. The NE-SW trend of the basin axis parallels the structure of the FMB and the older rocks of the Canadian Shield. An accumulation of marine and non-marine sediments developed, with episodic extrusive and intrusive magmatic activity. A phase of renewed rifting, during the Jurassic-Early Cretaceous, is related to seafloor spreading in the Canada Basin.

The Tertiary Eurekan Orogeny resulted in compressive deformation of Ellesmere Island and fault-controlled uplifts in the Sverdrup basin. Intrusive and extrusive magmatic activity, as well as extensive thrust-faulting and folding, are associated

with this orogeny. Isostatic uplift affected the shield after the horizontal compressive deformation which only affected the regions north of the Canadian Shield.

The youngest of the geological provinces, the Arctic Coastal Plain, refers to the narrow band of undeformed Recent strata lying along the northwestern margin of the Arctic Archipelago. Mesozoic and Palaeogene strata unconformably underlie these marine and fluvial sediments.

1.4 Previous Work

Schei (1904) first described the rocks at Lands Lokk, now considered part of the Bourne Complex. He referred to green, porphyritic rocks with phenocrysts of feldspar, olivine, and augite as probable intrusions. Peary (1907) described rocks near Lands Lokk as volcanic, but Christie (1957) suggested that Peary may have described a porous, nodular limestone that also occurs in that area.

Christie (1957) named the Bourne Group after Cape Bourne, a notable landmark in the region. He reported that as much as one-half of the rocks were diabase sills and were very difficult to distinguish from the flows. Christie also suggested that, because the intrusive rocks were widespread and intimately associated with the lava flows, they were probably contemporaneous.

Trettin (1969) replaced the term Group with Complex. He reported that the Bourne Complex was in fault contact with, and

elevated relative to, the Silurian Imina Formation. He stated that the Bourne rocks represented a marine assemblage of sedimentary and volcanic rocks intruded by dykes and sills. Trettin observed that the intrusions were older than the Tertiary or Late Cretaceous faults displacing them. He noted that the coarse-grained, porphyritic intrusives occurred only in the Bourne Complex, and not in the adjacent Imina Formation. This observation led him to propose a tentative, pre-Silurian age for the Bourne Complex.

In 1987 G.K. Muecke and D.C. Merrett visited Fjeldholmen Island. They collected samples of extrusive and intrusive rocks from the Bourne Complex, and intrusive samples from the Nansen Formation. In 1989 G.K. Muecke, D.H. Ritcey, and A.S. Henry collected samples of both extrusive and intrusive rocks from the Bourne Complex at Krueger Island.

1.5 Statement of Purpose

The age, origin, and tectonic setting of the Bourne Complex are unknown. Moreover, the affinities between the Bourne Complex, Pearya, and the Clements Markam Fold Belt are unclear.

This thesis attempts to determine the origin of the Bourne Complex on Krueger and Fjeldholmen Islands. Such a determination requires an investigation of the mineralogy, petrology, and petrochemistry of the collected samples. As fossils have not been found in the Bourne Complex, radiometric dating must place the complex in the time-stratigraphic framework of the region.

Hydrous alteration, low grade metamorphism, and obscure field relations combine to make field classification of the samples difficult. Petrographic and petrochemical evidence help to confirm or modify these classifications made in the field.

The specific research goals of this thesis include:

1) description and classification of the rocks on the basis of mineralogy, petrology, and petrochemistry;
2) whole-rock petrochemical analysis of the samples to determine their magmatic and tectonic affinities;
3) analysis of primary clinopyroxene compositions to determine the tectonic affinity of the rocks;
4) determination of the absolute age of selected samples through $^{40}Ar/^{39}Ar$ dating of primary amphibole phenocrysts; and
5) petrochemical comparison of the samples to determine if a comagmatic affinity exists.

CHAPTER 2: GEOLOGICAL SETTING

2.1 Introduction

This chapter reviews the tectonic framework and regional geology of the Canadian Arctic Islands. The region includes three primary tectonic provinces: the Canadian Shield, the Arctic Platform, and the Innuitian Tectonic Province (Fig. 2.1) (Trettin 1986). The Innuitian Province has the greatest relevance to this study. It contains four major stratigraphic successions, named for their depositional and tectonic settings. The first of these, a buried Middle and Upper Proterozoic succession, is not discussed here. The second is the Upper Proterozoic to Upper Devonian Franklinian mobile belt. It comprises the Franklinian Shelf, deep water basin, and Pearya terrane. The third and fourth major successions are the Carboniferous to Neogene Sverdrup Basin, and the Lower Cretaceous to Recent Arctic Continental Terrace Wedge, respectively (Trettin 1989).

Reviewed below are the geological provinces and subprovinces contained within the Canadian Arctic Archipelago. The major stratigraphic successions that exist within the Innuitian Tectonic Province receive additional attention as they have particular relevance to this thesis.

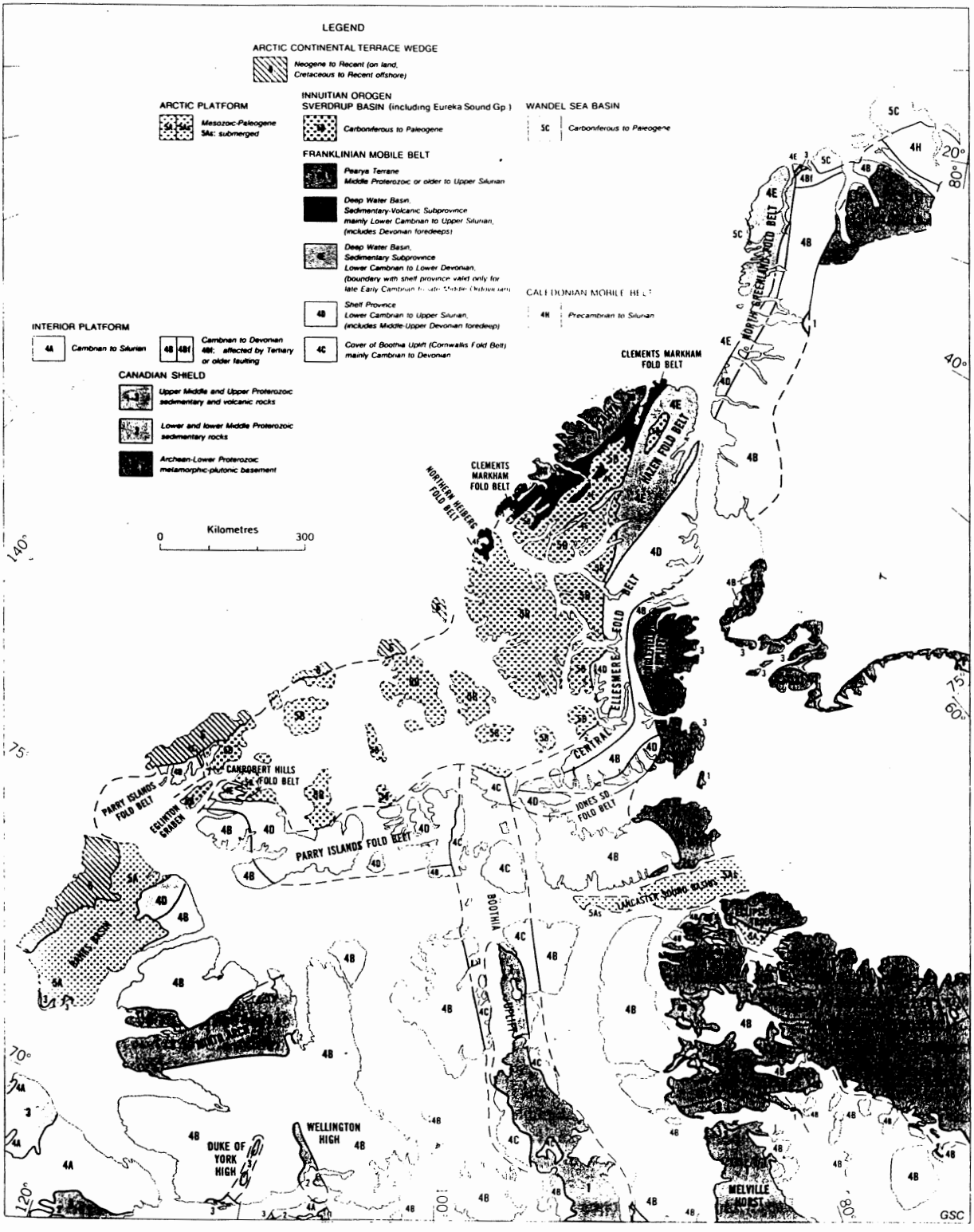

Figure 2.1 Geological provinces of the Canadian Arctic Islands (from Trettin 1989).

2.2 Canadian Shield and Arctic Platform

The Canadian Shield crops out in southeastern regions of the high Arctic islands (Figs. 2.1, 1.4). It consists of metamorphic-plutonic basement, deformed in Archean or Early Proterozoic time , and overlying, mildly metamorphosed, sedimentary and volcanic successions of Proterozoic age (Trettin 1986).

The metamorphic basement rocks, of amphibolite or granulite facies, represent a group of Archean terranes brought together in a series of Early Proterozoic orogenies. They exhibit contrasting structural trends, northerly on Ellesmere Island, and easterly on Devon Island (Trettin 1989).

The oldest sedimentary rocks, overlying the metamorphosed basement, crop out only on southern Victoria Island. Younger, Proterozoic basin deposits extend from the southwestern islands to northeastern Greenland. These are the oldest rocks that exhibit the predominant NE-SW structural trend of the high Arctic. Whether these deposits represent a passive margin related to a proto-Arctic Ocean, or a series of intra-cratonic basins, is unknown (Trettin 1989).

The shield extends into, and under, the adjacent Arctic Platform and the Innuitian Province to the northwest. The Arctic Platform consists of undeformed, shallow-marine shelf sediments. These carbonate and evaporite sediments overlie the northwestern flank of the Canadian Shield (Figs. 2.1, 1.4). The sedimentary rocks of the platform include middle Paleozoic, and Mesozoic to

Paleogene successions (Trettin 1989). The older of these exposures represents a once continuous cover that ranges in age from Early Cambrian to Late Devonian. Stratigraphically, the Arctic Platform is continuous with the Franklinian Shelf of the Innuitian Tectonic Province. The boundary between them is structural, coinciding with the limit of Franklinian deformation.

2.3 Innuitian Tectonic Province

The Innuitian Tectonic Province flanks the northwestern boundary of the Arctic Platform, exhibiting a characteristic NE-SW structural trend (Fig. 2.1). The southeastern boundary coincides with the limit of Phanerozoic deformation; this is also the northern boundary of the Arctic Platform. The northern limit of the Innuitian Tectonic Province is the boundary between continental and Mesozoic-Tertiary oceanic crust to the northwest. The Innuitian Tectonic Province encompasses most of the Arctic Islands, and contains the Franklinian mobile belt, Pearya, the Sverdrup Basin, and the Arctic Terrace Wedge.

2.3.1 Franklinian Mobile Belt

The Franklinian mobile belt (Fig. 2.1, 1.4) includes two distinct depositional subprovinces, the shelf, and the deep-water basin. The deep-water basin is further divided into a

southeasterly sedimentary subprovince and a northwesterly sedimentary and volcanic subprovince. Overlying strata conceal the base of the Franklinian mobile belt. Several orogenic events, including the accretion of Pearya and the Ellesmerian Orogeny, affected the mobile belt.

2.3.1.1 Franklinian Shelf

The Franklinian Shelf extends from northeastern Greenland to the southwestern Arctic Islands (Figs. 2.1, 1.4). It includes all strata of Early Cambrian to Early Devonian age that lie between the slope of the deep water basin and the Arctic Platform. The formations of the shelf are stratigraphically continuous with those of the Arctic Platform. The southern and eastern boundaries of the shelf are structural, not stratigraphic.

Carbonate, and to a lesser extent, clastic and evaporitic sediments which form this subprovince, thicken towards the shelf margin in Ellesmere Island. Early Cambrian rifting, subsequent lithospheric cooling, and sediment loading were responsible for subsidence and the accumulation of sediment.

2.3.1.2 Deep-Water Basin

The deep water basin contains two distinct geological domains: the southeastern sedimentary subprovince, and the northwestern sedimentary and volcanic subprovince. The latter,

crops out only in northern Ellesmere and Axel Heiberg islands. Facies changes link the strata of the exclusively sedimentary subprovince to the Franklinian Shelf. The northwestern domain however, contains volcanic units of island arc origin, and may represent an exotic terrane (Trettin 1986).

The sedimentary domain contains reworked carbonates, mudrocks, sandstones, and radiolarian cherts. Carbonate and clastic sediments, deposited by sediment gravity flows, originated on the slope and margin of the Franklinian Shelf. The major depositional units contained in this domain range from Early Cambrian to Middle Devonian in age. The rocks of the sedimentary subprovince form the Hazen Fold Belt (Fig. 2.2), deformed by the Ellesmerian Orogeny and probably affected by the accretion of Pearya.

The Northern Heiberg Fold Belt and the Clements Markam Fold Belt form the northwestern sedimentary and volcanic subprovince (NSVS) (Fig. 2.2). The two belts differ structurally and stratigraphically, although they have some units in common. A major transcurrent fault forms the boundary between this domain and the Hazen Fold Belt in northeastern Ellesmere Island. Some units of the sedimentary-volcanic subprovince correlate with units in the shelf province.

The NSVS contains four major volcanic units of island arc affinity that may represent an oceanic terrane of Proterozoic or early Paleozoic age (Trettin 1989). The Clements Markam Fold Belt contains several stratigraphically different rock units. A Silurian flysch unit in this belt is considerably different from

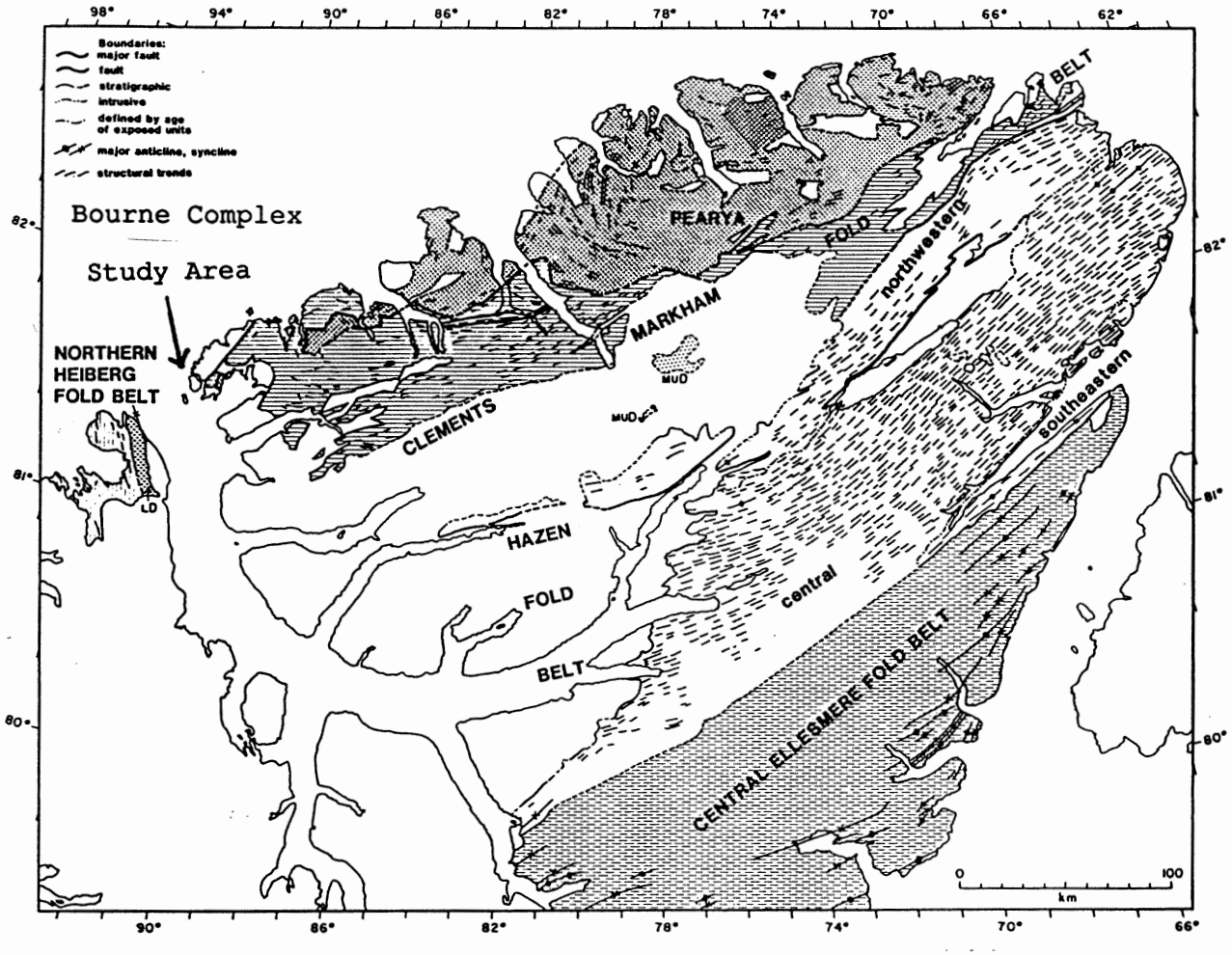

Figure 2.2 Stratigraphic and structural subdivisions, northern Ellesmere Island (from Trettin 1986).

flysch in the adjacent sedimentary subprovince, but similar to coeval flysch in north Greenland. This relationship, combined with the structural heterogeneity of the Clements Markam Fold Belt, suggests that it may represent an exotic composite terrane.

The Ellesmerian Orogeny affected the entire mobile belt during Late Devonian-Early Carboniferous time. Thin-skinned deformation occurred in the Shelf province and adjacent parts of the Deep Water Basin, and basement was involved in Pearya and the Clements Markam Fold Belt (Trettin 1989).

2.3.2 Pearya

Pearya, an exotic continental fragment, lies on the northwestern margin of Ellesmere Island, in fault contact with the Clements Markam Fold Belt (Fig. 2.2, 2.3). This composite terrane contains four major stratigraphic successions that differ in both age and lithology. The age of these successions ranges from Middle Proterozoic to Late Silurian. Trettin (1989) gives the most recent summary of the geology of this terrane.

The accretion of Pearya during the Late Silurian appears to have been the most important structural event to occur in the geological history of northern Ellesmere Island (Trettin 1989). Intense deformation, that may have reached as far inland as the Hazen Fold Belt, occurred when the sinistral strike-slip motion was halted and the terrane became attached to the Clements Markam Fold Belt.

Evidence that relates Pearya to the Caledonian-Appalachian

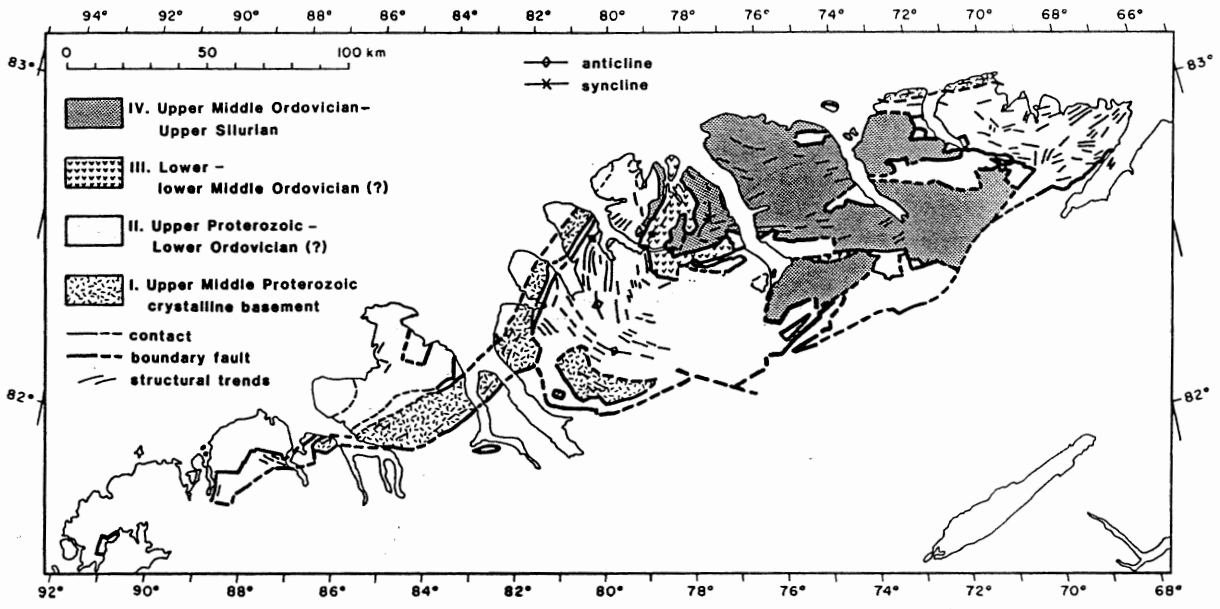

Figure 2.3 Major successions of Pearya terrane (from Trettin 1986).

region includes: the Grenvillian age of the Pearyan basement, the age of its mafic-ultramafic complexes, and the presence of a middle Ordovician collisional orogen similar to the Taconian and Grampian orogens. The basement of the Franklinian mobile belt is Archean, and the belt was not deformed during the Ordovician. The lower Silurian flysch of Pearya differs from coeval flysch of the mobile belt (Trettin 1989).

2.3.3 Sverdrup Basin

The Sverdrup Basin occupies the central and northwestern regions of the Franklinian Mobile Belt (Fig. 1.4). It is 1,300 km long, 400 km wide, and contains as much as 15,000 metres of basin fill (Trettin 1989; Balkwill 1978).

The basin began to develop during an Early Carboniferous-Early Permian rifting event. An angular unconformity, resulting from the Ellesmerian orogeny, separates the basin from the underlying fold belt. The presence of listric faults, associated coarse clastic sediment, and thinner crust beneath the axial regions indicates the extensional nature of the basin (Trettin 1989; Sobczak et al. 1986).

By the middle of the Carboniferous, basin subsidence had resulted in the formation of a shallow sea. During the early stages of deposition, evaporites and marine muds filled the axial regions of the basin. Carbonates and clastic sediments covered the margins. The presence of carbonates and evaporates reflected the subequatorial position of the region during late Paleozoic

time.

A basal unit of fine to coarse clastic material contains local intrusions of mafic volcanics in northern Axel Heiberg and northwestern Ellesmere Islands. The Melvillian Disturbance folded and faulted the Lower Permian rocks of the southern and eastern margins of the basin. Extrusion of Permian basalts probably relates to this event (Cameron 1989).

Thermal subsidence occurred from the Late Permian to Early Cretaceous. The region drifted north during the Mesozoic and deposition of carbonates and evaporites ended. Siltstone and shale accumulated in the axial regions during the Early Mesozoic. Deltaic progradation during the middle Mesozoic resulted in mostly terriginous, and little marine deposition to the basin.

A second phase of rifting began in the Middle Jurassic and was well underway by the Early Cretaceous. Extrusion of tholeiitic basalt, associated with the main stage of rifting, occurred at Axel Heiberg and northwestern Ellesmere Islands (Cameron 1989). Opening of the Canada Basin probably relates to this rifting (Williamson 1988). Eustatic sea level changes resulted in a series of regional transgressions and regressions. Fluctuations in sediment supply resulted from periodic uplifts of the cratonic shield to the south and east of the basin. The Tertiary Eurekan orogeny caused fault-controlled uplift within the Sverdrup, and terminated deposition to the basin.

2.4 Discussion

Plate tectonic theory proposes that mobile belts which form on continental margins are related to events occurring in adjacent ocean basins. If mobile belts, such as the Franklinian, develop on continental margins, then an ocean basin may have existed north of Ellesmere Island during Paleozoic time. Trettin and Balkwill (1979) suggest that the siliceous to intermediate volcanism that dominated northern Ellesmere Island during the Early and Middle Ordovician, reflects the existence of a south-dipping subduction zone beneath the northern margin of the North American Plate. Trettin (1989) proposes that the Ellesmerian Orogeny was probably caused by convergence of North America with another, unidentified, offshore plate. Ziegler (1989) hypothesizes that the Siberian Block was converging southward toward the northern margin of the North American Plate during the Middle to Late Paleozoic, and Scotese (1979) places the Siberian Block in the vicinity during the same time. These tentative hypotheses have important implications regarding the origin of the Bourne Complex.

The Bourne Complex crops out along the northwestern coast of Ellesmere Island. Trettin (1969) suggests a tentative Middle Paleozoic age for the Complex. These spatial and temporal positions suggest that the origin of the Complex may be related to magmatism associated with a Middle Paleozoic, south-dipping subduction zone.

2.5 Summary

In the Arctic Islands, three primary tectonic provinces contain several major geological provinces. One of these tectonic provinces, the Innuitian, includes the basins, terranes, and fold belts that encompass most of the region.

The deep-seated structural fabric of the Canadian Shield appears to control the depositional style of the overlying provinces. Several major orogenic events affected the region. The Ellesmerian and Eurekan orogenies, and the accretion of the Pearyan terrane deformed and metamorphosed the strata of Ellesmere Island. The development of Sverdrup Basin dominated the late Paleozoic and Mesozoic history of the region.

CHAPTER 3: FIELD RELATIONS AND PETROLOGY

3.1 Introduction

This chapter discusses the field relationships of the igneous rocks of the Bourne Complex, summarizes their mineralogical and textural characteristics, and makes a preliminary classification of the samples.

Time constraints precluded geological mapping of the Bourne Complex during the short visits to Fjeldholmen and Krueger Islands. Limited information pertaining to the extent, orientation, and juxtaposition of these volcanic rocks is reviewed below. Because generations of basic dykes cut the younger Sverdrup Basin sediments (Cameron 1989; Williamson 1988), basaltic dykes intruding the Nansen Formation on Fjeldholmen Island were also collected to provide a basis for their recognition in the Bourne Complex.

Thin sections reveal mineralogical and textural information not easily attained from hand samples. Textural information tentatively classifies the samples. Finally, the mineral chemistry of selected amphibole and clinopyroxene phenocrysts is presented and discussed.

3.2 Field Relations

On Fjeldholmen Island, an east-trending fault separates the southerly Carboniferous Nansen Formation from the northerly

Bourne Complex (Fig. 3.1). Thin basaltic dykes with north-trending orientations and nearly vertical dips intrude the limestone of the Nansen Formation. Samples FJ87-148 through FJ87-151 represent these dykes, which range from 40 cm to 3 metres in thickness. Exposed contacts with the limestone have well-developed chill margins.

North of a prominent gully that marks the fault separating the Nansen Formation from the Bourne Complex, fine-grained porphyritic dykes intrude volcanic flows of similar composition and texture. This similarity makes discrimination between the extrusive and intrusive units very difficult. Samples FJ87-131 through FJ87-147 were collected from semicontinuous outcrop of these east-trending units (Fig. 3.1). The igneous units intrude green-grey metawackes composed of medium-grained quartz and feldspar grains set in a fine-grained chloritic matrix.

On Krueger Island, igneous units of the Bourne Complex intrude fine-grained, metamorphosed siltstones. Contact relations between the different units are often obscured by frost shattering of the rock, and snow and ice cover.

Samples KR89-001 through KR89-039 were collected from igneous units at four different locations. The first location encompasses an area lying to the south of a small westerly-flowing creek which bisects the island. Outcrop on the north bank of the creek forms the second collection area. The third location lies along the west coast of the island, north of the creek. The fourth collection area lies north of the creek on the steep slopes of one of two prominent peaks on the island.

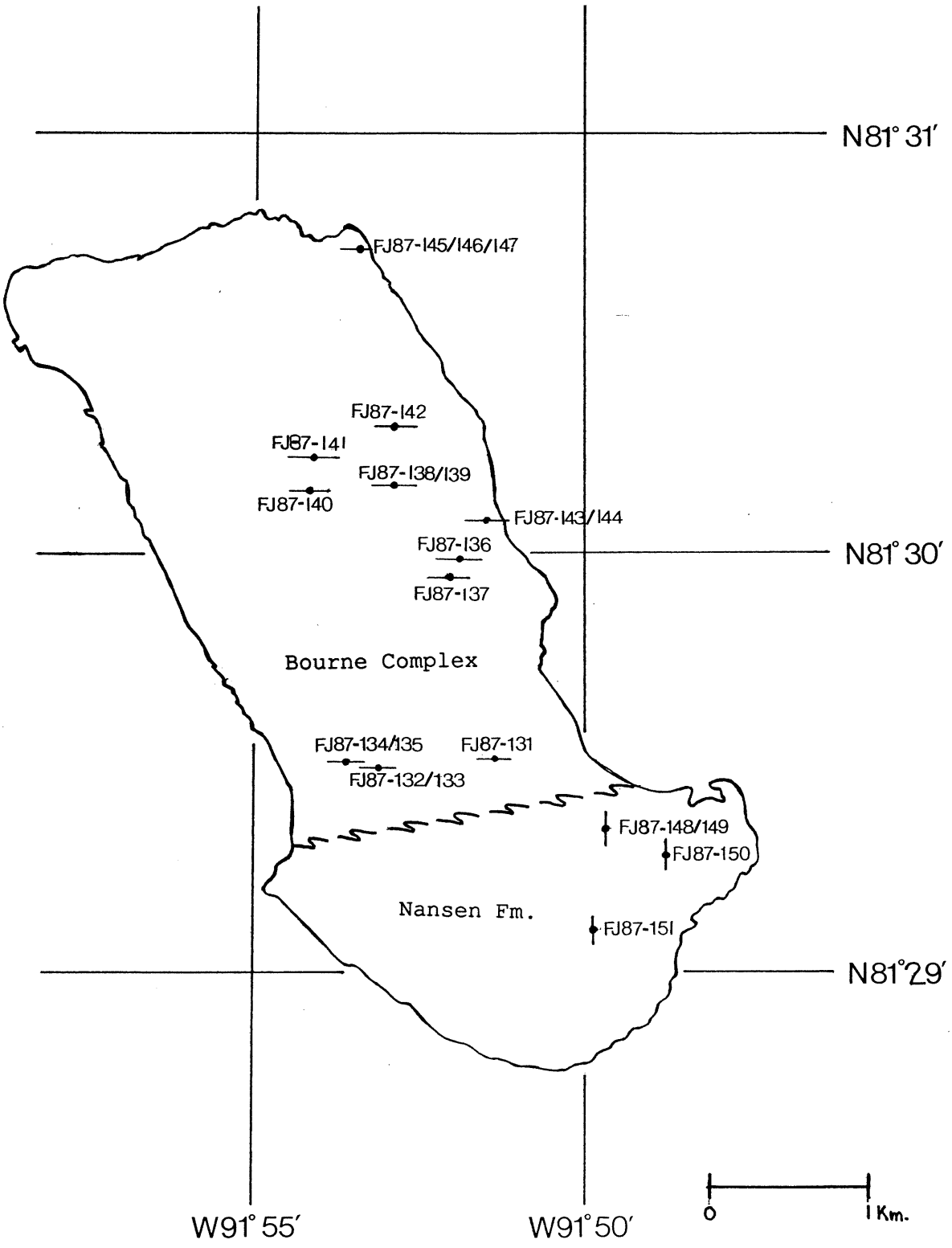

Figure 3.1 Sample location map of Fjeldholmen Island. Solid lines indicate sample locality, and orientation of dykes.

At the first location, the aphyric chill margins of porphyry dykes in contact with homogeneous diabase dykes suggest that the porphyry dykes intruded the diabase. All of the dykes on Krueger Island trend in an easterly direction and exhibit nearly vertical dips, with the exception of sample KR89-006, a relatively fresh, gabbroic dyke, and a number of associated basaltic dykes which trend to the north. These dykes are exposed on the north bank of the creek and may be associated with the north-trending dykes cutting the Nansen Formation. An easterly-trending swarm of porphyry dykes crop out along the western coast north of the creek at the third location. The dykes range in width from 1-5m (average 3m) and exhibit chilled margins adjacent to the country rock. Hornfelsed sediment occurs at the contact. The dykes are characterized by 1 cm plagioclase phenocrysts present in variable abundance. Very similar coarse-grained porphyry dykes, characteristic of the Bourne Complex (Trettin 1969), lie exposed at the fourth location in close proximity to porphyritic metavolcanic rocks.

3.3 Petrography

A summary of the primary and secondary mineral assemblages contained in the samples precedes a discussion of their textural characteristics. Appendix A contains complete petrographic descriptions of the individual samples.

3.3.1 Mineralogy

The igneous rocks of the Bourne Complex consist of a primary mineral assemblage containing plagioclase, clinopyroxene, orthopyroxene, hornblende, opaque oxides, and olivine. Chlorite, sericite, actinolite, calcite, sphene, epidote, opaque oxides, and quartz form a secondary, or alteration, assemblage.

All of the samples contain plagioclase, as either phenocrysts, large intergranular grains, or microcrystalline groundmass. In igneous rocks, plagioclase feldspar ranges in composition from sodium-rich albite to calcium-rich anorthite. Low-grade metamorphic rocks usually contain albite (Nesse 1986). Extinction angles measured from albite twins indicate albitic compositions for the plagioclase in the Bourne Complex samples. All of the plagioclase exhibits some degree of sericitic alteration, from weak in many of the dykes, to strong in the volcanic rocks on Krueger Island (Fig. 3.2). Some samples contain oscillatory zoned plagioclase phenocrysts (Fig. 3.3).

Of the 36 samples, 28 contain clinopyroxene as either phenocrysts, intergranular grains, or groundmass. Grains which are colourless in PPL predominate, indicating calcic compositions (Deer et al. 1966). Most of the samples with low clinopyroxene compositions exhibit moderate to strong chloritic or uralitic alteration, suggesting that primary clinopyroxene may have been converted to chlorite or, uralite, a form of actinolitic amphibole (Deer et al. 1966)(Fig. 3.4).

Less than one third of the samples contain orthopyroxene.

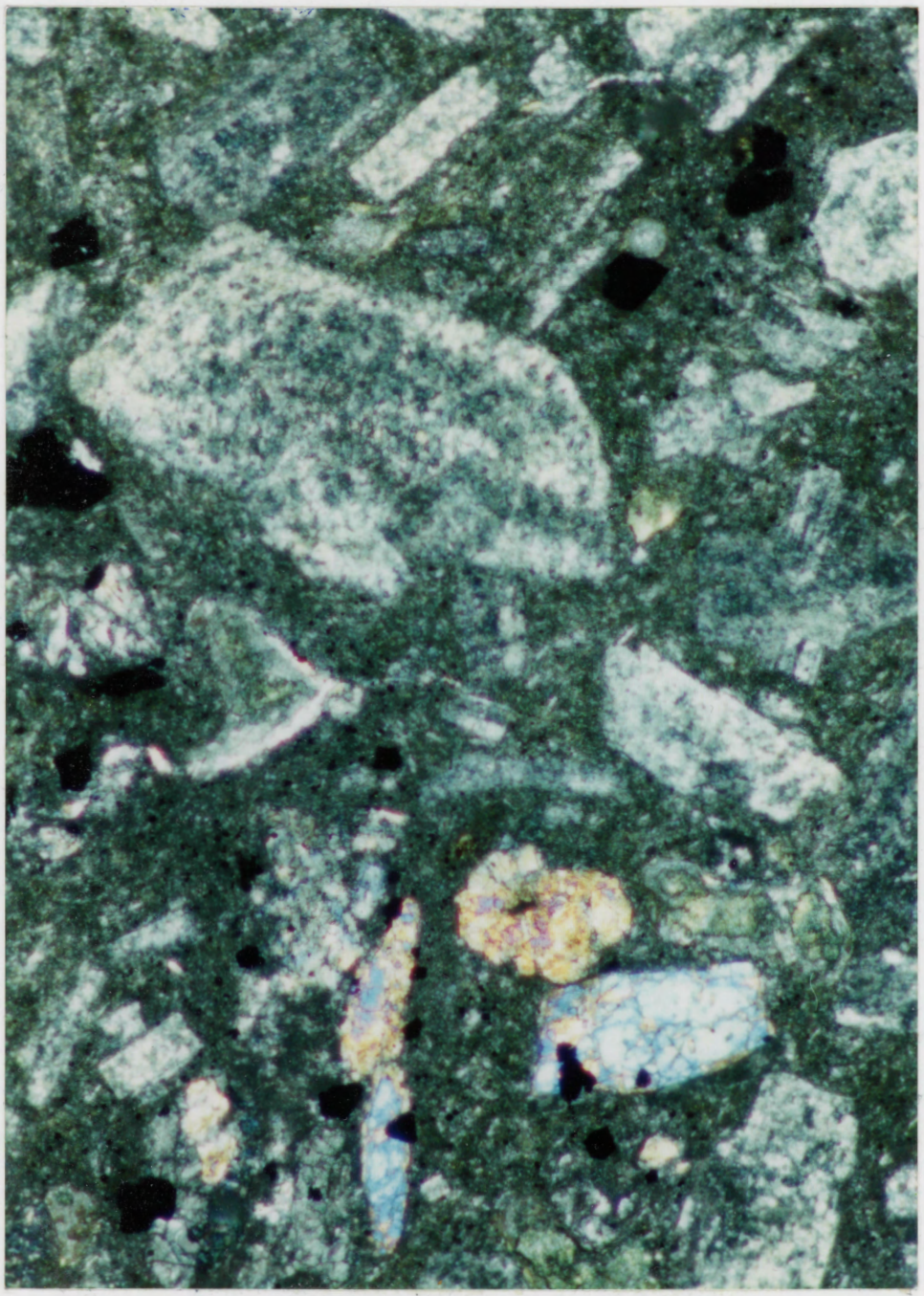

Figure 3.2. FJ87-132 (Porphyritic andesite) Phenocrysts of strongly sericitized plagioclase and smaller phenocrysts of clinopyroxene in a chloritic groundmass of sericitized plagioclase microlites. XN, 1 x 2 mm..

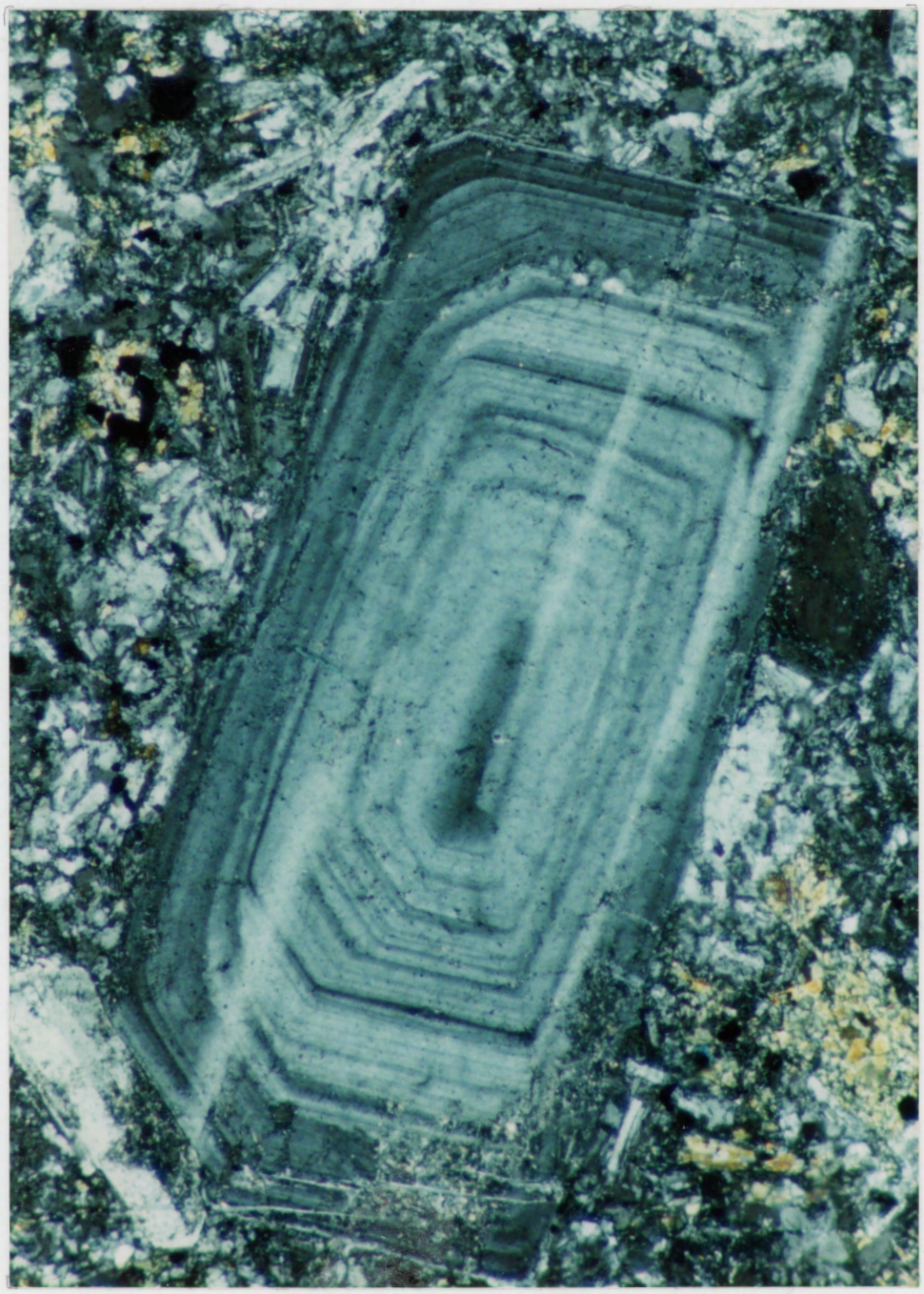

Figure 3.3. KR89-038 (Porphyritic andesite) Oscillatory zoning in plagioclase. XN, 1 x 2 mm.

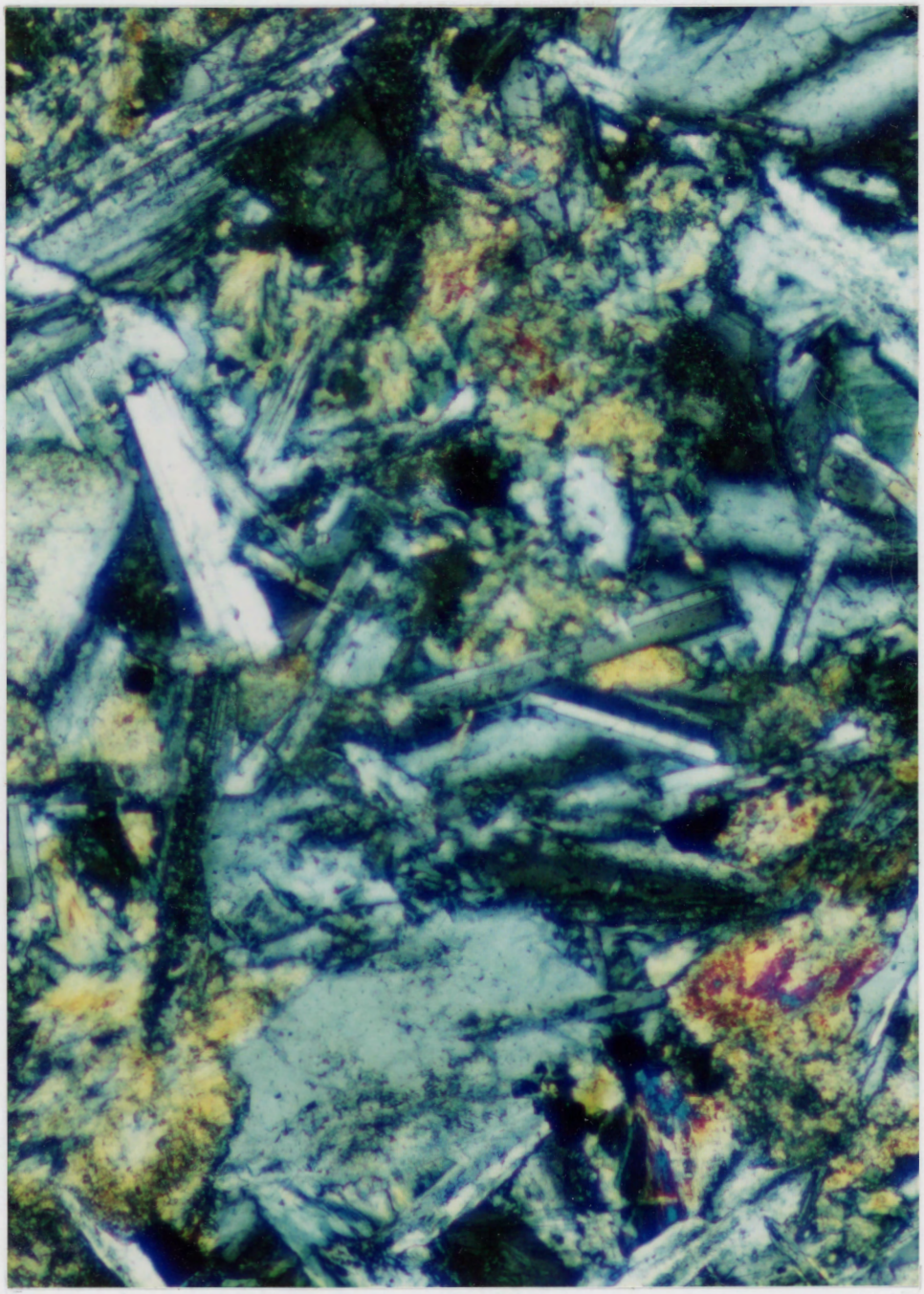

Figure 3.4. KR89-023 (Plagioclase porphyry dyke) Relatively unaltered plagioclase laths with intergranular actinolite. XN, 0.5 x 1 mm.

Where present as phenocrysts, orthopyroxene usually accounts for less than 5% of the mode. Groundmass and intergranular orthopyroxene compose up to 10% of some samples. Many samples contain uralite pseudomorphs after orthopyroxene, illustrating the tendency of this mineral to alter to uralite (Deer et al. 1966)(Fig. 3.5).

Six porphyritic andesite samples from Fjeldholmen Island contain subhedral to euhedral, moderately pleochroic hornblende (Fig. 3.6). Hornblende grains occur with basal sections exhibiting yellow - brown pleochroism and, rarely, as a variety with basal sections showing green - blue-green pleochroism. Sample KR89-006, the north-trending dyke from Krueger Island, contains large anhedral to subhedral grains of pleochroic-brown hornblende, a variety not observed in other samples (Fig. 3.7).

All but two of the samples contain opaque oxides. Most samples contain very finely disseminated anhedral grains. Coarser euhedral to subhedral grains often show triangular or square cross-sections indicative of ilmenite or magnetite.

Olivine occurs in samples FJ87-148, FJ87-151, and in sample KR89-008, from a Krueger Island dyke. In the first sample, olivine exists as medium-grained relict phenocrysts altered to chlorite and rimmed by very fine-grained opaque oxides. Relatively unaltered olivine occurs in the remaining two samples.

Chlorite occurs as the most common of the secondary minerals observed. It usually appears as pale-green, very fine-grained interstitial grains, but often exists as bright green patches. Many vesicles and veinlets are lined or completely filled with

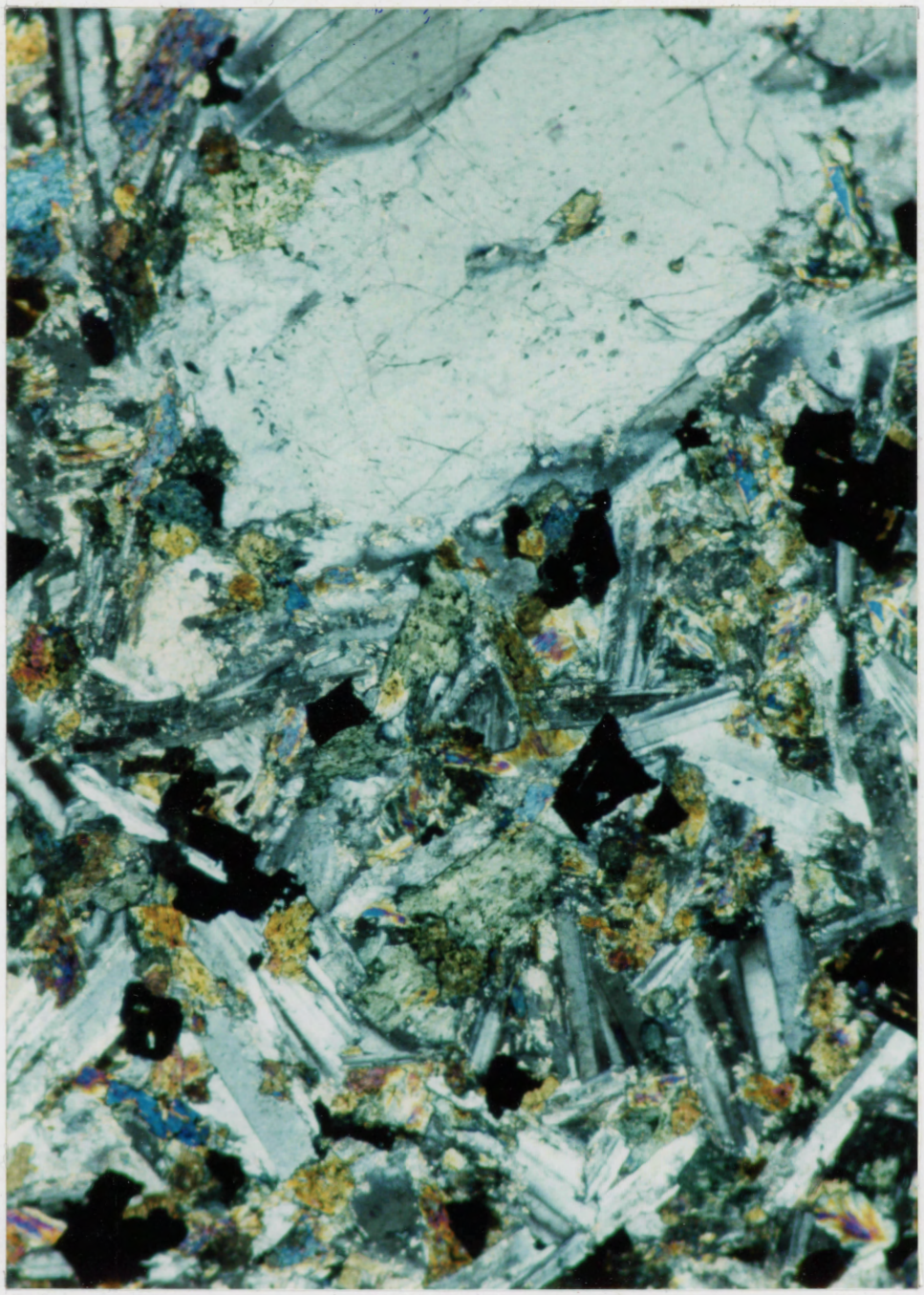

Figure 3.5. KR89-020 (Plagioclase porphyry dyke) A large plagioclase phenocryst with intergranular plagioclase laths and olive-green actinolite after orthopyroxene. XN, 2 x 3.5 mm.

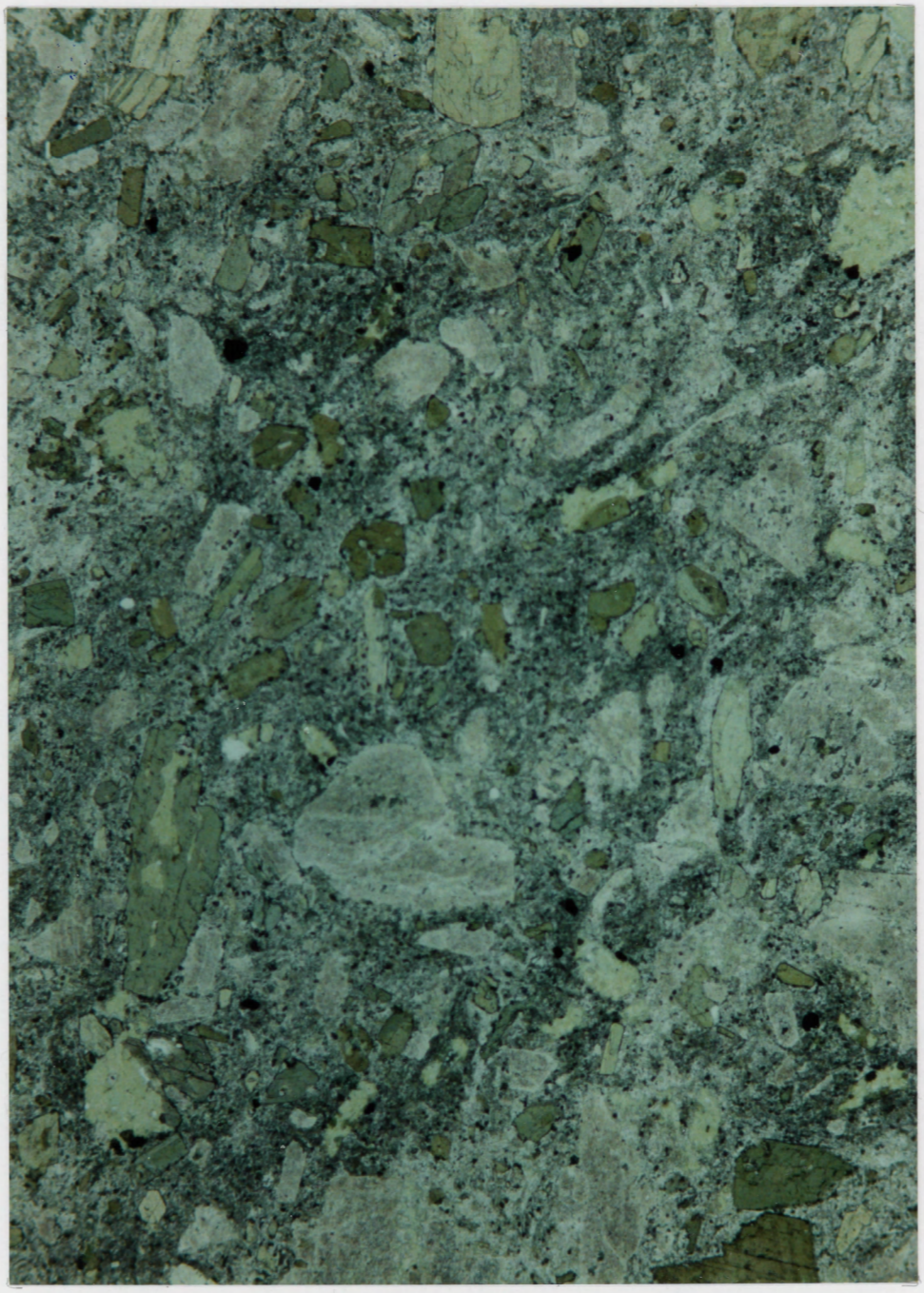

Figure 3.6. FJ87-146 (Porphyritic andesite) Sericitized plagioclase phenocrysts and subhedral hornblende in a sericitic/chloritic groundmass of plagioclase and opaque oxides. PPL, 5 x 7 mm.

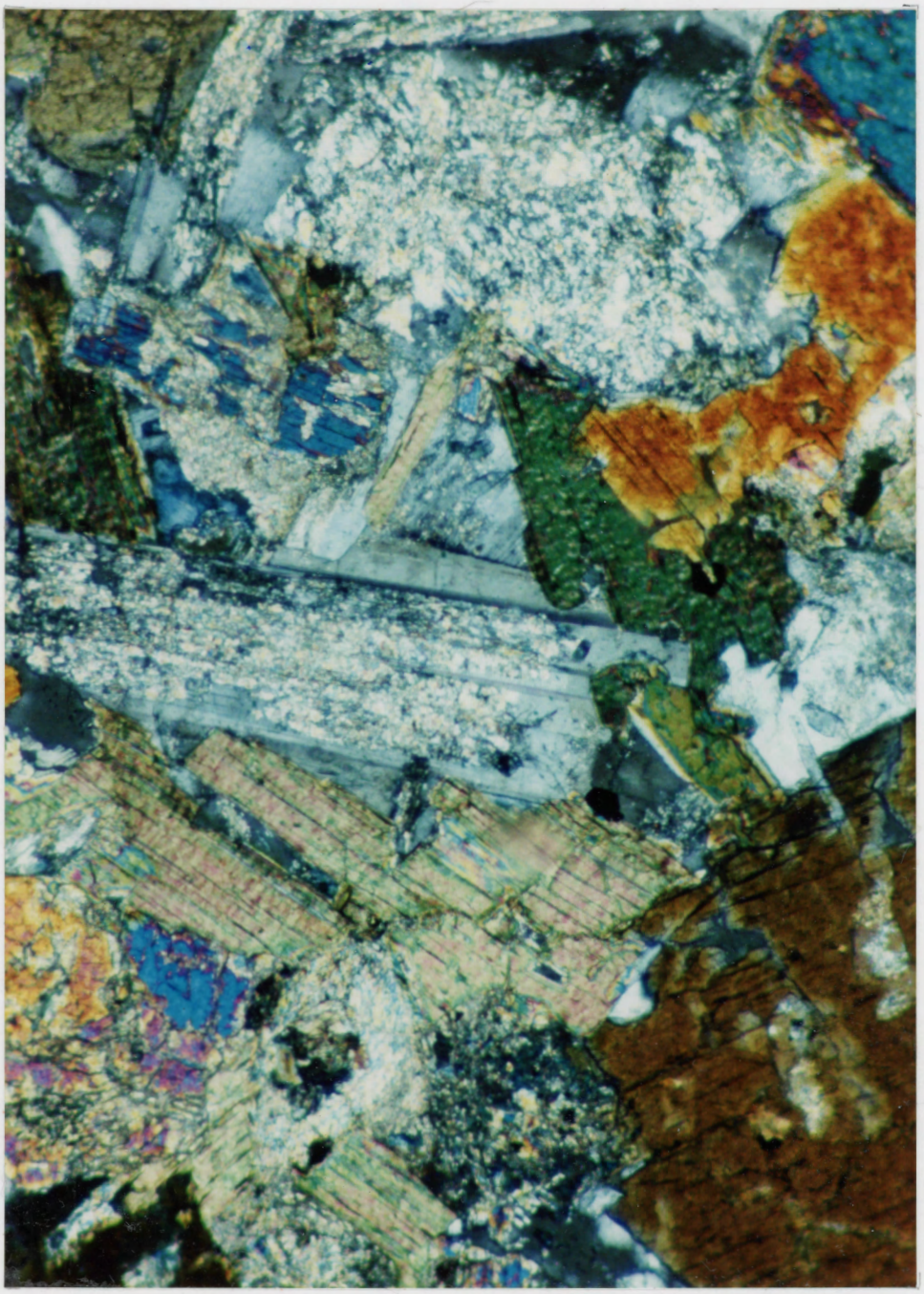

Figure 3.7. KR89-006 (North trending dyke) Dark brown hornblende, green and pink biotite, and sericitized plagioclase. XN, 1 x 2 mm.

Figure 3.8. FJ87-134 (porphyritic andesite) Ovoid amygdales lined with chlorite and filled with calcite, in a strongly chloritic groundmass of sericitized plagioclase laths. XN, 5 x 7 mm.

chlorite, often in association with calcite (Fig. 3.8). Chlorite constitutes up to 25% of some strongly altered samples, but on average composes 5 - 15% of a sample.

Many of the samples contain opaque oxides as alteration products of mafic minerals. Very fine-grained aggregates of opaque grains rim the boundaries of clinopyroxene and olivine phenocrysts. Sericitic alteration of plagioclase occurs in all of the samples to some degree, but is strongest in the porphyritic rocks of Krueger Island. Sericite appears as a very fine-grained aggregate in plagioclase phenocrysts and microlites. Actinolite occurs as bladed masses or aggregates. It typically exhibits first-order yellow birefringence colours, and pale-green pleochroism. Uralite, a variety of actinolite which often has the habit of the pyroxene it replaces, appears in many of the samples. In the Bourne Complex uralite occurs as pale-green to colourless aggregates of grains or bladed crystals.

Calcite occurs predominantly as a vein or amygdale infill, and rarely as a discrete grain. The discrete grains often occur with epidote and actinolite. Many amygdaloidal samples contain 5 - 10% calcite. Sphene exists in all of the Fjeldholmen Island samples but occurs rarely in the samples from Krueger Island. Appearing as very fine-grained masses of brown aggregate, it constitutes 20% of sample FJ87-148 and up to 10% of other samples. Epidote occurs in eight samples exclusive to Krueger Island. It invariably appears as highly birefringent, granular masses, and is commonly associated with calcite or actinolite (Figs. 3.9, 3.10). Quartz occurs as intergranular, anhedral

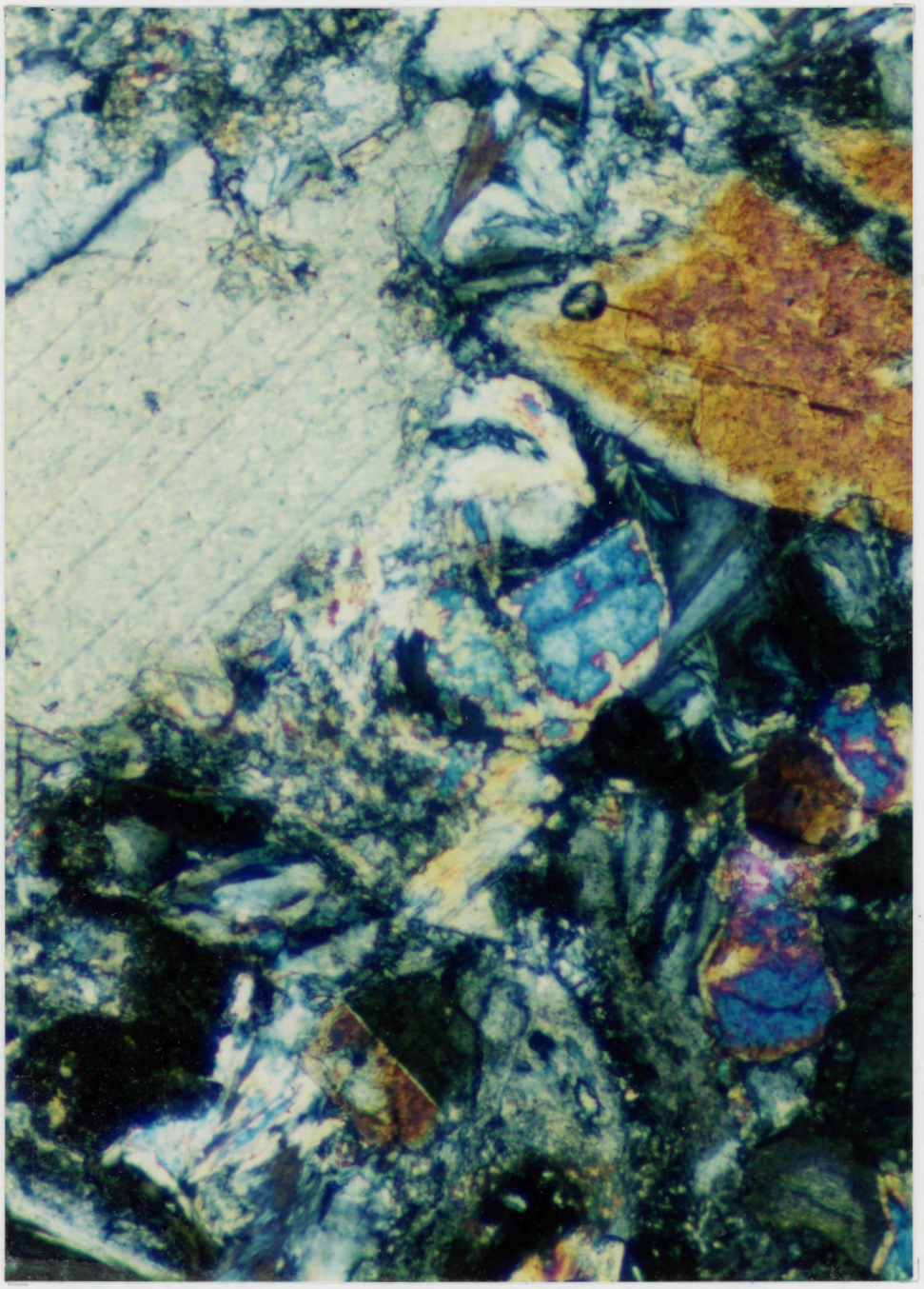

Figure 3.9. KR89-037 (Porphyritic andesite) Epidote (centre) with large calcite grain and clinopyroxene. XN, 0.5 x 1 mm.

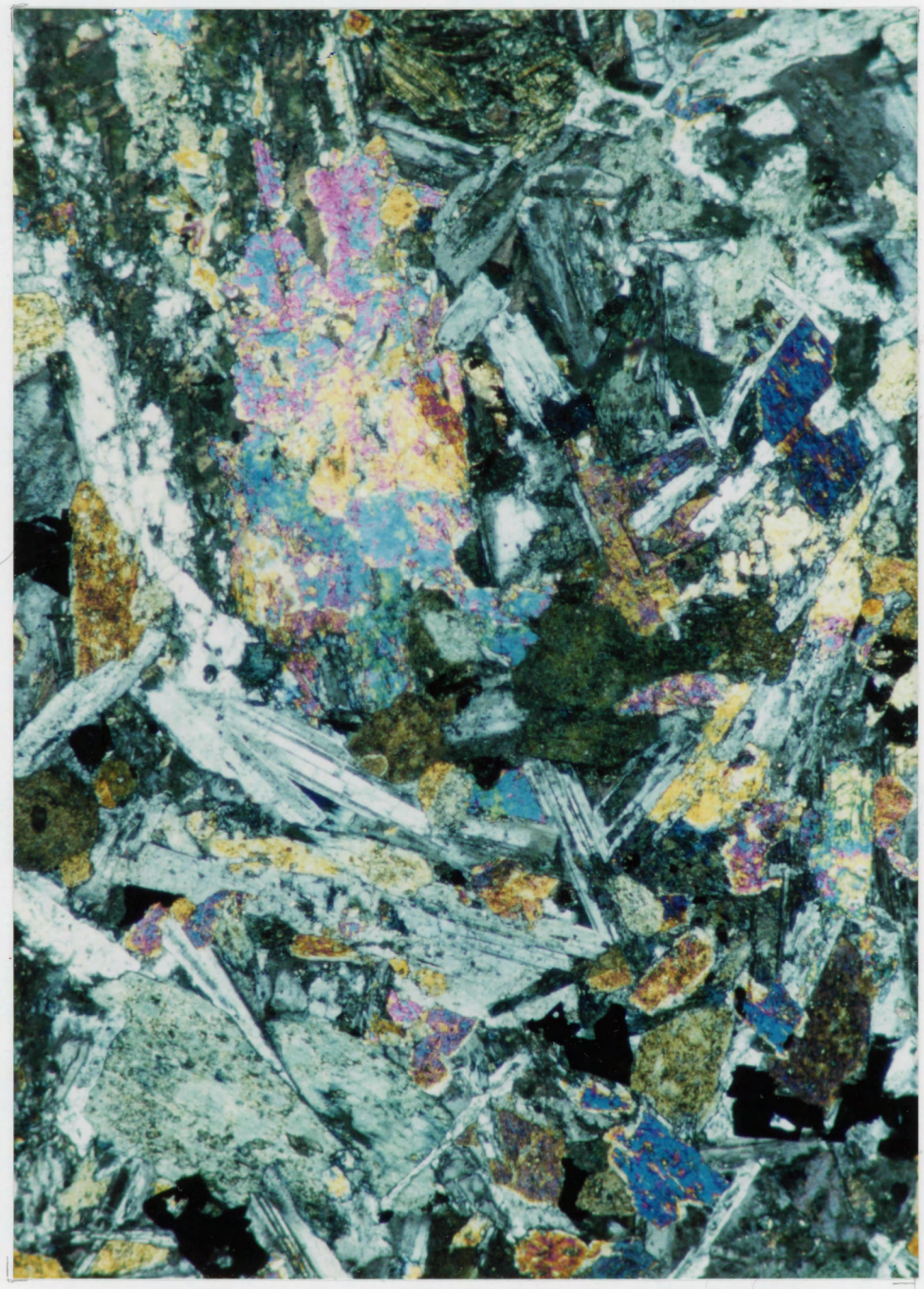

Figure 3.10. KR89-011 (Plagioclase porphyry dyke) Highly birefringent epidote in association with pale-green actinolite. XN, 2 x 3.5 mm.

grains in six strongly sericitized and moderately uralitized samples. In sample FJ87-145 it appears in symplectite intergrowth with plagioclase (Fig. 3.11).

Various forms and degrees of alteration affect the rocks of the Bourne Complex. An alteration mineral assemblage containing chlorite + actinolite + albite + epidote + quartz implies greenschist facies metamorphism. Such an assemblage is not necessarily diagnostic, but it is typical. Most of the Bourne Complex rocks contain chlorite and albite, many with associated actinolite and epidote. Microcrystalline quartz residing in groundmass is difficult to identify, and it may or may not be present in these samples. Nevertheless, at least six of the samples contain fine-grained secondary quartz. The abundance of chlorite precludes the attainment of upper greenschist facies. The secondary mineral assemblage observed most likely indicates greenschist facies metamorphism.

3.3.2 Texture

The samples from the Bourne Complex on Fjeldholmen Island fall into two separate and distinct textural groups. Twelve of the fourteen samples exhibit, to varying degrees, porphyryitic texture. These samples contain fine to medium-grained plagioclase, pyroxene, and amphibole phenocrysts set in a groundmass of microcrystalline to fine-grained felsic groundmass of dominantly plagioclase laths. Of these twelve porphyritic samples, nine exhibit relatively uniform texture, they contain

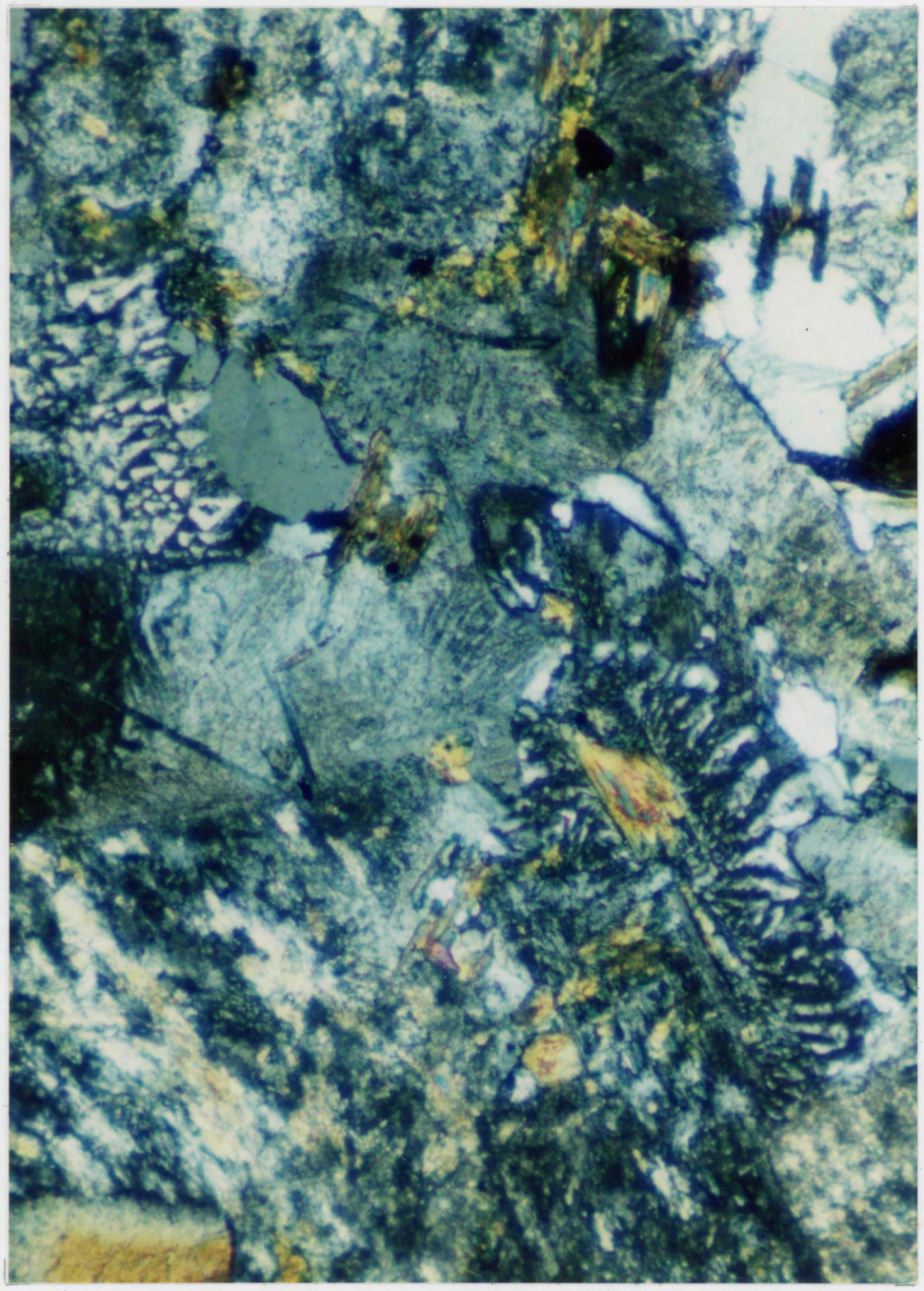

Figure 3.11. FJ87-145 (Plagioclase porphyry dyke) Quartz in symplectite intergrowth with plagioclase. XN, 0.5 x 1 mm.

microcrystalline groundmass and uniformly sized phenocrysts (Figs. 3.12, 3.13). The remaining three of these twelve samples contain a coarser, nearly medium-grained, intergranular groundmass which sets them apart from the other twelve. The concentration of phenocrysts, however, varies from moderately sparse to relatively abundant (Fig. 3.14).

The remaining two samples exhibit an aphyric, intergranular texture which is distinctly different from the porphyritic samples.

Of the three dykes which intrude the Nansen Formation two exhibit porphyritic texture, and the third an intergranular texture.

Textural similarities exist between the rocks of Fjeldholmen Island and Krueger Island. The metavolcanic rocks collected at the fourth location on Krueger Island exhibit porphyritic textures similar to the porphyritic textures found on Fjeldholmen Island. One of the north-trending dykes on Krueger Island displays an intergranular texture similar to one of the north-trending Nansen Formation dykes. In both these cases the Krueger Island textures are coarser than those found on Fjeldholmen Island.

Based primarily on textural and mineralogical characteristics, three groupings of rocks emerge from the sample set. These divisions are: 1) porphyritic andesite, 2) plagioclase porphyry dykes, and 3) north-trending dykes. The porphyritic andesite group contains twenty samples of dykes and flows, twelve of which come from Fjeldholmen Island. Samples in

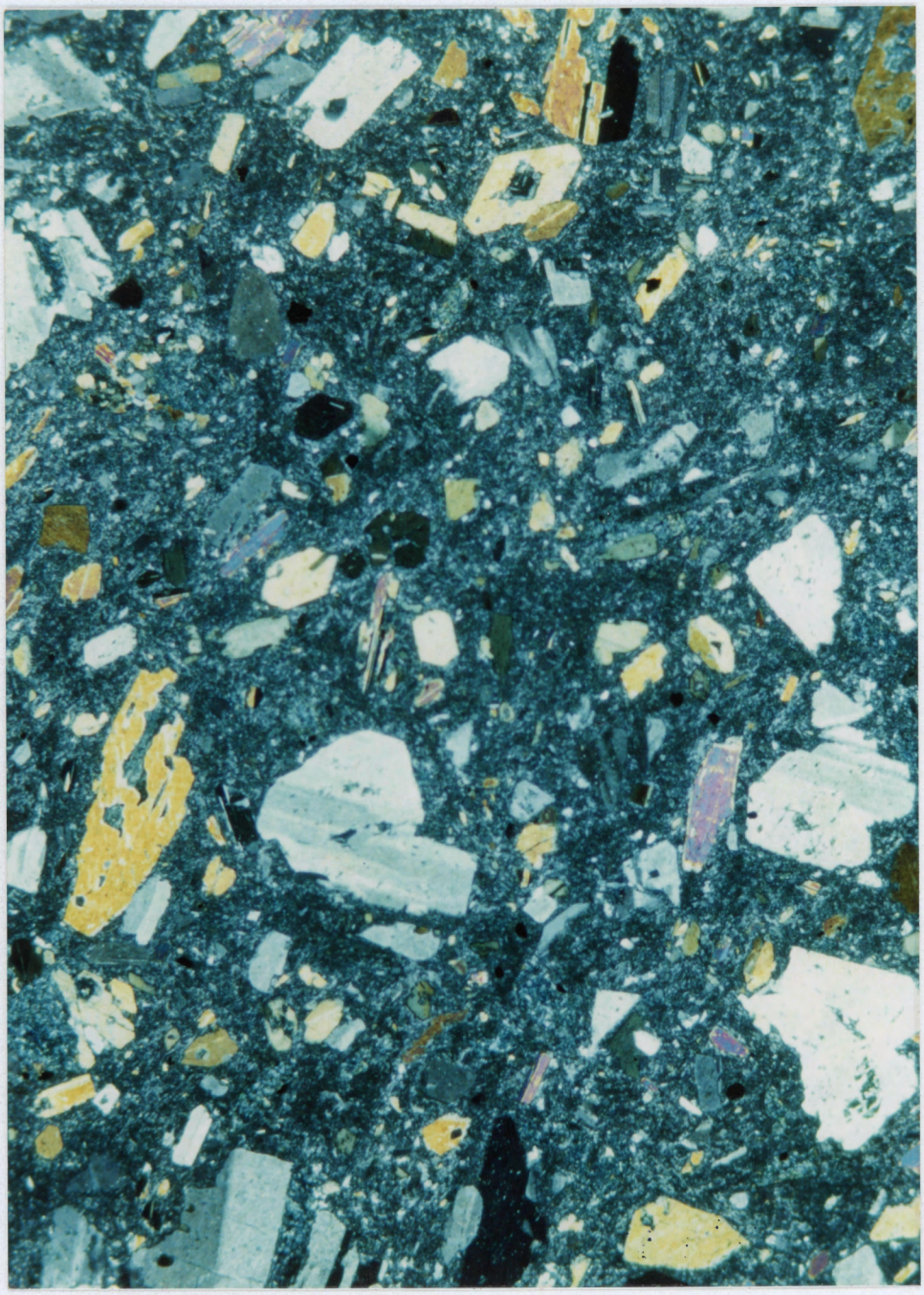

Figure 3.12. FJ87-146 (Porphyritic andesite) Porphyritic texture characteristic of many samples from Fjeldholmen Island. Uniformly sized plagioclase and hornblende phenocrysts set in a microcrystalline groundmass. XN, 5 x 7 mm.

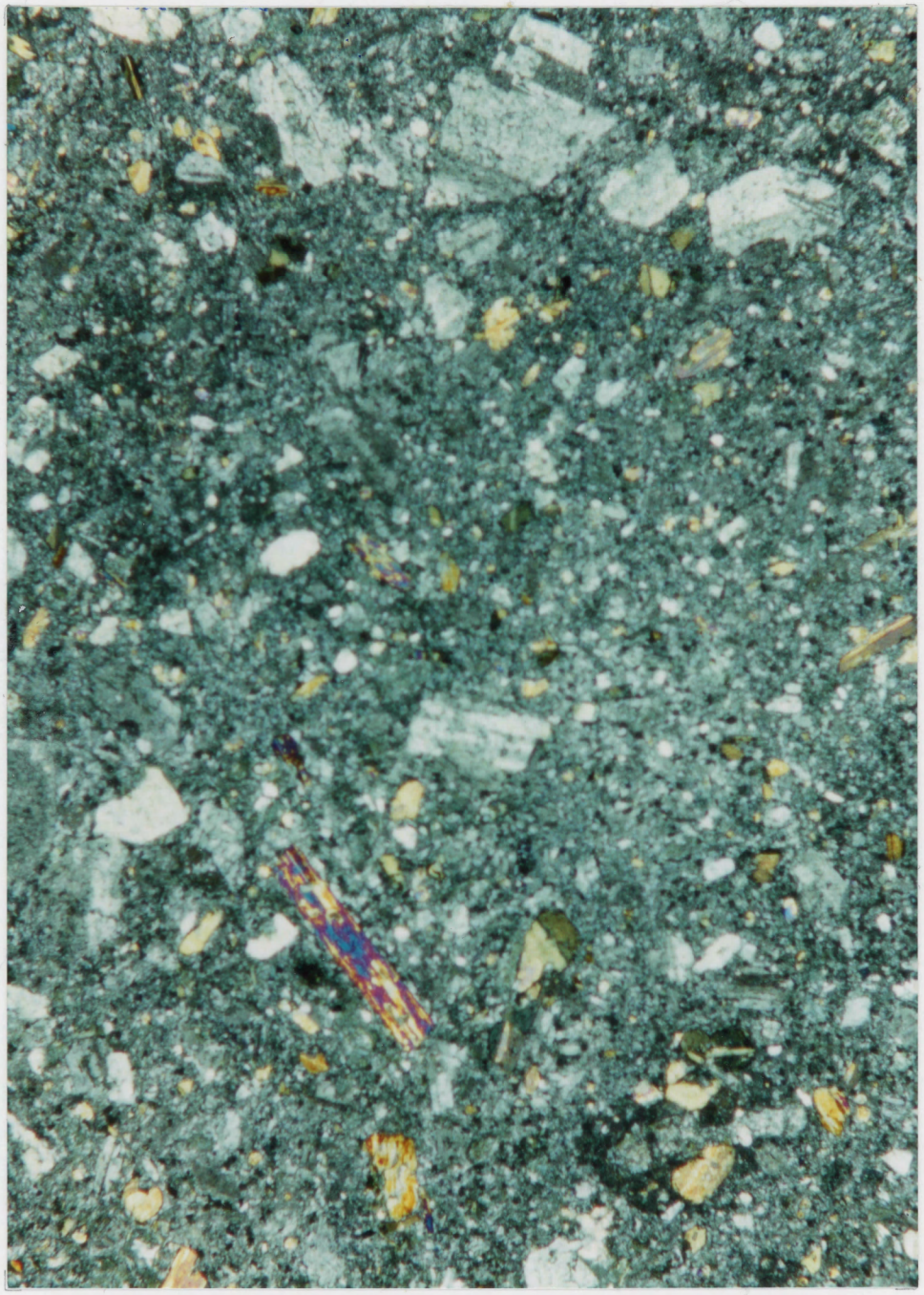

Figure 3.13. FJ87-131 (Porphyritic andesite) Porphyritic texture characteristic of many samples from Fjeldholmen Island. Plagioclase and hornblende phenocrysts set in a microcrystalline groundmass. XN, 4 x 7 mm.

Figure 3.14. FJ87-133 (Porphyritic andesite) Sparsely porphyritic texture with coarser groundmass. XN, 10 x 14 mm.

this group range from sparsely to moderately porphyritic and fine- to coarse-grained. The twelve samples termed plagioclase porphyry dykes come mainly from Krueger Island. They include samples from dykes composed primarily of large phenocrysts set in a relatively coarse groundmass. The north-trending dykes include the three samples from Nansen Formation dykes and sample KR89-006, a Krueger Island dyke of similar texture and orientation. These dykes all trend to the north which sets them apart from the easterly-trending units.

3.4 Mineral Chemistry

Many of the Bourne Complex samples contain phenocrysts of clinopyroxene and amphibole. The chemical compositions of clinopyroxene phenocrysts from seven samples were determined using the Jeol 733 superprobe at Dalhousie University. Values from several points on the rims and cores of a number of clinopyroxene grains from each sample were obtained. Appendix B contains the mean compositions of each sample.

MINPET software (Richard 1989) recalculated the mean oxide weight percent values to clinopyroxene structural formulae, on the basis of six oxygens. Figure 3.15 indicates that the core and rim compositions of the seven samples are augite.

Electron microprobe analysis determined the compositions of primary amphibole phenocrysts for six samples. Appendix B contains the mean whole grain compositions of each sample. AMPHIBOL software (Richard and Clarke 1990) calculated the

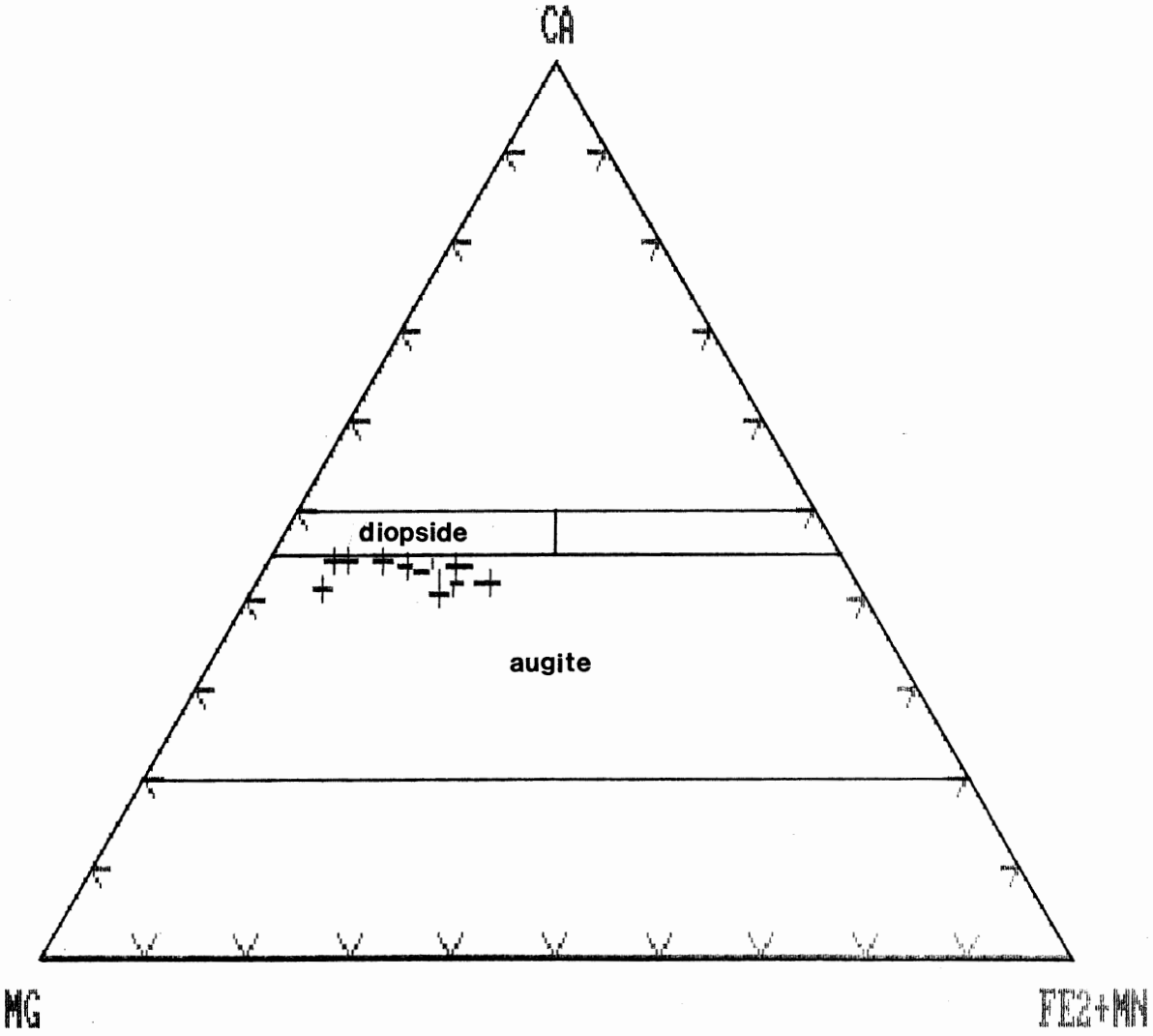

Figure 3.15 Classification of primary clinopyroxene phenocrysts (mean core and rim compositions). The phenocrysts are calcic-augite.

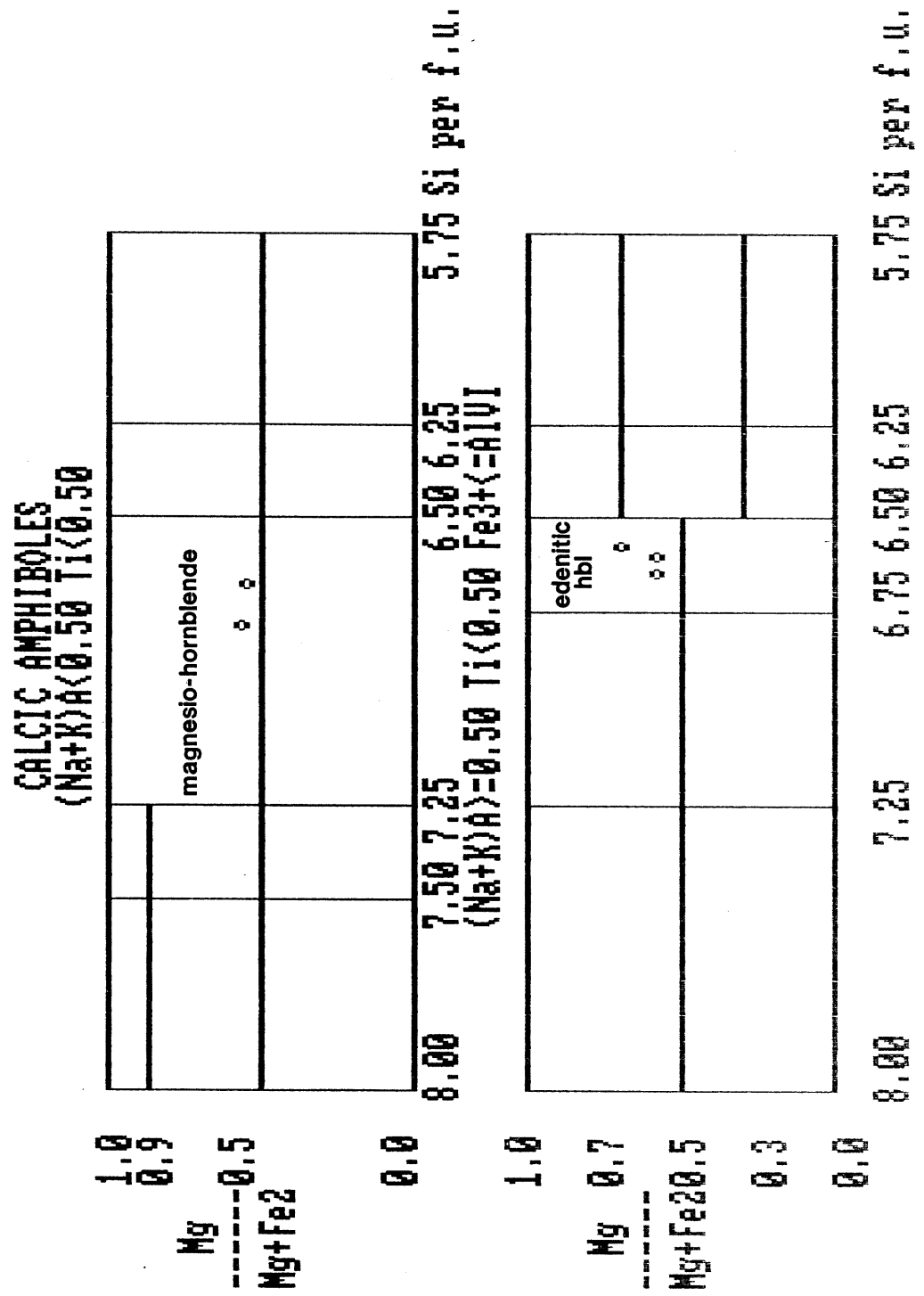

Figure 3.16 Classification of primary amphibole phenocrysts (mean core and rim compositions). Porphyritic andesite samples are classified as magnesio-hornblende and edenitic hornblende.

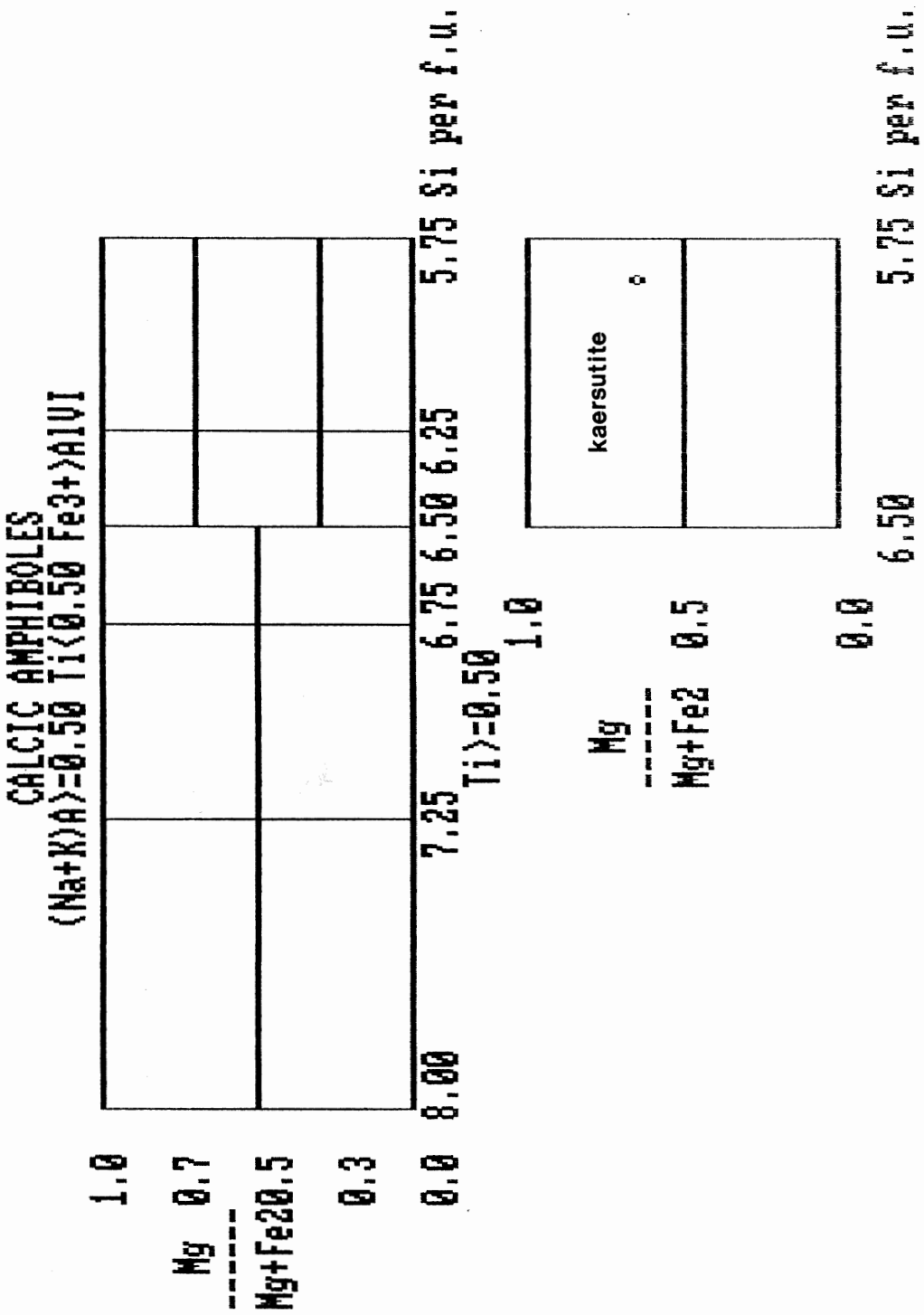

Figure 3.17 Classification of primary amphibole phenocrysts (mean core and rim compositions). Sample KR89-006 is kaersutite.

structural formulae of the mean core and rim compositions and plotted the mean values of the six cores. Figures 3.16 and 3.17 show that magnesio- and edenitic-hornblende occur in the porphyritic andesites, and that kaersutite occurs in the north-trending dyke.

CHAPTER 4: GEOCHEMISTRY

4.1 Introduction

This chapter presents and analyzes the geochemical characteristics of the igneous rocks of the Bourne Complex. A discussion on the probability of major element mobility precedes a test, using cluster analysis, of the classification made in Chapter 3. Geochemical and tectonomagmatic discrimination diagrams employing immobile trace elements and their ratios, classify and characterize the rocks.

4.2 Methods

Preparation of rock samples for X-ray fluorescence analysis, of major and trace element concentrations, follows a set procedure. Removal of all weathered, and foreign material from a 3 cm cube of sample, precedes crushing and milling the rock to a powder. Sieving, to a prescribed mesh size, and homogenization of the powder completes the preparation. Thirty-six samples were prepared in this manner and analyzed at the Atlantic Regional X-Ray Fluorescence Laboratory at Saint Mary's University. Duplicate samples, submitted as controls, provided a means of determining analytical precision. The laboratory returned analyses for ten major and minor elements, fifteen trace elements, and loss on ignition (LOI). The mass lost after heating a sample to 1050 degrees Celsius constitutes the LOI.

Low Nb concentrations in several samples prompted their reanalysis to lower detection limits. Of the thirty-six samples, twelve received further analysis for rare earth element (REE), and other trace element concentrations at the Instrumental Neutron Activation Analysis Facility at Saint Mary's University, Halifax.

4.3 Results

Appendix C contains the major, trace, and rare earth element compositions of thirty-six Bourne Complex samples; Table 4 contains a statistical synthesis of these results. Preliminary observations reveal a number of compositional trends. Many of the samples contain andesitic SiO_2 values (Middlemost 1985). Most of the samples identified from petrographic criteria as porphyritic andesite display depleted Nb and enriched TiO_2 relative to the plagioclase porphyry dykes, which exhibit high Fe_2O_3 and K_2O values, but low Na_2O. Of the samples previously identified as strongly altered, many are depleted in silica relative to their unaltered equivalents. Altered samples display anomalously high LOI values as well. Amygdaloidal samples, not unexpectedly, contain large amounts of CaO and MgO, and exhibit depleted barium values.

These early observations reveal compositional trends that appear to indicate mobility of selected major elements, and confirm, to some extent, the classification made from petrographic evidence.

Table 4a

XRF and INAA Analysis of Major and Minor Element Oxides (wt %) and Trace Elements (ppm) - porphyritic andesite (20 analyses, 7 for INAA)

	Range	Mean	SD
SiO_2	45.07 - 62.43	54.07	4.80
Al_2O_3	14.33 - 17.97	16.15	1.04
Fe_2O_3	5.95 - 12.07	8.41	1.76
MgO	2.80 - 7.47	4.58	1.14
CaO	2.52 - 10.40	5.95	2.41
Na_2O	2.72 - 7.13	5.23	1.42
K_2O	0.12 - 1.71	0.77	0.46
TiO_2	0.52 - 2.28	1.15	0.50
MnO	0.09 - 0.25	0.14	0.03
P_2O_5	0.10 - 0.40	0.20	0.08
LOI	1.20 - 7.70	3.06	1.57
Total	99.07 -100.84	99.81	0.53
Ba	20.00 -300.00	143.70	96.27
Rb	4.00 - 47.00	18.21	11.86
Sr	50.20 -384.50	218.40	110.43
Y	14.30 - 43.00	22.87	7.63
Zr	70.80 -285.00	148.72	61.68
Nb	0.70 - 11.00	5.06	2.88
Ga	11.00 - 25.00	18.25	3.19
Zn	55.00 -155.00	80.80	23.00
Cu	10.00 - 72.00	27.10	17.70
Ni	5.00 - 70.00	21.85	18.05
V	109.00 -289.00	198.15	46.04
Cr	17.00 -166.00	72.15	47.83
La	9.79 - 20.23	14.33	3.32
Ce	21.81 - 44.62	32.99	7.22
Nd	7.17 - 21.04	14.19	4.73
Sm	2.22 - 5.04	3.71	1.11
Eu	0.73 - 1.60	1.13	0.33
Tb	0.39 - 1.07	0.69	0.23
Yb	1.74 - 3.81	2.52	0.73
Lu	0.24 - 0.53	0.36	0.10
Cs	21.08 - 43.13	31.89	6.98
Hf	2.14 - 4.60	3.43	1.05
Ta	0.38 - 1.53	0.74	0.39
Th	3.77 - 6.45	4.68	0.99
U	1.69 - 2.53	2.13	0.31
Sc	14.71 - 21.53	18.18	2.42
Co	21.94 - 44.23	31.43	8.53

Table 4b

XRF and INAA Analysis of Major and Minor Element Oxides (wt %) and Trace Elements (ppm) - plagioclase porphyry dykes (12 analyses, 3 for INAA)

	Range	Mean	SD
SiO_2	46.85 - 50.12	48.15	0.78
Al_2O_3	12.17 - 18.34	15.44	1.90
Fe_2O_3	8.24 - 14.83	11.05	1.94
MgO	4.75 - 9.24	6.08	1.19
CaO	7.96 - 11.79	10.34	1.27
Na_2O	2.55 - 3.90	3.06	0.34
K_2O	0.34 - 1.30	0.60	0.28
TiO_2	0.95 - 3.03	1.53	0.64
MnO	0.15 - 0.21	0.18	0.02
P_2O_5	0.12 - 0.33	0.20	0.06
LOI	1.40 - 4.40	2.40	0.87
Total	98.93 - 100.00	99.30	0.32
Ba	47.00 - 317.00	164.75	83.50
Rb	10.00 - 47.00	20.75	11.16
Sr	151.00 - 305.00	247.41	42.59
Y	15.00 - 39.00	25.91	7.06
Zr	70.00 - 254.00	125.66	48.91
Nb	7.20 - 26.00	13.51	5.20
Ga	15.00 - 24.00	19.91	2.64
Zn	55.00 - 176.00	104.25	32.39
Cu	56.00 - 273.00	92.33	60.10
Ni	27.00 - 291.00	73.66	71.93
V	187.00 - 446.00	281.16	80.40
Cr	25.00 - 369.00	116.00	93.09
La	7.47 - 11.23	9.02	1.96
Ce	19.00 - 26.97	22.35	4.13
Nd	11.06 - 14.44	12.91	1.71
Sm	3.01 - 4.64	3.72	0.83
Eu	1.23 - 1.81	1.48	0.29
Tb	0.64 - 1.17	0.82	0.29
Yb	2.75 - 3.80	3.26	0.52
Lu	0.35 - 0.56	0.44	0.10
Cs	18.36 - 26.07	21.60	3.99
Hf	2.18 - 3.49	2.74	0.67
Ta	0.85 - 1.22	0.97	0.21
Th	0.82 - 1.59	1.11	0.41
Sc	33.10 - 35.94	34.07	1.61
Co	37.27 - 61.31	47.61	12.36

Table 4c

XRF and INAA Analysis of Major and Minor Element Oxides (wt %) and Trace Elements (ppm) - north-trending dykes (4 analyses, 2 for INAA)

	Range	Mean	SD
SiO_2	43.45 - 46.31	44.85	1.30
Al_2O_3	13.32 - 15.37	14.62	0.92
Fe_2O_3	9.17 - 12.52	10.56	1.42
MgO	4.62 - 8.69	7.07	1.79
CaO	8.62 - 12.78	10.49	1.82
Na_2O	1.71 - 3.36	2.74	0.78
K_2O	1.17 - 2.26	1.73	0.44
TiO_2	1.53 - 3.43	2.17	0.87
MnO	0.12 - 0.17	0.15	0.02
P_2O_5	0.34 - 0.81	0.51	0.20
LOI	2.80 - 6.10	4.50	1.48
Total	99.18 - 99.84	99.53	0.27
Ba	423.00 - 1328.00	838.75	417.35
Rb	29.00 - 79.00	55.25	21.88
Sr	419.00 - 927.00	604.50	222.89
Y	19.00 - 27.00	22.25	3.59
Zr	101.00 - 230.00	157.50	56.02
Nb	46.00 - 83.00	61.50	16.13
Ga	15.00 - 23.00	17.50	3.69
Zn	73.00 - 101.00	87.25	13.81
Cu	28.00 - 83.00	53.50	22.60
Ni	34.00 - 166.00	98.00	58.26
V	180.00 - 332.00	246.75	62.97
Cr	32.00 - 212.00	136.50	79.00
La	32.74 - 51.31	42.02	13.13
Ce	64.14 - 106.89	85.51	30.22
Nd	26.65 - 41.99	34.32	10.84
Sm	5.00 - 8.03	6.51	2.14
Eu	1.65 - 2.64	2.14	0.70
Tb	0.84 - 0.91	0.87	0.04
Yb	2.13 - 2.45	2.29	0.22
Lu	0.29 - 0.34	0.31	0.03
Cs	62.00 - 103.30	82.65	29.20
Hf	2.83 - 3.30	3.06	0.33
Ta	3.81 - 4.30	4.05	0.34
Th	3.87 - 5.01	4.44	0.80
U	0.90 - 0.93	0.91	0.02
Sc	23.17 - 25.08	24.12	1.35
Co	43.05 - 51.96	47.50	6.30

4.4 Chemical Classification

One system of igneous rock classification uses the modal mineral composition of the rocks. This system depends on precise petrographic descriptions of unaltered rocks. Glassy or cryptocrystalline rocks cannot be classified by these methods. A chemical classification system, however, enables the characterization of many different igneous rock types.

In the past many different criteria have been used in the chemical classification of volcanic rocks. Macdonald and Katsura (1964) employed silica content and the degree of alkalinity to classify the volcanic rocks of Hawaii. Cox et al. (1979) devised a system of classification for non-potassic volcanic rocks based on the same criteria.

Elements such as Si, Na, K, Ca, Ba, Rb, and Sr, and some of the light REE, are considered mobile under secondary alteration conditions (Henderson 1982). Petrographic evidence and preliminary observation of the chemical data suggest major and trace element mobility in the Bourne Complex igneous rocks. Elements which have become mobilized are not used in this study.

An immobile element, because of its very large or very small ionic radius, or high ionic charge, is not easily transported by the fluids which commonly accompany secondary alteration processes (Floyd and Winchester 1975; Winchester and Floyd 1977). Elements such as Ti, Zr, Nb, Y, and others fall into this group. Zirconium, an immobile element, is a good indicator of fractionation in volcanic rocks (Winchester and Floyd 1977;

Pearce and Norry 1979). Thus, in unaltered cogenetic rocks, alkali content increases with zirconium content, producing a tight linear trend (Winchester and Floyd 1977; Floyd and Winchester 1978). In Figure 4.1, a P_2O_5 - Zr plot, a linear trend indicates the restricted mobility of these elements. The four younger, north-trending dykes plot away from the trend defined by the porphyritic andesite and plagioclase porphyry dykes and are probably not genetically related. In contrast to Figure 4.1, a plot of $K_2O + Na_2O$ versus Zr (Fig. 4.2) displays a scatter of data points indicative of the mobility of K and/or Na in the Bourne Complex rocks. The demonstrated mobility of these elements, commonly used to classify volcanic rocks, precludes the use of alkali-silica diagrams in the classification of the Bourne Complex samples.

Many immobile elements are also termed incompatible. These high field strength elements have ionic radii, or electric charges, that are not easily accommodated in the crystal lattices of common rock-forming minerals. As a result, incompatible elements are the first to enter the liquid phase during partial melting, and are the last to form, or enter into, minerals upon cooling (Hess 1989). Rocks which originate from the same partial melt contain similar, and often characteristic, concentrations of these elements (Table 4d, Fig. 4.3). Addition or depletion of mobile elements may alter the absolute concentrations of incompatible elements in a specific rock, however, the incompatible element ratios within rocks formed from the same partial melt do not change with most fractionation processes. In

N = North Trending dykes.
A = Porphyritic Andesite.
P = Plagioclase Porphyritic dykes.

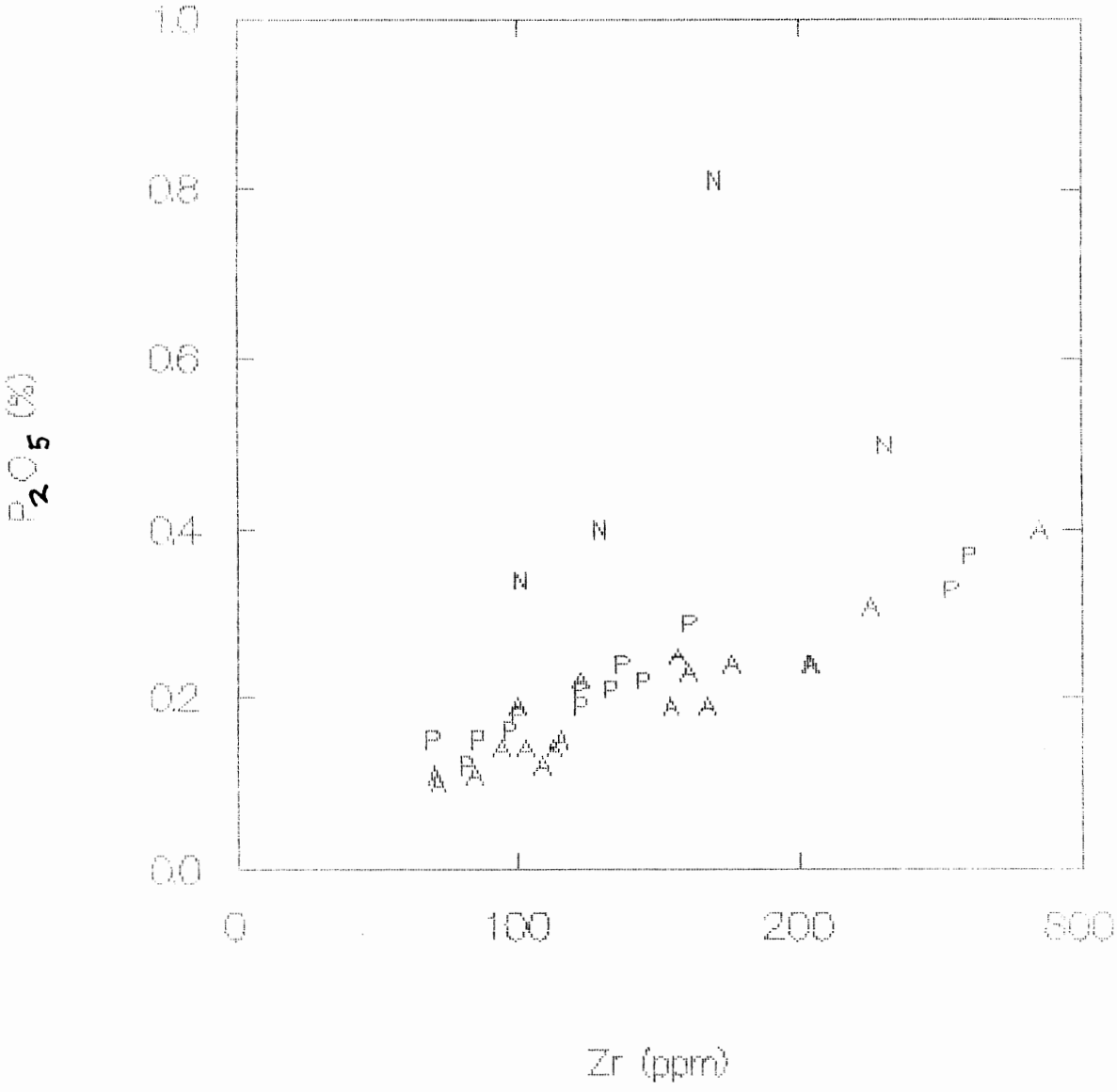

Figure 4.1 P_2O_5 - Zr binary plot. The linear trend illustrates the restricted mobility of these elements.

N = North Trending dykes.
A = Porphyritic Andesite.
P = Plagioclase Porphyritic dykes.

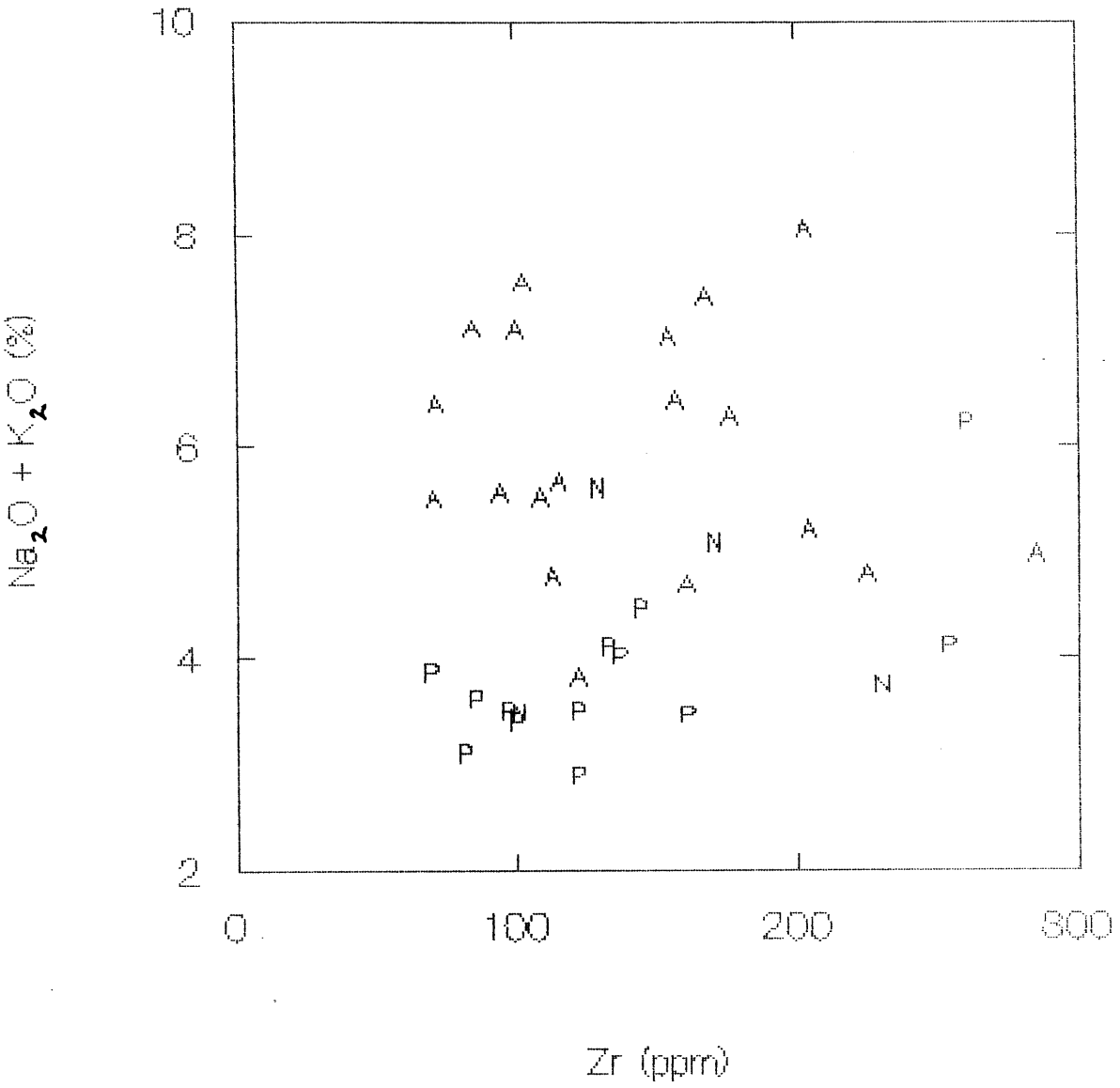

Figure 4.2 Na_2O+K_2O - Zr binary plot. The scatter of data points illustrates the mobility of one, or both, of these alkaline elements.

Table 4d

Pearson Correlation Matrices

Plagioclase Porphyry Dykes:

	Zr	Nb	Y	TiO_2	P_2O_5
Zr	1.000				
Nb	0.481	1.000			
Y	0.916	0.429	1.000		
TiO_2	0.887	0.527	0.880	1.000	
P_2O_5	0.963	0.432	0.921	0.906	1.000

North trending Dykes:

	Zr	Nb	Y	TiO_2	P_2O_5
Zr	1.000				
Nb	0.169	1.000			
Y	0.792	-0.210	1.000		
TiO_2	0.948	-0.123	0.782	1.000	
P_2O_5	0.449	0.879	-0.112	0.242	1.000

Porphyritic Andesite:

	Zr	Nb	Y	TiO_2	P_2O_5
Zr	1.000				
Nb	0.879	1.000			
Y	0.896	0.709	1.000		
TiO_2	0.773	0.577	0.850	1.000	
P_2O_5	0.939	0.876	0.884	0.821	1.000

a

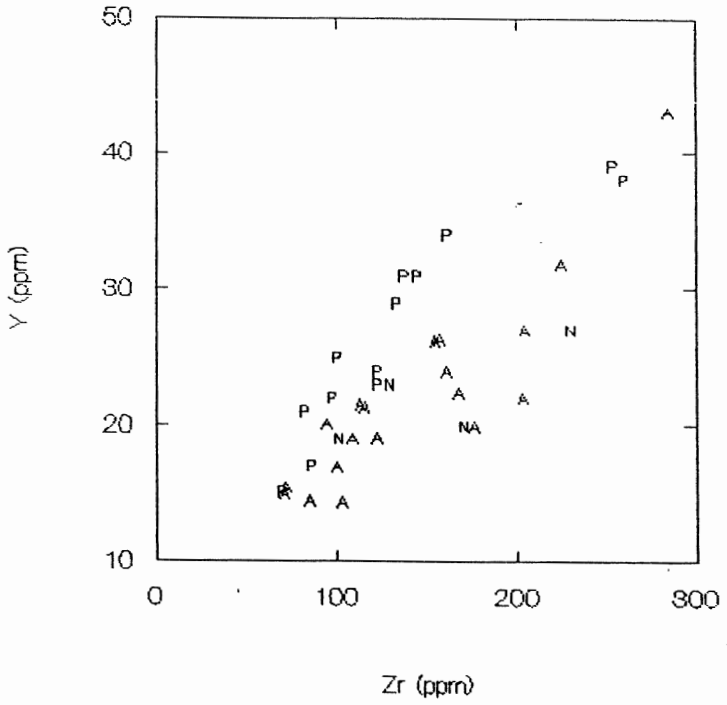

b

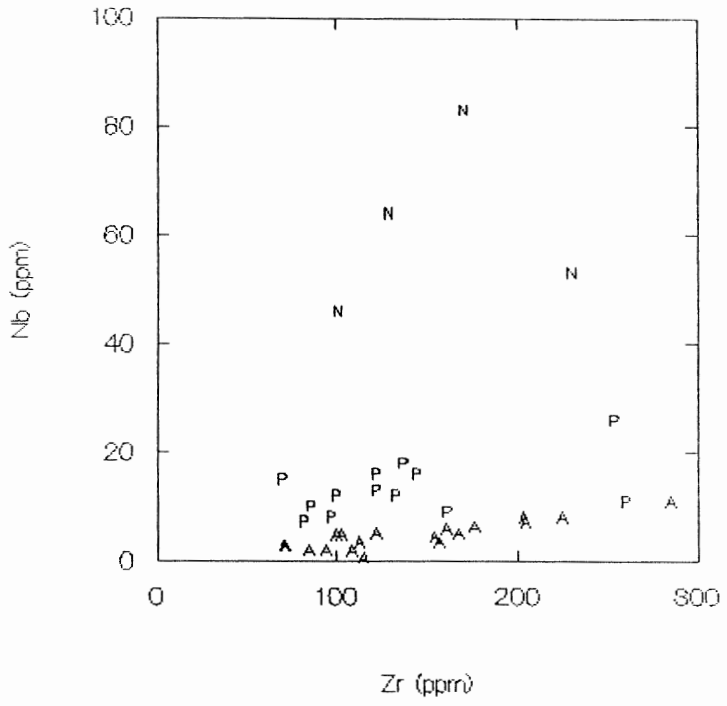

Figure 4.3 Binary plots which illustrate the restricted mobility of a) Y and b) Nb

c

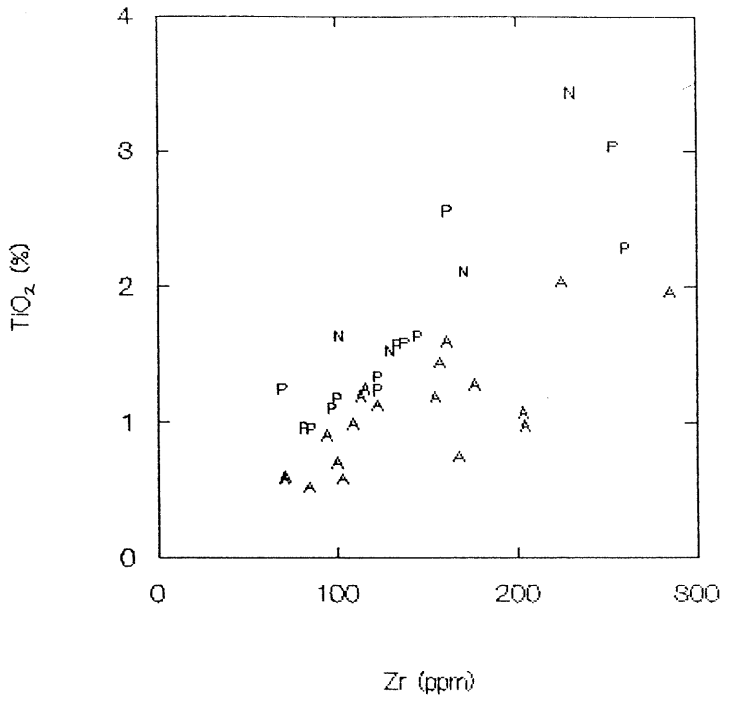

d

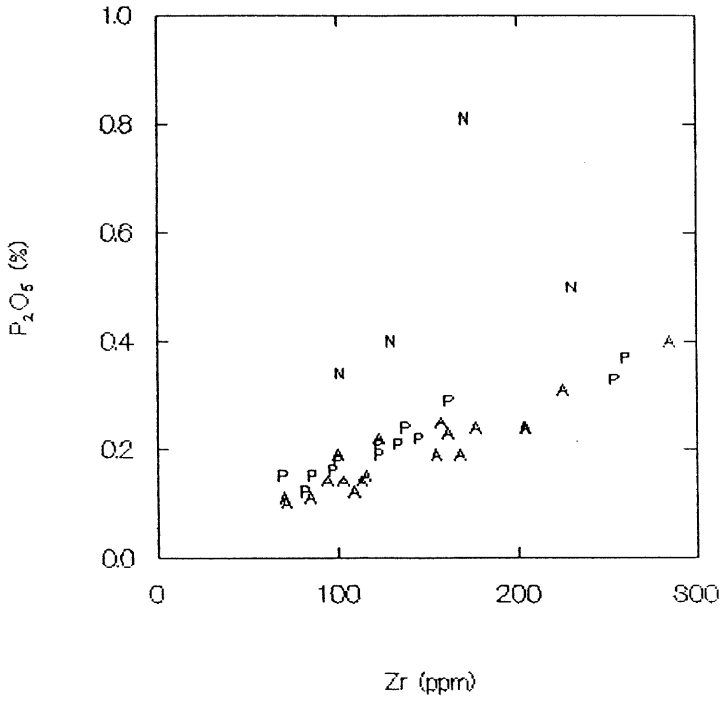

Figure 4.3 Binary plots which illustrate the immobility of c) TiO_2 and d) P_2O_5.

Table 4d, Pearson correlation matrices of immobile incompatible trace element concentrations for the three groups of rocks found in the Bourne Complex, show a good degree of correlation, indicating that the rocks have retained their original ratios. Thus, plots of incompatible element ratios can be used to show the magmatic affinity within a suite of rocks (Wilson 1989).

Plots of Nb, Y, Ti, and P, versus Zr (Fig. 4.3) show relatively linear trends and are a graphical representation of the Pearson correlations. The poorer correlation between TiO_2 and Zr may reflect small scale mobility manifested by the presence of metamorphic sphene (Cameron 1989). As Zr is considered strongly incompatible (until the final stages of crystallization), it is used as an index of differentiation; the higher the concentration of Zr, the more differentiated the rock. The linear trends in these plots indicate the restricted mobility of Nb, Y, Ti, Zr, and P in the samples.

Cluster analysis groups individuals or objects into clusters, so that variables in the same cluster are more like each other than they are like variables in other clusters. Cluster trees or dendrograms graphically portray the sample classifications. The primary value of cluster analysis lies in its ability to classify data according to natural relationships.

The cluster analysis module contained in SYSTAT (Wilkinson 1987) was used on ten ratios of five immobile elements (Ti, Nb, Y, P, and Zr) to cluster the Bourne Complex samples. Ratios, rather than absolute concentrations, eliminate the dilution or concentration effects of alteration. These ratios were

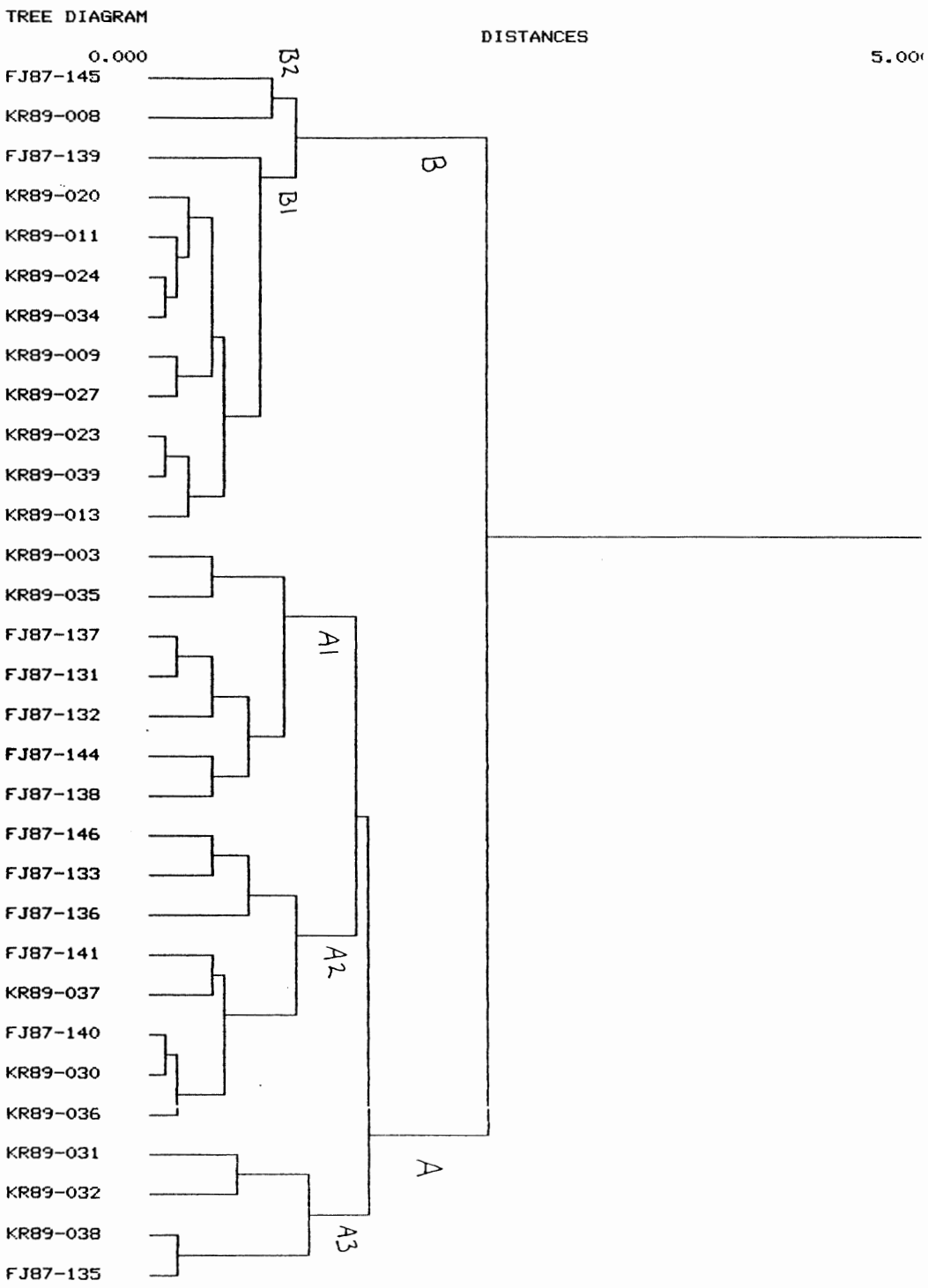

Figure 4.4 Cluster analysis using immobile trace element ratios, clusters the Bourne Complex samples into two distict groups: A, porphyritic andesites, and B, plagioclase porphyry dykes.

standardized prior to clustering to avoid placing emphasis on very high ratios. The north-trending dykes from the Nansen Formation were removed from the data set. The dykes are clearly younger (they intrude Carboniferous rock) and share no magmatic affinity with the Bourne complex.

Figure 4.4 is the resulting tree diagram, clearly showing two first order clusters containing five second order groups. The larger of the two clusters (A) contains all the samples previously classified as porphyritic andesite. The second, smaller cluster (B) contains samples of the plagioclase porphyry dykes. The smaller subclusters reflect chemical variations within the larger groups.

A distance scale measures the distance between branch points. On this scale, the farther the branch point is from the next branch point, the more significant the cluster. On Fig. 4.4 the first branches are more significant than the later branches. For example, the samples in B are more different from those in A, than A1, A2, and A3 are from each other. Cluster analysis shows that two chemically distinct groups of rocks, which correspond to the petrographic grouping, exist in the Bourne Complex

A chemical classification diagram devised by Winchester and Floyd (1977) uses the ratios Zr/TiO_2 and Nb/Y for the nomenclature of basaltic rocks (Fig. 4.5). The diagram clearly discriminates the rocks of the Bourne Complex. The rocks termed porphyritic andesite classify as andesite and andesitic basalt and are transitional to dacite compositions. The plagioclase porphyry dykes are subalkaline basalt transitional to alkali

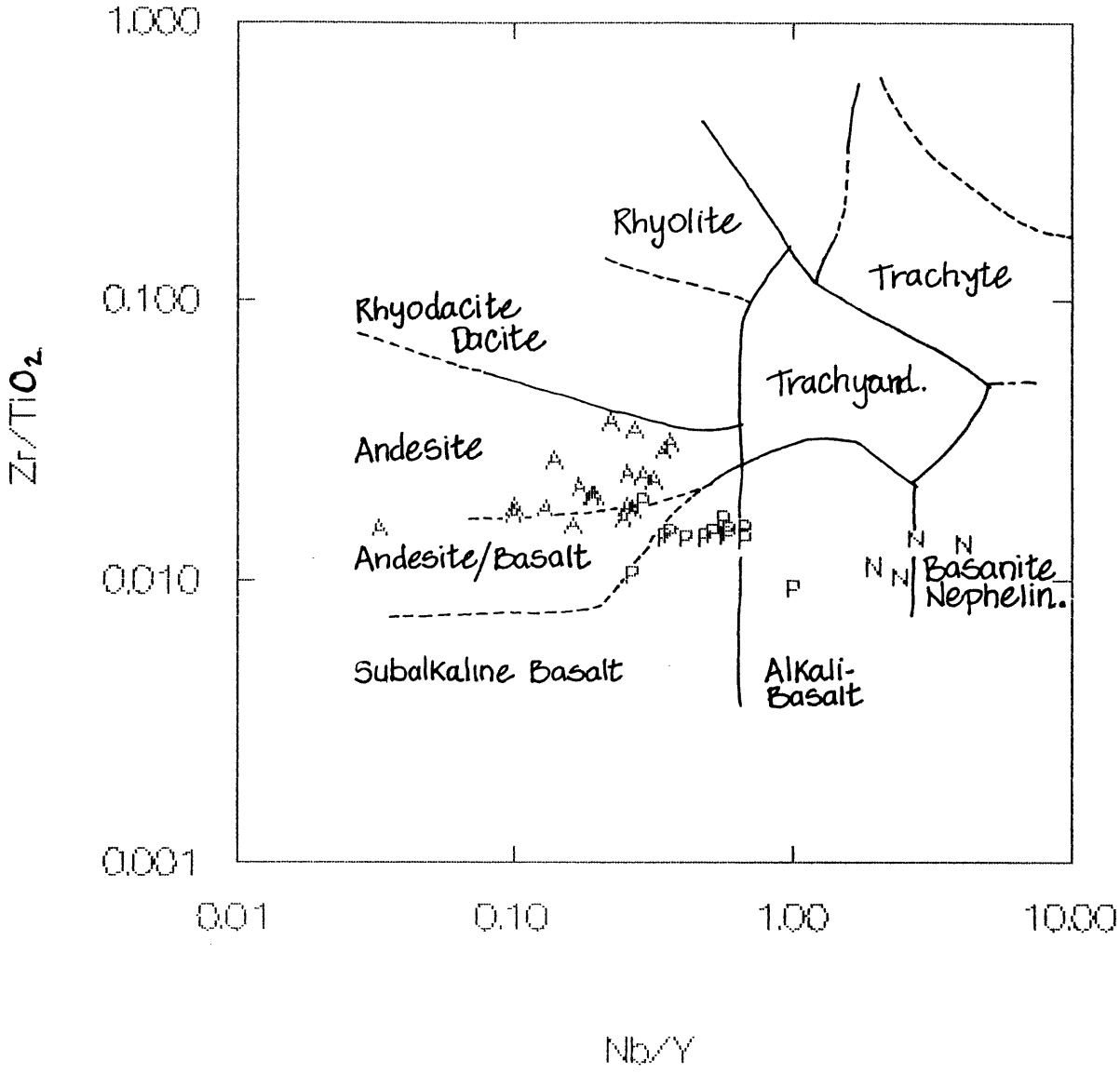

Figure 4.5 Zr/Tio_2 - Nb/Y chemical classification diagram. The Zr/Tio_2 ratio acts as an index of differentiation and the Nb/Y ratio is an alkalinity index. A = porphyritic andesite, P = plagioclase porphyry dyke, N = north-trending dyke (from Winchester and Floyd 1977).

basalt compositions. The north-trending dykes plot in the fields of alkali basalt and basanite-nephelinite. The diagram suggests that some of the samples may have been misclassified. The lone sample of plagioclase porphyry dyke for instance, which plots in the alkali-basalt field may, in fact, represent a younger dyke similar to the north-trending dykes.

4.5 Tectonomagmatic Discrimination

Tectonomagmatic discriminator diagrams use the compositions of fresh rocks, of known tectonic setting, to determine the character of ancient and possibly altered rocks. The field lines drawn around the clusters of data points which represent the rocks from a particular setting are, in most cases, strictly empirical. In some cases the positioning of the field lines can be explained geochemically.

A tectonomagmatic discriminator diagram, derived by Pearce and Cann (1973), uses the immobile trace elements Ti, Y, and Zr to discriminate within-plate basalt (WPB), from ocean-floor (OFB) and volcanic arc basalts (VAB) which form at plate margins. The diagram further discriminates calcalkaline basalt (CAB) from low-K tholeiite (LKT), both of which form in volcanic arc settings. Figure 4.6 shows the Bourne Complex data plotted on this diagram. The porphyritic andesite samples plot primarily in the CAB field. The north-trending dykes plot only in the WPB field, whereas the samples classified as plagioclase porphyry dykes plot in the

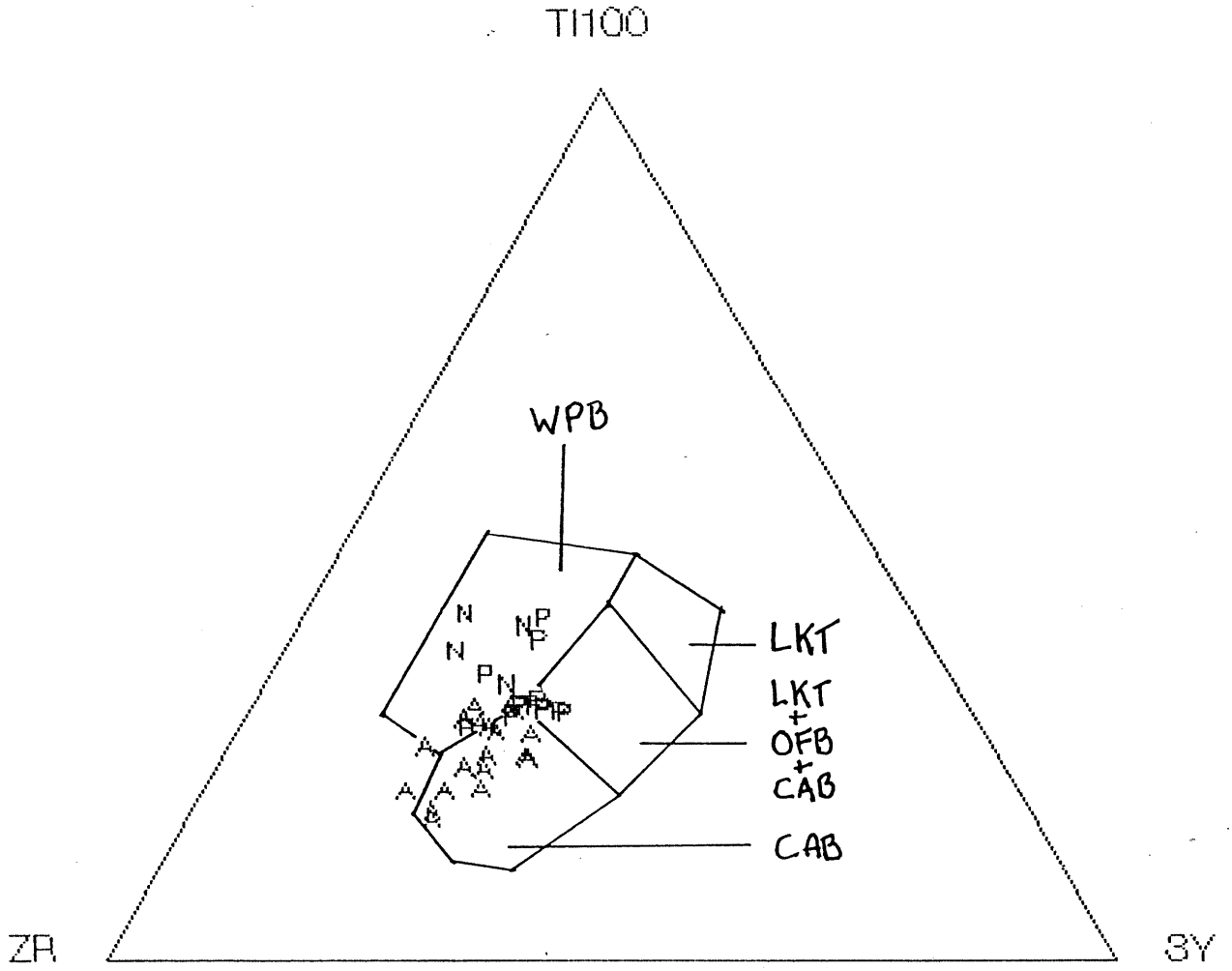

Figure 4.6 Ti-Y-Zr tectonomagmatic discrimination diagram for basalts. WPB=within-plate basalt, LKT=low-K tholeiite, OFB=ocean-floor basalt, CAB=calkalkaline basalt. Plotting symbols as in Fig. 4.5 (from Pearce and Cann 1973).

field designated as LKT, OFB, or CAB, as well as in the WPB field. Most of the plagioclase porphyry dykes plot as plate margin setting rocks; the three which plot in the WPB field may represent misclassified north-trending dykes. The diagram indicates that the plagioclase porphyry dykes and the porphyritic andesite are primarily plate-margin rocks, and that the north-trending dykes were deposited in a within-plate setting.

A Th-Hf-Ta diagram, devised by Wood (1980), discriminates rocks which form in a within-plate setting from those which form in a constructive, or destructive, plate-margin setting. The twelve samples which underwent instrumental neutron activation analysis (INAA) are plotted on this diagram to further characterize the Bourne Complex rocks (Fig. 4.7). The diagram clearly discriminates the samples. The porphyritic andesite samples plot as calc-alkaline, destructive plate margin basalts, consistent with the findings from Figure 4.6. The north-trending dykes plot as within-plate basalt, and the plagioclase porphyry dykes plot as E-type MORB. Wood (1980) suggests that samples containing more than 2% - 3% Ti-Fe oxides may plot closer to the Ta apex of the plot, reflecting the strong partitioning of Ta in these minerals. This may account for the plotted positions of samples close to, or on, the field boundary lines in Figure 4.7. Many of these samples contain greater than 2% opaque oxides and the two north-trending dyke samples contain more than 5%.

Many of the Bourne Complex samples contain fresh clinopyroxene phenocrysts. Microprobe analyses of these crystals can be used to determine the magma type of their host lava.

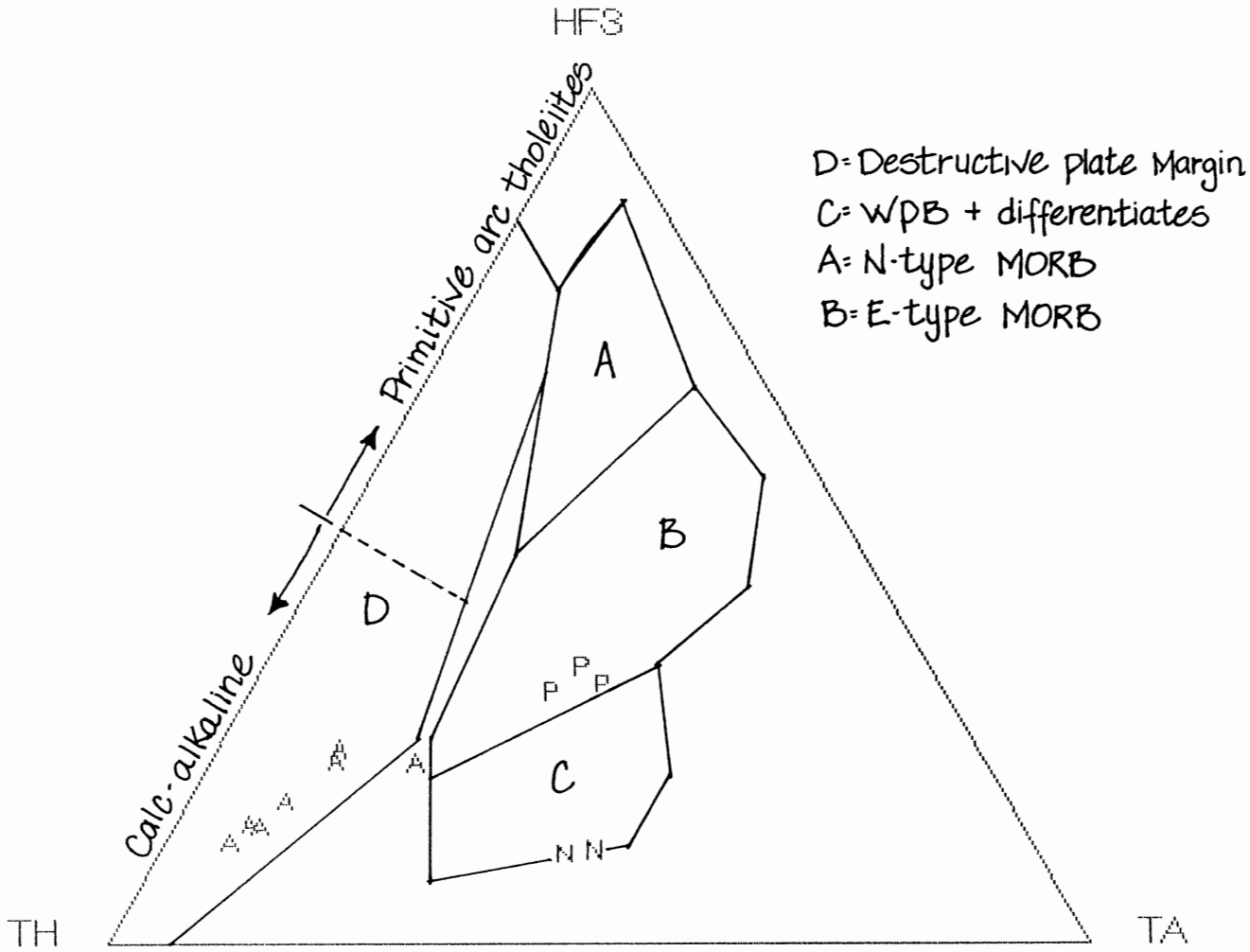

Figure 4.7 Hf-Ta-Th tectonomagmatic discrimination diagram for basalts and more differentiated rocks. Plotting symbols as in Fig. 4.5 (from Wood 1980).

Nisbet and Pearce (1977) present a method which uses the compositions of primary cpx phenocrysts to determine the tectonomagmatic affinity of basalts. F1 and F2 are the values of the discriminant functions which best discriminated the samples of a large database. The mean compositions of primary cpx phenocrysts from six porphyritic andesite samples and one plagioclase porphyry dyke sample were used in the discriminant function equations to calculate F1 and F2. Figure 4.8 shows these values plotted on the diagram developed by Nisbet and Pearce (1977). The diagram discriminates the porphyritic andesite samples as ocean floor or volcanic arc basalts with relatively good precision. The authors warn that the probability of successful discrimination using a small sample population is approximately 70%. The one sample which plots as within plate tholeiite may not be correctly discriminated as a result of the small sample population.

4.6 Summary

The demonstrated mobility of elements commonly used to classify volcanic rocks precludes the use of alkali-silica diagrams in the classification of the Bourne Complex samples. As a result, ratios of immobile, incompatible elements are employed to characterize and determine the tectonomagmatic affinity of the rocks. The Zr/Ti - Nb/Y chemical classification diagram (Fig. 4.5) indicates that the porphyritic andesite are andesite and basaltic andesite, that the plagioclase porphyry dykes have

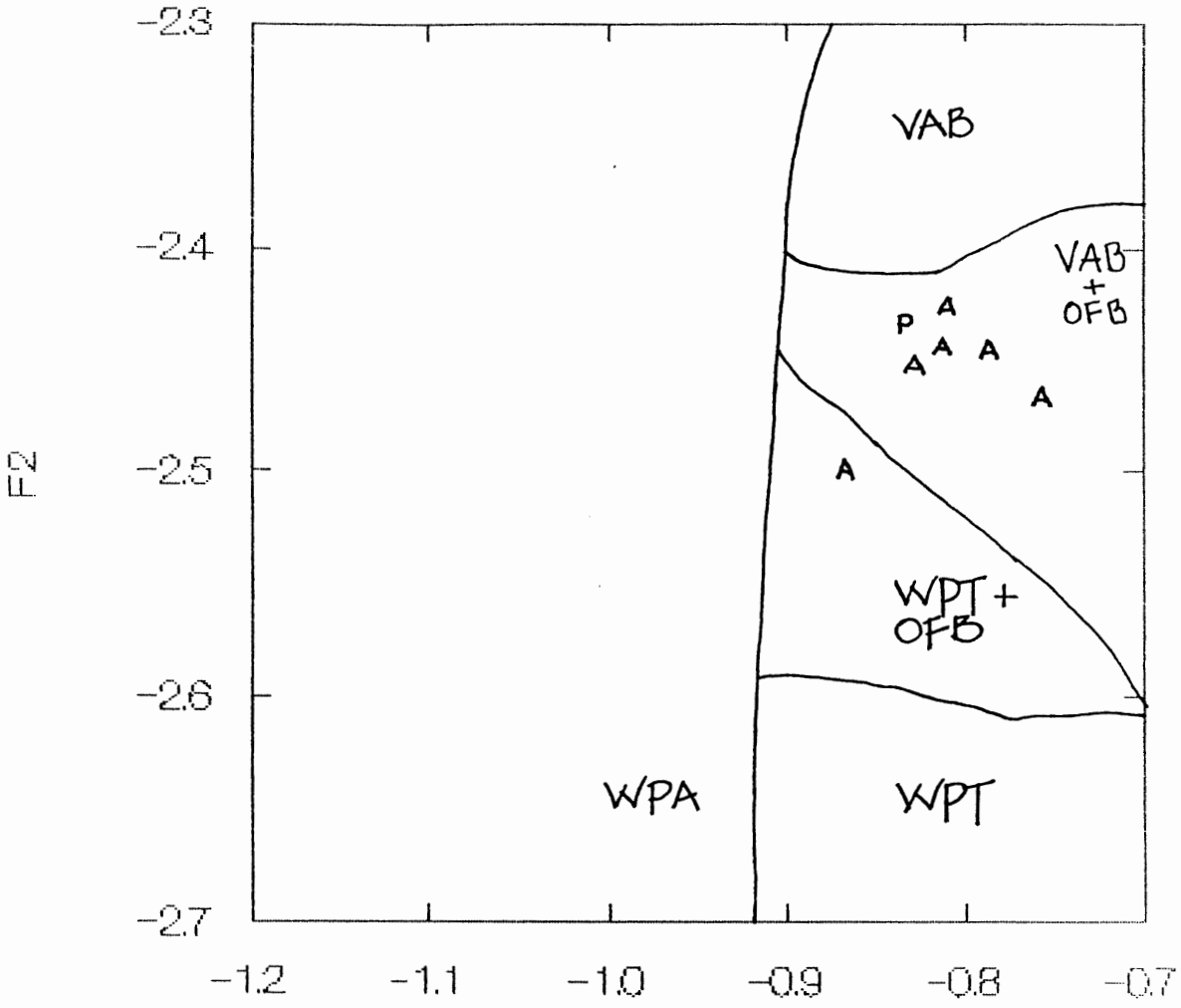

Figure 4.8 Tectonomagmatic discrimination diagram based on the composition of primary clinopyroxene phenocrysts. F1 and F2 are the discriminant functions calculated from the clinopyroxene compositions. Plotting symbols as in Fig. 4.6 (from Nisbet and Pearce 1977).

subalkaline basalt compositions, and that the north-trending dykes are alkali basalt transitional to basanite. The Ti-Y-Zr, and Hf-Ta-Th, tectonic discriminator diagrams (Fig. 4.6, Fig. 4.7) indicate that the porphyritic andesite originated at a destructive plate margin setting, that the plagioclase porphyry dykes indicate a destructive plate margin transitional to a MORB setting and that the north-trending dykes were emplaced in a within-plate setting.

CHAPTER 5: $^{40}Ar/^{39}Ar$ DATING

5.1 Introduction

This Chapter discusses the $^{40}Ar/^{39}Ar$ dating method, presents the results obtained from applying the method to selected Bourne Complex samples, and explains the techniques employed to interpret the results.

5.2 The $^{40}Ar/^{39}Ar$ Method

The $^{40}Ar/^{39}Ar$ dating method is a derivation of the potassium-argon (K-Ar) isotope method of dating rocks and minerals. The K-Ar method is based on the radioactive decay of ^{40}K to the daughter product ^{40}Ar over geologic time. Argon is an inert gas which does not combine chemically within minerals (Mason 1978). At high temperatures in a magma, radiogenic argon generated by decay of ^{40}K is lost through thermal diffusion. Upon solidification of the melt, radiogenic argon begins to accumulate, and is trapped in the crystal lattices of the minerals comprising the rock. The term "closure temperature" refers to the critical temperature at which individual minerals begin to retain radiogenic argon. By measuring the isotopic ratio of $^{40}K/^{40}Ar$ in a mineral, and knowing the rate of decay of ^{40}K to ^{40}Ar, the time elapsed since the cooling of this mineral through its closure temperature can be calculated.

The K-Ar method normally yields reliable ages for rapidly cooled igneous rocks that have simple cooling histories. However, rocks which experience elevated temperatures after crystallization or slow, complex cooling histories, may partially or completely lose accumulated radiogenic argon (McDougall and Harrison 1988). The K-Ar age obtained for these rocks may date the event which reheated the rocks, rather than the time of their emplacement. Furthermore, if only a partial loss of radiogenic argon occurred, the K-Ar age obtained may represent a date intermediate between the time of emplacement and the time of subsequent reheating (McDougall and Harrison 1988).

In the $^{40}Ar/^{39}Ar$ method, the rock or mineral to be dated is irradiated with fast neutrons in a nuclear reactor. This converts a known proportion of ^{39}K to ^{39}Ar, an isotope of argon that does not occur naturally. Heating by sequential temperature steps in a vacuum furnace extracts argon which is analysed isotopically in a mass spectrometer. This analysis measures the relative abundances of ^{40}Ar, ^{39}Ar, ^{37}Ar, and ^{36}Ar. The ratio $^{40}Ar/^{39}Ar$ is determined after correction for the presence of non-radiogenic (atmospheric) argon. The $^{40}Ar/^{39}Ar$ ratio is proportional to the $^{40}Ar/^{40}K$ ratio, and therefore is proportional to the age of the sample (McDougall and Harrison 1988).

The major advantage of the $^{40}Ar/^{39}Ar$ method over the K-Ar method is that the argon extracted at each temperature step can be analysed independently, and a series of apparent ages determined. A plot of the apparent age against the cumulative percentage of ^{39}Ar released is known as an age spectrum. A flat

pattern, termed a plateau, usually indicates that the sample has remained a closed system since initial closure, and has not lost radiogenic argon in a subsequent thermal event. Patterns which deviate from horizontal may indicate that a sample has lost some fraction of its radiogenic argon since crystallization, or that excess radiogenic or non-atmospheric initial argon are present.

The $^{40}Ar/^{39}Ar$ age spectrum approach makes the assumption that all ^{36}Ar in the sample is atmospheric in origin (negligible amounts are produced during irradiation). All non-radiogenic argon in the sample is assumed to have atmospheric composition (i.e. $^{40}Ar/^{36}Ar = 295.5$), and this ratio is used to correct for non-radiogenic ^{40}Ar. If excess radiogenic argon or non-atmospheric initial argon are present, then the standard procedure for calculating the amount of non-radiogenic ^{40}Ar will be incorrect.

$^{40}Ar/^{39}Ar$ isochron plots may be used to calculate $^{40}Ar/^{39}Ar$ ages without making assumptions about the isotopic composition of non-radiogenic argon in the sample (Jager and Hunziker 1979). The ratios $^{40}Ar/^{36}Ar$ and $^{39}Ar/^{36}Ar$, obtained from sequential heating of a sample, are plotted. The slope of a best-fit line through the data is proportional to the sample's age.

Inverse isochron plots, which plot $^{36}Ar/^{40}Ar$ versus $^{39}Ar/^{40}Ar$, have been employed recently to reduce the error introduced by using ^{36}Ar values in both ratios. The measurement of the quantity of ^{36}Ar present in a sample is not as precise as it is for the other isotopes because of the relatively low concentrations of ^{36}Ar present in most samples. The ratio of

non-radiogenic ^{36}Ar to ^{40}Ar in a sample is represented by the Y intercept of a best-fit line through the data points, and the age of the sample is obtained from the X intercept. Inverse isochron plots are used to determine the $^{40}Ar/^{39}Ar$ ages of the Bourne Complex samples.

5.3 Results

The $^{40}Ar/^{39}Ar$ method was used to date primary hornblende phenocrysts contained in three porphyritic andesite samples from Fjeldholmen Island. Microprobe analysis of these samples reveals average potassium concentrations of 0.20%. Samples FJ87-136, -138, and -146 were irradiated in the Mc Master University nuclear reactor and analysed at the Argon Dating Laboratory, located at Dalhousie University. Appendix D contains the gas release data and the age spectra for the analysed samples.

5.4 Interpretation

Figures 5.1, 5.2, and 5.3 are the inverse isochron plots for the three samples analysed. The plots show both corrected and uncorrected values. The uncorrected values represent the ratios measured at each heating step. The corrected values are derived by applying a "blank correction" to the raw data. In effect, this removes any residual argon present in the analytical

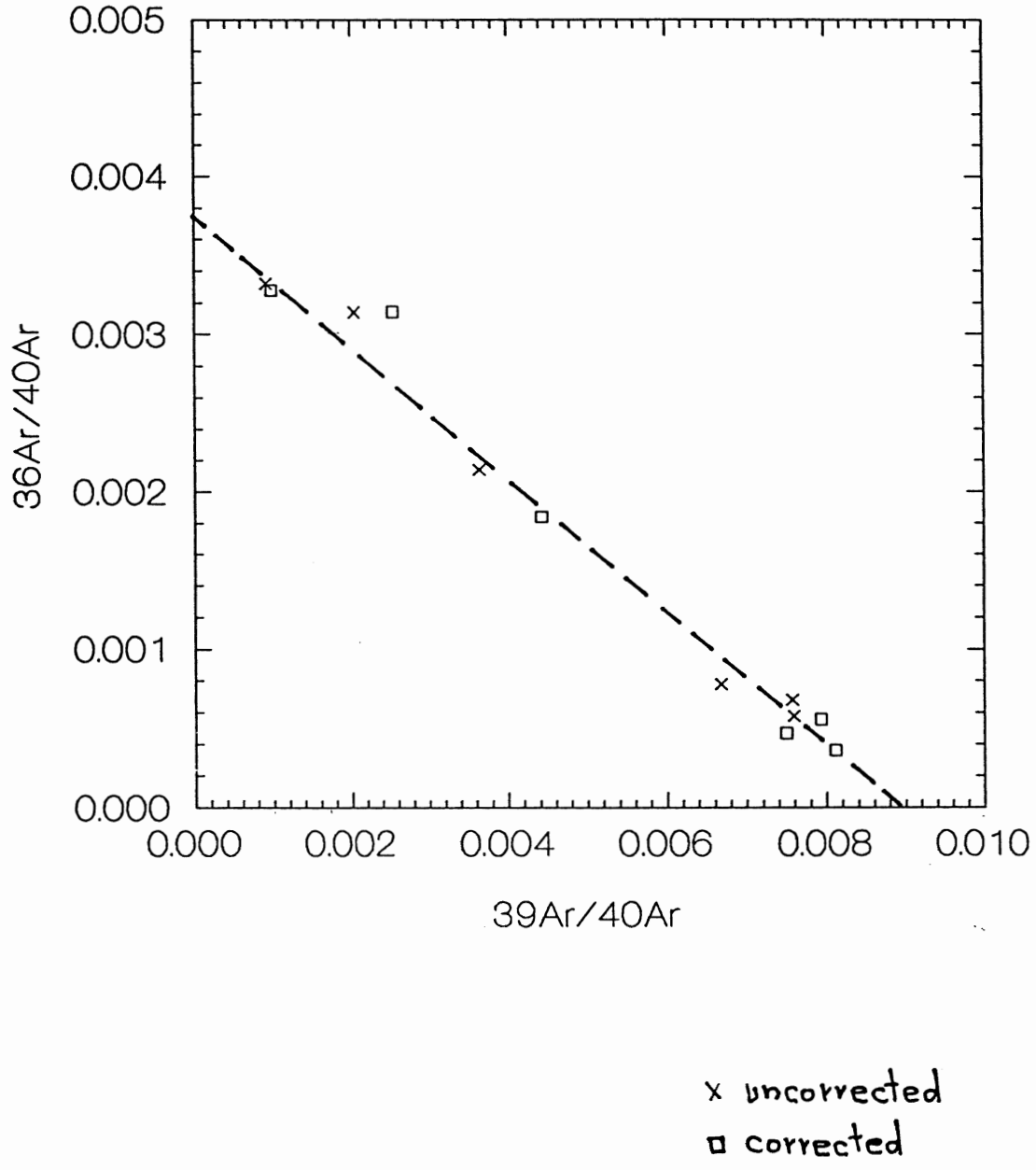

Figure 5.1 Inverse isochron plot for sample FJ87-136.

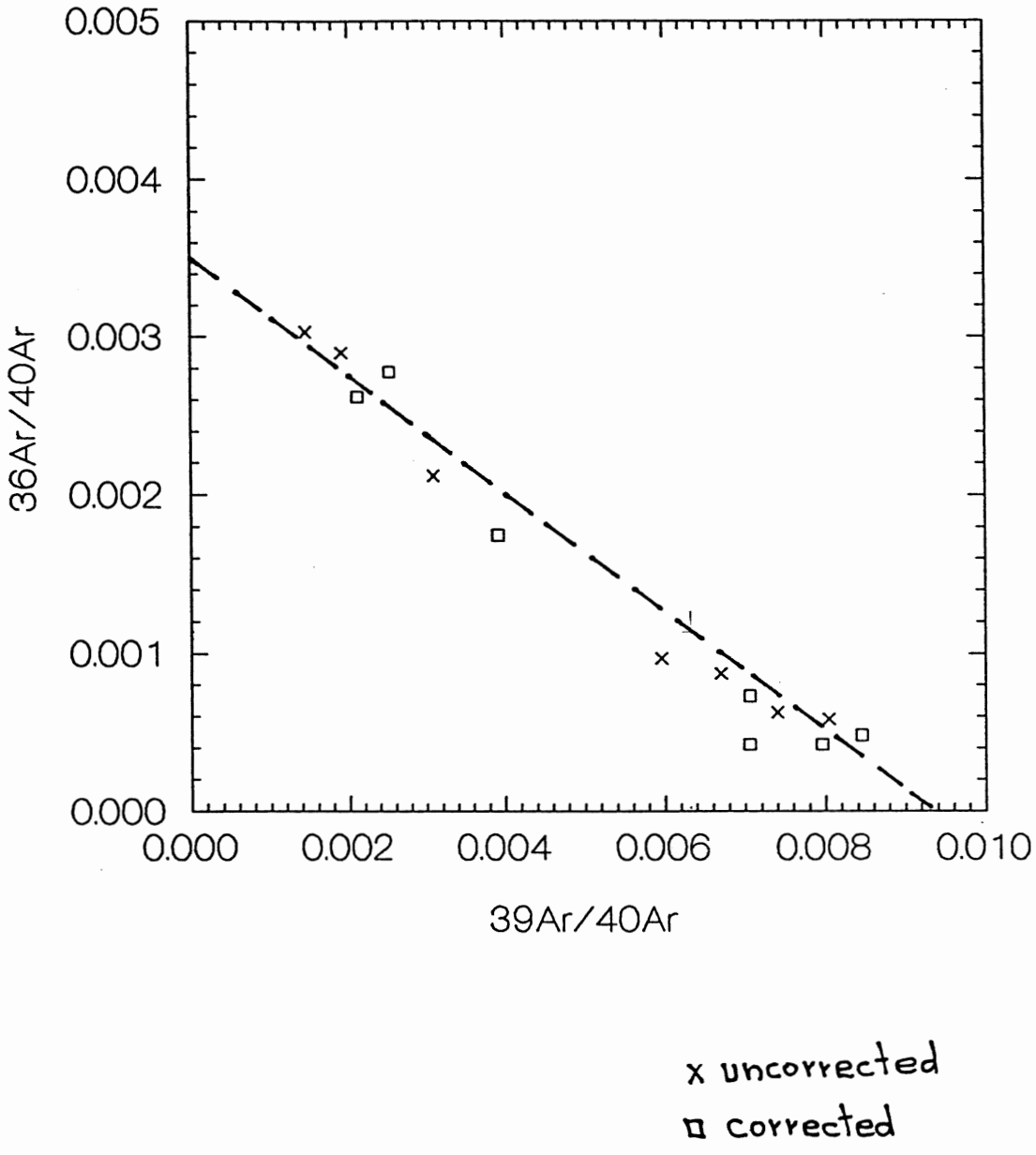

Figure 5.2 Inverse isochron plot for sample FJ87-138.

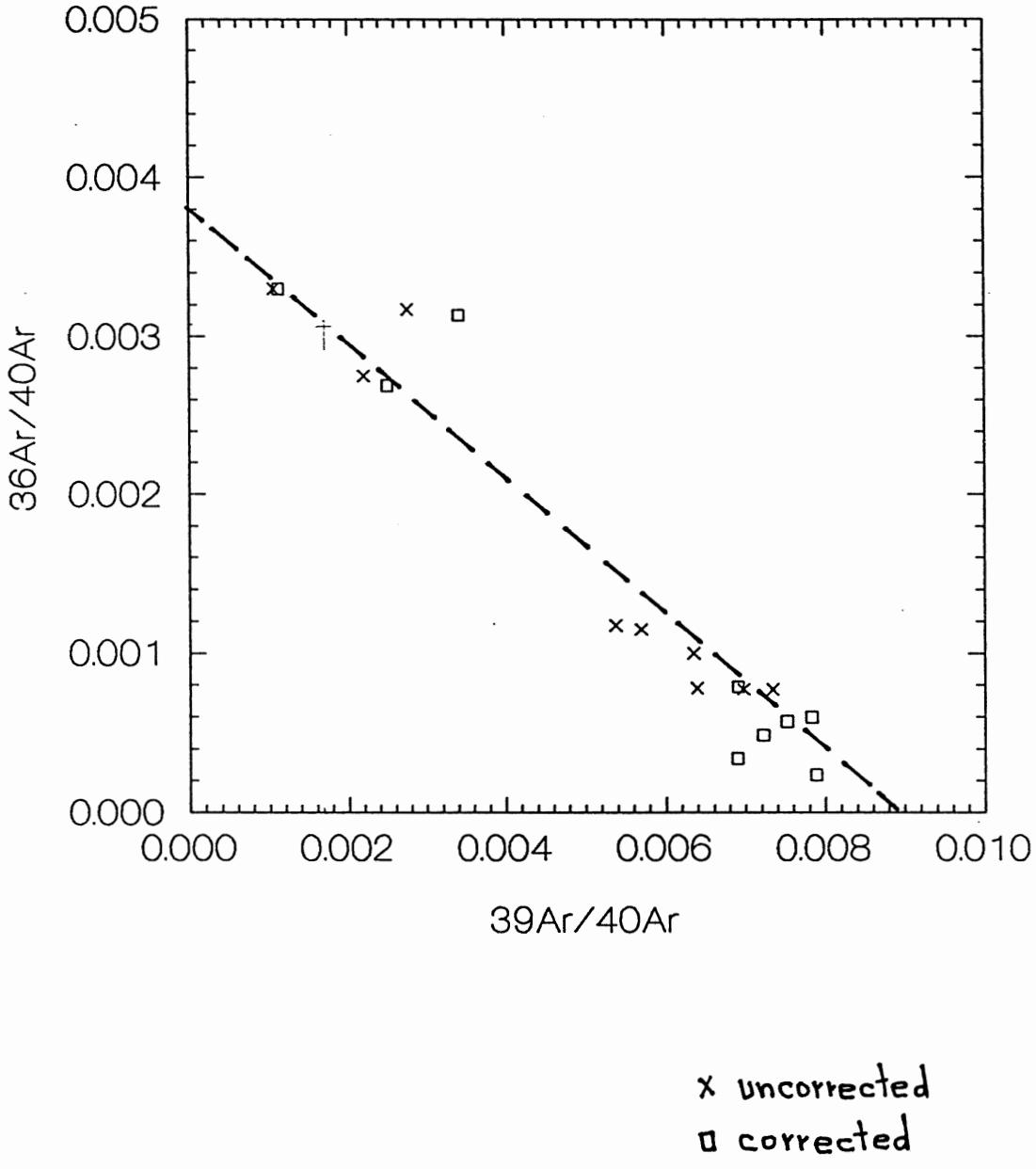

Figure 5.3 Inverse isochron plot for sample FJ87-146.

equipment. Analyses performed subsequent to these analyses suggest that the blank correction employed is an over-correction. Consequently, values midway between the corrected and uncorrected values are assumed in the following analysis. A least squares linear regression line, fitted using the method of York (1969), takes into account analytical error on both axes. When the X intercepts (the $^{39}Ar/^{40}Ar$ ratios) are substituted into the fundamental age equation, the following ages are obtained:

FJ87-136 = 380 +/- 14 Ma

FJ87-138 = 378 +/- 7 Ma

FJ87-146 = 394 +/- 20 Ma

The SUMS goodness of fit parameter (York 1969) indicates how well data fit a linear regression line. Simply stated, a SUMS value approximately equal to the number of data points indicates that the scatter of the data is to be expected from analytical error. SUMS values greater than this indicate that the scatter of the data is not the result of experimental error alone. SUMS values of 8.9 and 4.0, determined for samples FJ87-136 and FJ87-138 respectively, suggest that the scatter of data points is the result of analytical error, and that the ages determined using the X intercepts of the best fit lines are reliable. For sample FJ87-146, the SUMS value obtained for the goodness of fit of the linear regression line is 25.6, a value which indicates that more than experimental error is responsible for the scatter of the data points. As a result, the age aquired for sample FJ87-146 is

not considered reliably determined.

Because the 380 +/- 14 Ma, and 378 +/- 7 Ma ages are considered reliable, a best-estimate age of 380 +/- 10 Ma is assigned to the porphyritic andesite. The plagioclase porphyry dykes which intrude the andesite are younger, however, $^{40}Ar/^{39}Ar$ dating is required to place an exact age on these rocks.

CHAPTER 6: SUMMARY AND CONCLUSIONS

6.1 Summary

The Bourne Complex comprises three distinct groups of basic igneous rocks intruding fine-grained metasediments. Porphyritic andesite, as dykes and flows, is associated with plagioclase porphyry dykes and north-trending basic dykes. The plagioclase porphyry dykes and porphyritic andesite (dykes) exhibit an easterly trend, setting them apart from the north-trending dykes, which intrude the Carboniferous Nansen Formation. As the plagioclase porphyry dykes do not intrude the Nansen Formation, the field relationships suggest that they are of pre-Carboniferous age, but younger than the porphyritic andesite.

The porphyritic andesite contains fine-grained plagioclase, hornblende, and clinopyroxene phenocrysts set in a chloritized groundmass of microcrystalline, plagioclase microlites. Textural differences set it apart from the plagioclase porphyry dykes which contain abundant coarse plagioclase phenocrysts set in a groundmass of intergranular plagioclase, clinopyroxene, and hornblende. The presence of chlorite, actinolite, albite, epidote, and quartz, as secondary minerals, indicates greenschist facies metamorphism for both groups of rocks.

The demonstrated mobility of major elements precludes the use of alkali - silica classification schemes. The restricted mobility of selected incompatible trace elements allows the use of these elements for chemical classification and tectonomagmatic

discrimination purposes. Cluster analysis (Fig. 4.4), using 10 immobile trace element ratios, assembles the rocks into two distinct groups that support the field and petrographic classification.

The Zr/TiO_2-Nb/Y diagram (Fig. 4.5) designates the porphyritic andesite as andesitic basalts and andesites which approach dacite compositions. The plot characterizes the plagioclase porphyry dykes as subalkaline basalt transitional to alkali-basalt. The north-trending dykes classify as alkali basalt transitional to basanite-nephelinite.

The Ti-Y-Zr tectonomagmatic discrimination diagram (Fig. 4.6) characterizes the porphyritic andesite as being emplaced in a volcanic-arc tectonic setting, the plagioclase porphyry dykes as volcanic-arc basalts or MORB transitional to within-plate basalt, and the north-trending dykes as within-plate basalt.

Figure 4.7, a Hf-Ta-Th tectonomagmatic discrimination diagram, indicates that the porphyritic andesite was emplaced in a destructive plate-margin setting and has calcalkaline affinities. The plagioclase porphyry dykes plot as E-type MORB, and the north-trending dykes as within-plate basalt.

A final tectonomagmatic discriminator (Fig. 4.8) uses the discriminant functions calculated from the mean compositions of primary clinopyroxene phenocrysts to indicate that the porphyritic andesite is of volcanic arc or ocean-floor basalt affinity.

The porphyritic andesite samples, evaluated by $^{40}Ar/^{39}Ar$ dating of hornblende, yield a best estimate age of 380 ma.

6.2 Conclusions

Ziegler (1989) hypothesized that the Siberian Block was converging southward toward the northern margin of the North American Plate during the Middle to Late Paleozoic. Trettin and Balkwill (1979) suggested that the siliceous to intermediate volcanism, that dominated Northern Ellesmere Island during the Early and Middle Ordovician, reflects the existence of a south-dipping subduction zone beneath the northern margin of the North American Plate. Trettin (1989), Trettin and Balkwill (1979) proposed that the Ellesmerian Orogeny was probably caused by convergence of North America with another, unidentified, offshore plate. Trettin et al. (1987) presented a U-Pb (sphene) age of 390 +/- 10 ma for the Cape Woods pluton, which dates plutonism attributed to crustal thickening related to the accretion of Pearya and may represent the time of accretion of Pearya. These observations have important implications regarding the origin of the Bourne Complex.

The Bourne Complex crops out along the northwestern coast of Ellesmere Island. Argon isotope ages, from hornblende, obtained for the porphyritic andesite, date these rocks at circa 380 +/- 10 mya. These spatial and temporal positions suggest that the origin of the porphyritic andesite may be related to magmatism associated with crustal thickening that resulted from the transpressive accretion of Pearya at circa 390 Ma. The association of immature sediments with calcalkaline volcanics and hypabyssal intrusives suggests that the Bourne Complex represents

a fragment of an arc-related basin that originated during the final stages of the docking of the Pearya terrane.

On northern Axel Heiberg Island, dioritic/granodioritic intrusives yielded K/Ar dates for biotite of 367 +/- 25 Ma, and U-Pb zircon dates of 360 +/- 3 Ma (Trettin, 1989). These ages date the Ellesmerian Orogeny and related magmatism. The undated plagioclase porphyry dykes, which from field evidence post-date the Bourne Complex volcanics and pre-date the development of the Sverdrup Basin, show geochemical characteristics of E-type MORBs. These distinct dykes may represent back-arc basin magmatism subsequent to the docking of Pearya, but radiometric dating is needed to verify this speculation.

Finally, the North-trending dykes, which cut Sverdrup Basin lithologies, probably represent one of the Late Cretaceous phases of basin magmatism. The earlier Carboniferous, Permian and Early Cretaceous volcanics are all tholeiitic to mildly alkaline in character. However, the Late Cretaceous volcanics of northern Ellesmere Island are strongly alkaline. Again radiometric dating on these intrusives will be needed to confirm this suggestion.

APPENDIX A: Petrography

Fjelholmen Island:

FJ87-131: Porphyritic flow(?)

Fine-grained plagioclase, hornblende and actinolite phenocrysts, minor clinopyroxene and actinolite microphenocrysts, set in a microcrystalline groundmass of strongly sericitized plagioclase microlites, chlorite, sphene, and opaque oxides. Moderate to strong alteration.

20% moderately to strongly sericitized, subhedral plagioclase phenocrysts; 0.5 - 1.0 mm
20% pleochroic yellow - green, euhedral to subhedral hornblende; 0.2 - 1.0 mm
5% pleochroic pale green - green, subhedral actinolite after pyroxene; 0.2 - 0.7 mm
5% anhedral clinopyroxene microphenocrysts; 0.2 - 0.3 mm
25% sericitized plagioclase microlites
15% very fine-grained chlorite
5% very fine-grained sphene
5% hazy opaque oxides; < 0.1mm

FJ87-132: Porphyritic flow(?)

Fine- to medium-grained plagioclase phenocrysts, small blebs of chlorite, and fine- to medium-grained clinopyroxene phenocrysts set in a microcrystalline groundmass of strongly sericitized plagioclase microlites, chlorite, sphene, and hazy opaque oxides. Strong alteration.

30% moderately to strongly sericitized, subhedral plagioclase laths; 0.7 - 1.2 mm
20% blebs of very fine-grained chlorite; < 1mm
5% subhedral clinopyroxene, some altering to sphene; 0.4 - 1.0 mm
30% sericitized plagioclase microlites
10% very fine-grained granular sphene
5% blocky opaque oxides; 0.01-0.05mm

FJ87-133: Sparsely porphyritic dyke

Minor fine- to medium-grained clinopyroxene, fine-grained orthopyroxene, and plagioclase phenocrysts set in a groundmass of fine-grained, randomly oriented plagioclase laths, intergranular chlorite, clinopyroxene, and opaque oxides. Slight alteration.

1% subhedral, mildly sericitized plagioclase phenocrysts; 0.7 - 3.5 mm
1% subhedral clinopyroxene phenocrysts; 0.5 - 1.0 mm
1% euhedral orthopyroxene phenocrysts; 1.0 mm

45% euhedral to subhedral plagioclase microlites; 0.3 - 0.5 mm
20% intergranular chlorite
15% anhedral clinopyroxene microphenocrysts; 0.2 - 0.4 mm
15% subhedral, very fine-grained opaque oxides

FJ87-134: Porphyritic amygdaloidal flow

Fine- to medium-grained plagioclase and minor fine-grained clinopyroxene phenocrysts set in a groundmass of randomly oriented plagioclase microlites, intergranular chlorite, sphene, and clinopyroxene. Abundant ovoid amygdales filled with chlorite and calcite. Moderate alteration.

10% slightly sericitized, subhedral plagioclase glomerocrysts; 1.0 - 2.0 mm
5% anhedral clinopyroxene glomerocrysts; 0.5 - 1.0 mm
25% amygdales rimmed with very fine-grained sphene, lined with chlorite and filled with calcite; 1.5 - 2.0 mm
25% subhedral plagioclase microlites; 0.2 - 0.4 mm
20% intergranular chlorite blebs
10% very fine-grained sphene
5% intergranular anhedral clinopyroxene

FJ87-135: Porphyritic flow

Fine- to medium-grained plagioclase phenocrysts and minor fine-grained clinopyroxene microphenocrysts set in a groundmass of strongly sericitized plagioclase microlites, chlorite, sphene, and opaque oxides. Strong alteration.

30% subhedral, sericitized, plagioclase phenocrysts,; 0.5 - 2.0 mm
5% anhedral to subhedral clinopyroxene microphenocrysts; 0.1 - 0.5 mm
40% sericitized plagioclase microlites
10% intergranular chlorite
10% hazy opaque oxides
5% very fine-grained sphene

FJ87-136: Porphyritic dyke(?)

Fine- to medium-grained plagioclase phenocrysts, abundant fine-grained hornblende, and minor fine-grained actinolite phenocrysts set in a microcrystalline groundmass of sericitized plagioclase, sphene, and opaque oxides. Sample shows a distinct banded coarsening of phenocrysts. Slight alteration.

30% subhedral to euhedral plagioclase phenocrysts; 0.2 - 3.0 mm
25% euhedral hornblende phenocrysts, pleochroic yellow-green; 0.1 - 1.0 mm
10% hazy, equant, opaque oxides; 0.1 - 0.3 mm
5% subhedral, pleochroic green actinolite; 0.1 - 0.7 mm

25% microcrystalline, sericitized plagioclase
5% very fine-grained sphene

FJ87-137: Porphyritic flow(?)

Fine- to medium-grained slightly sericitized plagioclase phenocrysts and fine-grained clinopyroxene, hornblende, and actinolite phenocrysts set in a microcrystalline groundmass of sericitized plagioclase, chlorite, and opaque oxides. Slight alteration.

25% subhedral plagioclase phenocrysts; 0.5 - 2.0 mm
10% subhedral to euhedral, pleochroic yellow - green hornblende phenocrysts; 0.2 - 1.0 mm
5% subhedral, pleochroic green actinolite phenocrysts
10% anhedral to subhedral clinopyroxene phenocrysts; 0.2 - 1.0 mm
20% anhedral, very fine-grained plagioclase
10% very fine-grained sphene
10% hazy, fine-grained and dusty opaque oxides
10% patchy chlorite

FJ87-138: Porphyritic flow(?)

Fine- to medium-grained plagioclase, fine-grained hornblende and actinolite phenocrysts set in a microcrystalline groundmass of sericitized plagioclase, chlorite, sphene and opaque oxides. Slight alteration.

30% subhedral to euhedral plagioclase phenocrysts; 0.5 - 2.0 mm
10% subhedral to euhedral, pleochroic yellow - green hornblende phenocrysts; 0.2 - 1.5 mm
5% subhedral to euhedral, pleochroic green actinolite phenocrysts; 0.2 - 1.5 mm
5% anhedral quartz; 0.2 - 0.4
1% anhedral to subhedral clinopyroxene phenocrysts; 0.2 mm
20% patchy chlorite
20% anhedral, very fine-grained plagioclase
5% hazy, fine-grained opaque oxides
5% very fine-grained sphene

FJ87-139: Diabase dyke

Coarse-grained plagioclase forms an intergranular texture with medium-grained clinopyroxene, quartz, and opaque oxides. Moderate to strong alteration.

40% strongly sericitized, lath-shaped plagioclase; 2.0 - 5.0 mm
20% subhedral clinopyroxene, often corroded, altering to actinolite; 1.0 - 2.0 mm
10% subhedral, blocky, opaque oxides; 0.5 - 1.0 mm
15% irregular blebs of intergranular chlorite
10% anhedral, intergranular quartz

5% very fine-grained sphene

FJ87-140: Sparsely porphyritic dyke

Sparse medium-grained sericitized plagioclase phenocrysts set in an intergranular groundmass of fine-grained laths of plagioclase, chlorite, fine-grained orthopyroxene, and fine-grained clinopyroxene. Sparsely amygdaloidal. Slight alteration.

1% blocky, subhedral moderately sericitized plagioclase phenocrysts; 1.0 - 2.0 mm
5% chlorite-lined, calcite-filled ovoid amygdales; 2.0 mm
40% subhedral plagioclase laths; 0.3 - 1.0 mm
20% intergranular chlorite
10% subhedral clinopyroxene phenocrysts; 0.2 - 0.5 mm
10% subhedral orthopyroxene phenocrysts; 0.2 - 0.4 mm
10% blocky, subhedral, hazy, opaque oxides; 0.01 - 0.2 mm
5% very fine-grained sphene

FJ87-141: Porphyritic amygdaloidal flow

Fine- to medium-grained plagioclase phenocrysts and small calcite-filled amygdales set in a microcrystalline groundmass of plagioclase microlites, sphene, and chlorite. Moderate alteration.

30% subhedral to euhedral, slightly sericitized plagioclase; 0.5 - 2.0 mm
5% chlorite-lined, calcite-filled amygdales; 2.0 mm
10% chlorite as discrete patches; 0.5 - 1.0 mm
20% anhedral to subhedral sericitized plagioclase microlites
25% very fine-grained chlorite
10% very fine-grained sphene

FJ87-144: Porphyritic to glomeroporphyritic flow(?)

Fine- to medium-grained, zoned, plagioclase phenocrysts, fine-grained clinopyroxene and actinolite phenocrysts set in a groundmass of plagioclase microlites, very fine-grained sphene, opaque oxides, and chlorite. Moderate alteration.

45% zoned, subhedral to euhedral plagioclase phenocrysts. Cores, or rings within the grain, strongly sericitized. Phenocrysts weakly aligned; 0.5 - 1.0 mm
5% variably sized subhedral to euhedral clinopyroxene phenocrysts, many with cores altering to actinolite; 0.2 - 1.0 mm
5% subhedral actinolite phenocrysts after pyroxenes; 0.2 - 0.8 mm
10% chlorite, as irregular blebs and replacing clinopyroxene
20% anhedral to subhedral plagioclase microlites
5% very fine-grained sphene
10% very fine-grained opaque oxides

FJ87-145: Diabase dyke

Fine- to medium-grained strongly sericitized plagioclase laths form an intergranular texture with fine-grained clinopyroxene, orthopyroxene, fine-grained actinolite after pyroxenes, and fine-grained blocky opaque oxides. Secondary quartz forms intergrowth textures around plagioclase. Moderate to strong alteration.

30% strongly sericitized plagioclase laths; 0.5 - 1.0 mm
15% subhedral intergranular clinopyroxene; 0.2 - 0.8 mm
10% anhedral intergranular orthopyroxene; 0.4 - 0.6 mm
15% intergranular, actinolite after pyroxenes; 0.2 - 0.4 mm
15% subhedral, equant opaque oxides; 0.1 - 0.3 mm
10% secondary quartz in symplectite intergrowth with plagioclase
5% very fine-grained sphene

FJ87-146: Porphyritic flow

Fine- to medium-grained plagioclase, fine-grained hornblende and actinolite phenocrysts set in a microcrystalline groundmass of sericitized plagioclase, sphene, chlorite, and opaque oxides. Slight alteration.

25% slightly sericitized, subhedral plagioclase phenocrysts; 0.5 - 2.0 mm
10% subhedral to euhedral, pleochroic yellow - green hornblende phenocrysts; 0.2 - 1.5 mm
10% subhedral clinopyroxene phenocrysts; 0.2 - 0.7 mm
5% subhedral to euhedral, pleochroic green actinolite phenocrysts; 0.2 - 1.0 mm
1% euhedral apatite; 0.1 mm
30% very fine-grained sericitized plagioclase
5% fine-grained opaque oxides
5% chlorite
10% very fine-grained sphene

FJ87-148: Sparsely porphyritic dyke

Relict olivine phenocrysts and minor glomeroporphyritic clusters of clinopyroxene, orthopyroxene, and plagioclase set in a very fine-grained matrix of sericitized plagioclase microlites, fine-grained clinopyroxene, very fine-grained sphene, and opaque oxides. Minor calcite-filled amygdales and veinlets. Slight alteration.

3% subhedral relict olivine phenocrysts; 2.0 mm
3% subhedral, sericitized plagioclase phenocrysts and glomerocrysts; 0.5 - 2.0 mm
3% subhedral, clinopyroxene glomerocrysts; 0.5 - 1.0 mm
3% anhedral, orthopyroxene phenocrysts; 0.5 mm
3% calcite-filled amygdales; 0.5 mm
40% sericitized plagioclase microlites
20% very fine-grained sphene

15% very fine-grained opaque oxides
10% anhedral, fine-grained clinopyroxene

FJ87-150: Intergranular dyke

Microphenocrysts of hornblende and clinopyroxene form an intergranular texture with sericitized plagioclase microlites and opaque oxides. Small chlorite-calcite filled amygdales. Moderately altered.

10% slightly ovoid, chlorite-calcite filled amygdales; 0.5 - 0.8 mm
50% sericitized, lath shaped, plagioclase microlites; 0.2 mm
10% subhedral hornblende microphenocrysts; 0.1 mm
10% subhedral clinopyroxene microphenocrysts; 0.1 mm
10% blocky, subhedral to euhedral opaque oxides; 0.05 - 0.1 mm
10% very fine-grained sphene

FJ87-151: Porphyritic dyke

Medium-grained phenocrysts of olivine, clinopyroxene, and relict olivine set in a groundmass of very fine-grained clinopyroxene, hornblende, opaque oxides, and sericitized plagioclase. Calcite as microcrystalline groundmass and veins with chlorite. Amygdaloidal. Moderate alteration.

5% subhedral relict olivine phenocrysts altered to chlorite and opaque oxides; 1.0 - 1.5 mm
5% glomeroporphyritic, subhedral clinopyroxene phenocrysts; 1.0 mm
10% calcitic and chloritic amygdales; < 2.0 mm
30% sericitized plagioclase microlites
20% pleochroic brown subhedral hornblende; 0.1 mm
10% granular anhedral to subhedral clinopyroxene; 0.1 mm
5% blocky, subhedral opaque oxides; 0.1 mm
5% very fine-grained sphene

Appendix A: Petrography

Krueger Island:

KR89-003: Diabase dyke

Fine- to medium-grained sericitized plagioclase laths form a subhedral granular texture with fine- to medium-grained actinolite and rare fine-grained hornblende. Moderate to strong alteration.

50% strongly sericitized, subhedral plagioclase laths; 0.5 - 2.0 mm
20% subhedral actinolite after clinopyroxene; 0.2 - 1.5 mm
1% subhedral hornblende; 1.0 mm
10% secondary, anhedral quartz, as discrete patches; 0.5 mm
10% blocky opaque oxides as discrete grains and clusters; 0.2 - 0.3 mm
10% chlorite associated with actinolite

KR89-006: Intergranular dyke

Fine- to medium-grained plagioclase laths with abundant intergranular fine-grained biotite, hornblende, and minor clinopyroxene. Moderate alteration.

30% moderately to strongly sericitized, randomly oriented, subhedral, plagioclase laths; 0.5 - 2.0 mm
30% pleochroic, brown, subhedral hornblende; 0.5 - 1.0 mm
20% pleochroic green and yellow - brown, colour-zoned anhedral biotite; 0.5 - 1.0 mm
5% fine-grained clinopyroxene; 0.5 mm
10% subhedral, very fine-grained intergranular clinopyroxene; .02 mm
5% blocky, subhedral equant opaque oxides; 0.1 mm

KR89-008: Sparsely porphyritic dyke

Fine-grained olivine glomerocrysts set in an amygdaloidal groundmass of plagioclase microlites and intergranular clinopyroxene and calcite. Moderate alteration.

10% subhedral to euhedral, olivine glomerocrysts; < 1.0 mm
10% spherical, calcite filled amygdales; 1.0 mm
40% moderately sericitized plagioclase microlites; 0.2 - 0.5 mm
10% intergranular, anhedral to subhedral clinopyroxene; 0.2 - 0.4 mm
10% intergranular anhedral calcite; 0.3 mm
15% opaque oxides, rimming olivine and as larger, discrete grains
5% very fine-grained epidote

KR89-009: Aphyric dyke(?)

Randomly oriented plagioclase microlites with very fine-grained intergranular clinopyroxene and orthopyroxene. Slight alteration.

70% slightly sericitized plagioclase microlites; 0.2 - 0.5 mm
10% intergranular, subhedral orthopyroxene; 0.05 - 0.2 mm
10% intergranular, subhedral clinopyroxene; 0.05 - 0.2 mm
10% overprinting, blocky, subhedral opaque oxides; 0.1 - 0.2 mm

KR89-011: Porphyritic dyke

Medium-grained plagioclase phenocrysts set in a groundmass of fine-grained plagioclase laths, intergranular actinolite, epidote, hornblende, and chlorite. Slight alteration.

15% subhedral, slightly rounded, slightly sericitized plagioclase phenocrysts; 1.0 - 6.0 mm
40% randomly oriented, slightly sericitized plagioclase laths; 0.5 - 1.0 mm
20% subhedral, pleochroic green - blue-green actinolite; 1.0 mm
10% anhedral epidote; 0.3 - 1.0 mm
5% chlorite 0.2 - 0.4 mm
5% pleochroic green to blue-green hornblende; 0.3 - 1.0 mm
5% blocky, equant opaque oxides

KR89-013: Porphyritic dyke

Medium-grained plagioclase phenocrysts and one medium-grained euhedral clinopyroxene phenocryst set in a groundmass of fine-grained plagioclase laths, intergranular actinolite after clinopyroxene and orthopyroxene, hornblende, and epidote. Slight alteration.

1% euhedral clinopyroxene phenocryst; 3.5 mm
10% subhedral, slightly rounded, plagioclase phenocrysts; 1.0 - 6.0 mm
40% randomly oriented, slightly sericitized plagioclase laths; 0.5 - 1.0 mm
30% pleochroic green to blue-green actinolite ; 0.3 - 1.0 mm
10% blocky,equant, opaque oxides
5% intergranular subhedral epidote; 0.2 - 0.4 mm
5% subhedral, pleochroic yellow - green hornblende; 0.3 - 0.6 mm

KR89-020: Porphyritic dyke

Medium-grained plagioclase phenocrysts set in a groundmass of fine-grained plagioclase laths, intergranular clinopyroxene, actinolite, and hornblende. Slight alteration.

10% subhedral, slightly rounded, plagioclase phenocrysts; 1.0 - 6.0 mm

50% randomly oriented, slightly sericitized plagioclase laths; 0.5 - 1.0 mm
20% pleochroic green to blue-green actinolite replacing pyroxene; 0.3 - 1.0 mm
10% subhedral fine-grained clinopyroxene; 0.5 mm
5% blocky, equant, opaque oxides
5% pleochroic yellow - brown subhedral hornblende

KR89-023: Sparsely phyric dyke

Sparse medium-grained plagioclase phenocrysts set in a groundmass of fine-grained, randomly oriented plagioclase laths, intergranular actinolite, clinopyroxene, chlorite, and epidote. Slight alteration.

1% anhedral, rounded, plagioclase glomerocrysts; 2.0 mm
45% randomly oriented, slightly sericitized, plagioclase laths; 0.5 - 1.0 mm
30% subhedral pleochroic green - blue-green actinolite; 0.3 - 0.7 mm
5% patchy, anhedral - subhedral epidote; 0.5 mm
10% subhedral clinopyroxene; 0.3 mm
5% blocky, equant opaque oxides; 0.1 - 0.2 mm
5% chlorite

KR89-024: Porphyritic dyke

Abundant medium to coarse-grained plagioclase phenocrysts and fine- to medium-grained clinopyroxene phenocrysts are set in a groundmass of fine-grained plagioclase laths, clinopyroxene, actinolite, hornblende, intergranular chlorite, and opaque oxides. Slight alteration.

20% subhedral, plagioclase phenocrysts; 1.0 - 6.0 mm
10% anhedral, clinopyroxene phenocrysts; 0.5 - 2.0 mm
40% randomly oriented, subhedral, plagioclase laths; 0.5 - 1.0 mm
10% intergranular, anhedral, clinopyroxene; 0.2 - 0.5 mm
5% intergranular chlorite
5% intergranular actinolite
5% blocky,subhedral, opaque oxides; 0.2 mm
2% calcite as irregular blebs
3% subhedral, pleochroic yellow - brown hornblende; 0.1 mm

KR89-027: Porphyritic dyke

Medium- to coarse-grained plagioclase phenocrysts set in a groundmass of randomly oriented, fine-grained plagioclase laths, fine-grained clinopyroxene and orthopyroxene, intergranular calcite and chlorite, and opaque oxides. Slight alteration.

10% subhedral, sericitized plagioclase phenocrysts; 1.0 - 6.0 mm
40% randomly oriented, subhedral, plagioclase laths; 0.5 - 1.0 mm

15% intergranular, anhedral, clinopyroxene; 0.2 - 0.5 mm
5% intergranular, subhedral orthopyroxene; 0.3 - 0.5 mm
10% intergranular chlorite
10% calcite as irregular intergranular blebs
5% blocky,subhedral, opaque oxides; 0.2 mm
5% intergranular actinolite associated with chlorite and calcite
Tr. very fine-grained subhedral hornblende

KR89-030: Aphyric metavolcanic

Very fine-grained strongly sericitized plagioclase microlites with abundant opaque oxides, minor actinolite, traces of intergranular quartz, and chlorite - sericite blebs. Intense alteration.

40% strongly sericitized plagioclase microlites; 0.1 mm
20% opaque oxides, as granular rims or filling veinlets; 0.05 mm
10% chlorite - sericite blebs; 0.3 mm
2-3% intergranular, anhedral quartz; 0.01 mm
2-3% anhedral actinolite
10% chlorite as discrete patches and disseminated
10% calcite as intergranular microcrystalline groundmass

KR89-031: Porphyritic metavolcanic

Medium-grained, strongly sericitized, subhedral plagioclase phenocrysts and fine- to medium-grained clinopyroxene phenocrysts set in a groundmass of strongly sericitized plagioclase microlites, very fine-grained quartz, chlorite, and opaque oxides. Strong alteration.

15% strongly sericitized plagioclase phenocrysts; 0.5 - 2.5 mm
5% subhedral to euhedral clinopyroxene phenocrysts; 0.2 - 2.0 mm
5% subhedral to euhedral orthopyroxene phenocrysts; 0.2 - 0.6 mm
40% sericitized plagioclase microlites
10% anhedral disseminated quartz; 0.05 mm
15% granular opaque oxides
10% spherical clusters of granular chlorite; 0.5 mm

KR89-032: Glomeroporphyritic metavolcanic

Fine- to medium-grained moderately sericitized plagioclase set in a groundmass of sericitized plagioclase microlites, chlorite, and opaque oxides. Minor calcitic amygdales and veinlets. Moderate alteration.

20% subhedral sericitized plagioclase glomerocrysts; 0.5 - 3.0 mm
50% sericitized plagioclase microlites
15% calcite in veinlets and vesicles
10% chlorite rimming vesicles and as discrete patches
5% finely disseminated opaque oxides

KR89-034: Sparsely porphyritic dyke

Fine- to medium-grained plagioclase and minor clinopyroxene phenocrysts set in a groundmass of plagioclase microlites, fine-grained clinopyroxene, intergranular calcite and chlorite, and opaque oxides. Minor calcite filled vesicles. Very slight alteration.

5% subhedral plagioclase phenocrysts; 0.5 - 1.5 mm
<1% anhedral clinopyroxene phenocrysts; 2.0 mm
5% slightly ovoid calcite - chlorite filled vesicles; 1.2 mm
40% randomly oriented plagioclase microlites
25% intergranular subhedral clinopyroxene microphenocrysts; 0.4 mm
10% very fine-grained intergranular chlorite
10% fine-grained opaque oxides associated with chlorite; 0.1 - 0.6 mm
5% very fine-grained pleochroic green - brown hornblende; 0.1 mm

KR89-035: Porphyritic metavolcanic

Medium-grained intensely sericitized plagioclase phenocrysts set in a groundmass of strongly sericitized plagioclase microlites, strongly altered fine-grained clinopyroxene and orthopyroxene, and opaque oxides. Veinlet filled with epidote. Strong alteration.

30% sericitized plagioclase phenocrysts; 1.0 - 3.0 mm
20% sericitized plagioclase microlites
40% very fine granular to fine-grained pleochroic green - blue-green actinolite, after clinopyroxene and orthopyroxene; 0.2 - 0.9 mm
5% opaque oxides; 0.1 - 0.4 mm
5% fine granular epidote filling veinlet; 0.05 - 0.1 mm

KR89-036: Aphyric metavolcanic

Fine- to medium-grained intensely sericitized plagioclase phenocrysts set in a groundmass of strongly sericitized plagioclase microlites, fine-grained clinopyroxene and orthopyroxene altering to actinolite, and opaque oxides. Strong alteration.

10% fine-grained sericitized plagioclase phenocrysts; 0.5 - 1.0 mm
40% sericitized plagioclase microlites
15% fine-grained subhedral intergranular clinopyroxene; 0.1 - 0.5 mm
15% fine-grained subhedral intergranular orthopyroxene; 0.2 - 0.3 mm
10% fine-grained pleochroic green - blue-green actinolite, after clinopyroxene and orthopyroxene; 0.2 - 0.5 mm
10% elongate opaque oxides; 0.1 - 0.3 mm

KR89-037: Sparsely porphyritic metavolcanic

Fine- to medium-grained intensely sericitized plagioclase phenocrysts set in a groundmass of strongly sericitized plagioclase microlites, strongly altered fine-grained clinopyroxene and orthopyroxene, fine-grained epidote, and opaque oxides. Strong

alteration.

5% fine-grained sericitized plagioclase phenocrysts; 0.5 - 1.0 mm
30% sericitized plagioclase microlites
20% fine-grained pleochroic green - blue-green actinolite, after clinopyroxene and orthopyroxene; 0.2 - 0.5 mm
10% fine to medium-grained clinopyroxene; 0.5 - 1.0 mm
10% fine to medium-grained orthopyroxene; 0.3 - 0.6 mm
10% elongate opaque oxides; 0.1 - 0.3 mm
5% fine- to medium grained epidote; 0.5 - 1.0 mm
5% fine granular epidote in veins
5% calcite as discrete blebs or filling veins

KR89-038: Porphyritic metavolcanic

Fine- to medium-grained sericitized plagioclase phenocrysts, relatively pristine plagioclase phenocrysts, and actinolite phenocrysts set in a groundmass of strongly sericitized plagioclase microlites and opaque oxides. Very thin epidote filled veinlet. Strong alteration.

10% fine-grained sericitized plagioclase phenocrysts; 0.5 - 1.0 mm
15% fine- to medium-grained relatively pristine plagioclase phenocrysts 5% with oscillatory zoning; 0.5 - 3.0 mm
15% fine-grained actinolite phenocrysts after pyroxene; 0.4 - 0.9 mm
1% pleochroic yellow - brown hornblende; 1.0 mm
45% sericitized plagioclase microlites
5% very fine-grained opaque oxides
4% very fine granular epidote filling veinlet
5% anhedral intergranular quartz; 0.1 mm

KR89-039: Aphyric diabase dyke

Fine-grained slightly sericitized plagioclase laths form an intergranular texture with fine-grained clinopyroxene, actinolite, intergranular chlorite, minor very fine-grained hornblende, and minor fine granular epidote. Slight alteration.

40% slightly sericitized plagioclase laths; 0.1 - 0.9 mm
20% subhedral clinopyroxene microphenocrysts; 0.1 - 0.7 mm
10% subhedral actinolite after pyroxenes; 0.3 - 0.5 mm
10% intergranular chlorite as discrete blebs; 0.2 mm
10% fine-grained blocky opaque oxides; 0.1 - 0.3 mm
5% very fine-grained pleochroic yellow - brown hornblende; 0.1 mm
5% very fine granular vein-filling epidote

APPENDIX B: Mineral Data

Table B1 - Mean Clinopyroxene Analyses
Major Element Oxides (wt %)

	FJ87-131 (2)	FJ87-132 (22)	FJ87-133 (22)	FJ87-135 (10)	FJ87-137 (17)
SiO_2	51.940	51.048	50.701	52.014	52.612
TiO_2	0.365	0.500	1.222	0.300	0.226
Al_2O_3	3.140	2.031	2.644	1.475	2.196
Cr_2O_3	0.145	0.016	0.026	0.006	0.206
FeO	6.385	10.755	11.299	12.011	6.554
MnO	0.160	0.308	0.283	0.355	0.177
MgO	17.300	14.151	13.355	12.819	16.529
CaO	20.585	20.501	19.881	20.963	21.551
Na_2O	0.170	0.240	0.338	0.253	0.202
Total	100.200	99.554	99.750	100.205	100.260

Table B1 Continued

	FJ87-139 (7)	FJ87-144 (8)
SiO_2	50.863	51.159
TiO_2	0.734	0.540
Al_2O_3	1.847	1.988
Cr_2O_3	0.016	0.034
FeO	13.500	11.821
MnO	0.290	0.324
MgO	12.089	13.671
CaO	19.727	19.486
Na_2O	0.226	0.309
Total	99.291	99.334

APPENDIX B: MINERAL DATA

Table B2 - Mean Amphibole Analyses
Major Element Oxides (wt %)

	FJ87-131 (8)	FJ87-136 (8)	FJ87-137 (7)	FJ87-138 (6)	FJ87-146 (17)
SiO_2	43.686	45.610	44.620	45.577	46.066
TiO_2	1.859	1.558	1.957	1.425	1.281
Al_2O_3	9.976	9.969	9.803	9.028	8.479
Cr_2O_3	0.003	0.021	0.014	0.027	0.038
FeO	15.378	16.548	15.673	16.242	14.907
MnO	0.216	0.268	0.233	0.260	0.257
MgO	12.565	11.643	11.960	12.070	12.951
CaO	11.080	10.310	11.087	10.770	10.757
Na_2O	1.706	1.521	1.756	1.510	1.393
K_2O	0.219	0.108	0.223	0.078	0.088
Total	96.688	97.555	97.330	96.987	96.217

Table B2 Continued

	KR89-006 (6)
SiO_2	40.145
TiO_2	3.423
Al_2O_3	13.337
Cr_2O_3	0.027
FeO	12.628
MnO	0.162
MgO	11.852
CaO	11.952
Na_2O	2.728
K_2O	1.122
Total	97.375

Appendix C: Whole Rock Geochemistry

Table C1 - Major and Minor Element Oxides and Loss on Ignition (wt %), XRF and INAA Trace Elements (ppm)

	FJ87-131	FJ87-132	FJ87-133	FJ87-134	FJ87-135
SiO2	58.220	53.860	52.030	48.140	62.430
Al2O3	15.420	17.150	14.330	14.780	15.470
Fe2O3	7.150	8.000	11.750	8.650	6.010
MgO	4.840	4.210	4.750	6.000	3.170
CaO	4.440	6.810	5.510	9.480	2.520
Na2O	5.600	4.690	3.660	5.490	7.110
K2O	0.800	0.870	1.330	0.180	0.310
TiO2	0.570	0.870	2.140	1.240	0.840
MnO	0.140	0.130	0.180	0.210	0.120
P2O5	0.100	0.140	0.400	0.150	0.190
LOI	2.700	3.600	3.500	6.500	1.900
Total	99.980	100.330	99.580	100.820	100.070
Ba	113.000	149.000	300.000	48.000	24.000
Rb	18.000	14.600	25.000	6.600	7.800
Sr	156.500	284.400	148.000	194.100	67.400
Y	15.400	20.100	43.000	21.300	22.400
Zr	71.800	94.100	285.000	115.000	167.000
Nb	2.900	2.000	11.000	0.700	5.000
Pb	.	.	.	.	.
Ga	13.000	16.000	25.000	11.000	16.000
Zn	73.000	85.000	117.000	73.000	69.000
Cu	15.000	10.000	32.000	46.000	19.000
Ni	15.000	14.000	5.000	70.000	12.000
TiO2	0.600	0.910	1.940	1.250	0.740
V	184.000	217.000	244.000	210.000	132.000
Cr	116.000	56.000	17.000	166.000	49.000
La	-	-	-	-	12.040
Ce	-	-	-	-	30.450
Nd	-	-	-	-	13.500
Sm	-	-	-	-	3.770
Eu	-	-	-	-	1.180
Tb	-	-	-	-	0.790
Yb	-	-	-	-	3.090
Lu	-	-	-	-	0.440
Cs	-	-	-	-	29.430
Hf	-	-	-	-	3.950
Ta	-	-	-	-	0.710
Th	-	-	-	-	3.770
U	-	-	-	-	1.880
Sc	-	-	-	-	17.380
Co	-	-	-	-	21.940

Table C1 Continued

	FJ87-136	FJ87-137	FJ87-138	FJ87-139	FJ87-140
SiO2	57.910	58.500	57.990	47.640	50.980
Al2O3	16.450	14.910	16.430	12.170	14.860
Fe2O3	7.370	7.230	7.370	14.830	11.510
MgO	3.540	5.030	4.250	5.810	4.310
CaO	4.010	5.210	3.060	8.960	6.170
Na2O	6.890	4.700	6.990	2.880	5.140
K2O	0.210	0.810	0.120	0.580	1.090
TiO2	0.740	0.560	0.590	2.840	2.390
MnO	0.130	0.140	0.130	0.210	0.180
P2O5	0.190	0.110	0.110	0.290	0.370
LOI	2.100	2.900	2.200	3.100	2.600
Total	99.540	100.100	99.240	99.310	99.600
Ba	32.000	131.000	20.000	47.000	214.000
Rb	4.000	19.000	5.500	14.000	17.000
Sr	156.200	151.500	79.800	151.000	281.000
Y	16.900	14.900	14.400	34.000	38.000
Zr	100.000	70.800	84.600	161.000	260.000
Nb	4.900	2.900	2.000	9.000	11.000
Pb	.	.	.	.	.
Ga	18.000	15.000	18.000	24.000	21.000
Zn	69.000	75.000	79.000	96.000	99.000
Cu	14.000	10.000	13.000	273.000	25.000
Ni	6.000	18.000	9.000	57.000	10.000
TiO2	0.700	0.590	0.510	2.520	2.270
V	208.000	176.000	159.000	412.000	274.000
Cr	31.000	112.000	51.000	67.000	19.000
La	13.880	-	9.790	-	-
Ce	31.000	-	21.810	-	-
Nd	12.460	-	7.170	-	-
Sm	3.120	-	2.220	-	-
Eu	0.950	-	0.730	-	-
Tb	0.580	-	0.470	-	-
Yb	2.190	-	1.820	-	-
Lu	0.340	-	0.260	-	-
Cs	29.960	-	21.080	-	-
Hf	2.370	-	2.140	-	-
Ta	0.490	-	0.380	-	-
Th	4.470	-	4.010	-	-
U	1.970	-	2.090	-	-
Sc	21.530	-	19.960	-	-
Co	44.230	-	27.380	-	-

Table C1 Continued

	FJ87-141	FJ87-144	FJ87-145	FJ87-146	FJ87-146 (dup)
SiO2	52.650	53.500	50.120	60.580	60.520
Al2O3	17.540	16.300	12.810	16.050	15.950
Fe2O3	7.870	8.730	14.000	5.950	5.960
MgO	2.800	5.280	4.750	3.920	4.270
CaO	6.850	3.700	7.960	2.860	2.880
Na2O	6.270	6.640	2.820	7.130	7.130
K2O	0.160	0.390	1.300	0.420	0.410
TiO2	1.540	1.170	3.280	0.610	0.610
MnO	0.120	0.140	0.210	0.100	0.100
P2O5	0.250	0.190	0.330	0.140	0.150
LOI	3.500	3.600	1.400	1.500	1.600
Total	99.550	99.640	98.980	99.260	99.580
Ba	31.000	50.000	317.000	65.000	60.000
Rb	6.300	12.300	47.000	8.100	6.800
Sr	50.200	122.800	290.000	113.600	112.400
Y	26.300	26.200	39.000	14.300	14.800
Zr	156.900	154.200	254.000	102.800	102.900
Nb	3.400	4.500	26.000	4.900	4.800
Pb	.	.	.	.	.
Ga	22.000	20.000	24.000	17.000	17.000
Zn	83.000	94.000	176.000	63.000	61.000
Cu	72.000	40.000	63.000	12.000	11.000
Ni	10.000	20.000	33.000	17.000	19.000
TiO2	1.430	1.190	3.000	0.580	0.590
V	226.000	210.000	446.000	137.000	147.000
Cr	20.000	54.000	26.000	97.000	95.000
La	-	-	-	14.010	-
Ce	-	-	-	30.290	-
Nd	-	-	-	10.480	-
Sm	-	-	-	2.640	-
Eu	-	-	-	0.760	-
Tb	-	-	-	0.390	-
Yb	-	-	-	1.740	-
Lu	-	-	-	0.240	-
Cs	-	-	-	29.270	-
Hf	-	-	-	2.480	-
Ta	-	-	-	0.450	-
Th	-	-	-	5.680	-
U	-	-	-	2.480	-
Sc	-	-	-	18.140	-
Co	-	-	-	26.050	-

Table C1 Continued

	FJ87-148	FJ87-150	FJ87-151	KR89-003	KR89-006
SiO2	46.310	43.450	44.120	55.500	45.540
Al2O3	13.320	14.620	15.370	16.630	15.200
Fe2O3	12.520	9.170	10.000	8.040	10.560
MgO	4.620	8.080	6.920	4.620	8.690
CaO	9.530	12.780	11.040	5.770	8.620
Na2O	2.570	1.710	3.360	4.490	3.340
K2O	1.170	1.770	1.730	1.030	2.260
TiO2	3.570	1.700	2.240	1.090	1.600
MnO	0.140	0.120	0.170	0.180	0.170
P2O5	0.500	0.340	0.810	0.120	0.400
LOI	5.300	6.100	3.800	1.600	2.800
Total	99.550	99.840	99.560	99.070	99.180
Ba	423.000	570.000	1328.000	209.000	1034.000
Rb	29.000	66.000	47.000	25.000	79.000
Sr	561.000	419.000	927.000	345.000	511.000
Y	27.000	19.000	20.000	19.000	23.000
Zr	230.000	101.000	170.000	109.000	129.000
Nb	53.000	46.000	83.000	1.900	64.000
Pb	.	.	.	.	.
Ga	23.000	16.000	16.000	21.000	15.000
Zn	101.000	97.000	78.000	59.000	73.000
Cu	28.000	83.000	53.000	22.000	50.000
Ni	34.000	123.000	69.000	50.000	166.000
TiO2	3.410	1.630	2.100	0.980	1.520
V	332.000	236.000	239.000	199.000	180.000
Cr	32.000	212.000	122.000	132.000	180.000
La	-	-	51.310	-	32.740
Ce	-	-	106.890	-	64.140
Nd	-	-	41.990	-	26.650
Sm	-	-	8.030	-	5.000
Eu	-	-	2.640	-	1.650
Tb	-	-	0.910	-	0.840
Yb	-	-	2.130	-	2.450
Lu	-	-	0.290	-	0.340
Cs	-	-	103.300	-	62.000
Hf	-	-	3.300	-	2.830
Ta	-	-	4.310	-	3.810
Th	-	-	5.010	-	3.870
U	-	-	0.900	-	0.930
Sc	-	-	23.170	-	25.080
Co	-	-	43.050	-	51.960

Table C1 Continued

	KR89-008	KR89-009	KR89-011	KR89-013	KR89-020
SiO2	46.850	48.060	47.820	48.220	48.560
Al2O3	14.170	15.170	16.080	16.840	15.730
Fe2O3	10.790	10.880	11.210	10.020	11.610
MgO	9.240	5.860	5.780	6.010	4.800
CaO	9.100	10.440	9.750	11.670	9.950
Na2O	3.100	3.240	3.050	2.690	3.900
K2O	0.760	0.780	0.440	0.400	0.570
TiO2	1.280	1.770	1.510	1.170	1.820
MnO	0.160	0.200	0.200	0.190	0.200
P2O5	0.150	0.240	0.190	0.120	0.220
LOI	4.400	3.000	2.900	1.800	2.300
Total	100.000	99.640	98.930	99.130	99.660
Ba	303.000	176.000	111.000	88.000	175.000
Rb	28.000	34.000	17.000	10.000	23.000
Sr	262.000	224.000	295.000	305.000	235.000
Y	15.000	31.000	23.000	21.000	31.000
Zr	70.000	137.000	122.000	82.000	144.000
Nb	15.000	18.000	13.000	7.200	16.000
Pb	.	.	.	.	.
Ga	19.000	20.000	22.000	18.000	21.000
Zn	78.000	87.000	131.000	135.000	83.000
Cu	57.000	66.000	114.000	86.000	68.000
Ni	291.000	40.000	69.000	45.000	27.000
TiO2	1.240	1.560	1.200	0.930	1.610
V	187.000	290.000	257.000	241.000	310.000
Cr	369.000	124.000	146.000	68.000	42.000
La	-	-	-	-	11.230
Ce	-	-	-	-	26.970
Nd	-	-	-	-	14.440
Sm	-	-	-	-	4.640
Eu	-	-	-	-	1.810
Tb	-	-	-	-	1.170
Yb	-	-	-	-	3.800
Lu	-	-	-	-	0.560
Cs	-	-	-	-	26.070
Hf	-	-	-	-	3.490
Ta	-	-	-	-	1.220
Th	-	-	-	-	1.590
U	-	-	-	-	.
Sc	-	-	-	-	35.940
Co	-	-	-	-	44.250

Table C1 Continued

	KR89-023	KR89-024	KR89-027	KR89-030	KR89-030 (dup)
SiO2	48.600	47.990	48.140	45.070	45.080
Al2O3	15.030	18.130	18.340	15.430	15.310
Fe2O3	10.440	8.240	8.840	12.070	12.120
MgO	6.750	6.560	5.240	5.080	5.230
CaO	11.660	11.700	11.790	8.020	8.000
Na2O	3.100	3.270	2.940	4.210	3.970
K2O	0.400	0.340	0.450	0.580	0.570
TiO2	1.330	1.070	1.330	2.120	2.120
MnO	0.180	0.150	0.150	0.250	0.250
P2O5	0.160	0.150	0.180	0.310	0.320
LOI	1.500	1.800	1.800	7.700	7.400
Total	99.150	99.400	99.200	100.840	100.370
Ba	1131.000	41.000	114.000	82.000	87.000
Rb	11.000	11.000	17.000	12.700	14.700
Sr	2261.000	63.000	249.000	169.600	168.900
Y	22.000	17.000	25.000	31.800	30.600
Zr	97.000	86.000	100.000	224.600	222.700
Nb	8.000	10.000	12.000	8.100	6.700
Pb	.	.	.	.	.
Ga	15.000	20.000	20.000	21.000	21.000
Zn	115.000	55.000	89.000	155.000	155.000
Cu	112.000	79.000	63.000	16.000	15.000
Ni	43.000	92.000	59.000	8.000	8.000
TiO2	1.070	0.940	1.150	2.030	2.030
V	254.000	190.000	216.000	289.000	291.000
Cr	91.000	153.000	123.000	100.000	104.000
La	-	7.470	8.360	-	-
Ce	-	19.000	21.090	-	-
Nd	-	11.060	13.250	-	-
Sm	-	3.010	3.520	-	-
Eu	-	1.230	1.400	-	-
Tb	-	0.640	0.670	-	-
Yb	-	2.750	3.230	-	-
Lu	-	0.350	0.420	-	-
Cs	-	18.360	20.380	-	-
Hf	-	2.180	2.550	-	-
Ta	-	0.850	0.850	-	-
Th	-	0.820	0.930	-	-
U	-	.	.	-	-
Sc	-	33.180	33.100	-	-
Co	-	61.310	37.270	-	-

Table C1 Continued

	KR89-031	KR89-032	KR89-034	KR89-035	KR89-036
SiO2	54.350	54.760	47.560	48.290	49.500
Al2O3	16.950	17.970	16.530	17.940	16.560
Fe2O3	7.360	7.340	9.480	8.700	10.060
MgO	4.250	3.620	6.720	5.780	5.810
CaO	6.370	3.530	11.210	10.400	8.220
Na2O	5.150	6.870	2.550	3.400	2.990
K2O	1.140	1.180	0.340	1.370	1.710
TiO2	1.420	1.200	1.590	1.230	1.650
MnO	0.130	0.140	0.160	0.140	0.150
P2O5	0.240	0.240	0.210	0.140	0.230
LOI	2.900	3.600	2.900	2.600	2.300
Total	100.260	100.450	99.250	99.990	99.180
Ba	249.000	258.000	131.000	178.000	278.000
Rb	23.800	21.000	13.000	42.300	47.000
Sr	349.600	355.000	223.000	285.900	314.000
Y	19.900	22.000	24.000	21.500	24.000
Zr	175.600	203.000	122.000	112.900	160.700
Nb	6.300	8.000	16.000	3.500	5.900
Pb	.	.	.	.	.
Ga	18.000	19.000	17.000	19.000	17.000
Zn	73.000	90.000	88.000	72.000	57.000
Cu	34.000	26.000	56.000	29.000	68.000
Ni	32.000	17.000	95.000	39.000	53.000
TiO2	1.260	1.060	1.300	1.190	1.590
V	164.000	160.000	258.000	229.000	215.000
Cr	27.000	37.000	158.000	133.000	142.000
La	13.800	20.230	-	-	-
Ce	33.970	44.620	-	-	-
Nd	16.540	21.040	-	-	-
Sm	4.170	5.040	-	-	-
Eu	1.380	1.360	-	-	-
Tb	0.720	0.870	-	-	-
Yb	2.300	2.690	-	-	-
Lu	0.340	0.380	-	-	-
Cs	32.830	43.130	-	-	-
Hf	4.080	4.390	-	-	-
Ta	0.800	0.850	-	-	-
Th	4.230	6.450	-	-	-
U	1.690	2.530	-	-	-
Sc	19.790	15.810	-	-	-
Co	33.660	25.460	-	-	-

Table C1 Continued

	KR89-037	KR89-038	KR89-039
SiO2	47.690	59.480	48.350
Al2O3	15.730	16.110	14.380
Fe2O3	9.680	7.540	12.350
MgO	7.470	2.990	5.540
CaO	10.380	5.790	10.000
Na2O	2.720	4.560	3.270
K2O	1.100	0.660	0.840
TiO2	1.250	1.010	1.940
MnO	0.170	0.090	0.210
P2O5	0.220	0.240	0.210
LOI	2.700	1.200	1.900
Total	99.110	99.670	98.990
Ba	261.000	182.000	243.000
Rb	32.300	15.900	24.000
Sr	384.500	358.900	211.000
Y	19.100	27.000	29.000
Zr	122.300	204.100	133.000
Nb	5.100	7.300	12.000
Pb	.	.	.
Ga	18.000	20.000	19.000
Zn	76.000	55.000	118.000
Cu	21.000	18.000	71.000
Ni	26.000	6.000	33.000
TiO2	1.110	0.980	1.520
V	221.000	109.000	313.000
Cr	60.000	24.000	25.000
La	-	16.580	-
Ce	-	38.830	-
Nd	-	18.150	-
Sm	-	5.040	-
Eu	-	1.600	-
Tb	-	1.070	-
Yb	-	3.810	-
Lu	-	0.530	-
Cs	-	37.530	-
Hf	-	4.600	-
Ta	-	1.530	-
Th	-	4.220	-
U	-	2.270	-
Sc	-	14.710	-
Co	-	41.290	-

(1) . = not detected.
(2) - = not analysed.

APPENDIX D

FJ87-136 HORNBLENDE SUMMARY

°C	mV 39	% 39	AGE(Ma)	% ATMOS	37/39	40/36	39/36	% IIC
750	6	3	134 +/- 28	93	25.7	318	.6	7
850	2	1	77 +/- 69	98	75.8	301	.2	33
950	7	4	357 +/- 10	63	29.4	467	1.6	4
1000	58	34	372 +/- 3	20	22	1472	11.1	3
1025	23	13	403 +/- 3	23	27.5	1284	8.5	4
1075	48	28	384 +/- 2	17	23.3	1731	13.1	3
1125	12	7	425 +/- 4	33	26.6	904	4.9	3
1175	9	6	432 +/- 6	43	24.2	693	3.1	3
1200	7	4	423 +/- 9	53	31.9	554	2.1	4

TOTAL GAS AGE = 377 Ma

J = 2.17E-03

ERROR ESTIMATES AT ONE SIGMA LEVEL

37/39,40/36 AND 39/36 Ar RATIOS ARE CORRECTED FOR INTERFERING ISOTOPES

% IIC - INTERFERING ISOTOPES CORRECTION

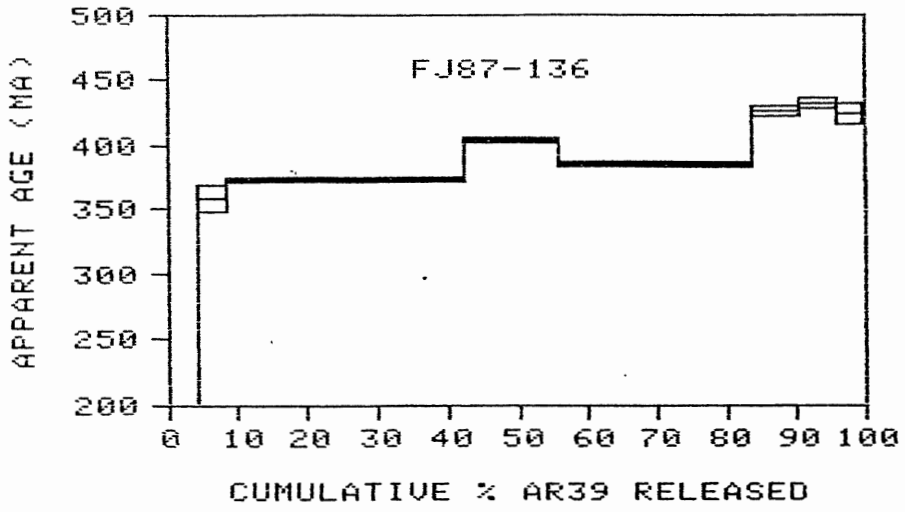
FJ87-136
APPARENT AGE (MA)
500
450
400
350
300
250
200
0
10
20
30
40
50
60
70
80
90
100
CUMULATIVE % AR39 RELEASED

FJ87-138 HORNBLENDE SUMMARY

°C	mV 39	% 39	AGE(Ma)	% ATMOS	37/39	40/36	39/36	% IIC
750	4	2	270 +/- 26	86	14	345	.6	2
850	2	<1	265 +/- 39	89	34.6	330	.4	6
950	5	2	420 +/- 13	63	26.8	472	1.4	3
1000	41	16	388 +/- 3	26	22.2	1145	7.6	3
1050	81	32	364 +/- 2	17	21.8	1717	13.8	3
1100	50	20	387 +/- 3	18	24.8	1601	11.8	3
1150	26	10	416 +/- 4	29	23.6	1029	6.1	3
1200	33	13	-	-	-	-	-	-
1250	11	4	423 +/- 7	48	25.3	614	2.6	3

J = 2.17E-03

ERROR ESTIMATES AT ONE SIGMA LEVEL

37/39,40/36 AND 39/36 Ar RATIOS ARE CORRECTED FOR INTERFERING ISOTOPES

% IIC - INTERFERING ISOTOPES CORRECTION

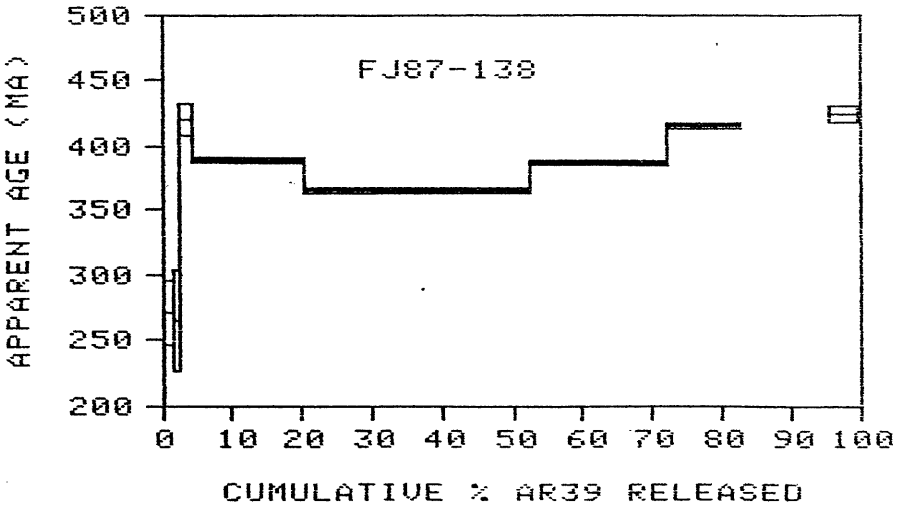
FJ87-138
APPARENT AGE (MA)
500
450
400
350
300
250
200
0
10
20
30
40
50
60
70
80
90
100
CUMULATIVE % AR39 RELEASED

FJ87-146 HORNBLENDE SUMMARY

°C	mV 39	% 39	AGE(Ma)	% ATMOS	37/39	40/36	39/36	% IIC
750	8	4	87 +/- 21	94	10.8	315	.8	4
850	3	2	88 +/- 57	98	35.3	303	.3	14
950	6	3	304 +/- 21	81	33.3	363	.7	5
1000	26	13	389 +/- 4	30	25.7	999	6.3	3
1025	35	18	388 +/- 3	23	25	1292	9	3
1050	15	8	419 +/- 3	23	24.4	1282	8.1	3
1100	56	29	371 +/- 3	23	23.9	1295	9.5	3
1150	15	8	422 +/- 4	35	25.2	851	4.5	3
1200	26	13	404 +/- 4	34	23.9	870	4.9	3
1225	5	3	434 +/- 9	55	25.9	541	1.9	3

TOTAL GAS AGE = 373 Ma

J = 2.17E-03

ERROR ESTIMATES AT ONE SIGMA LEVEL

37/39,40/36 AND 39/36 Ar RATIOS ARE CORRECTED FOR INTERFERING ISOTOPES

% IIC - INTERFERING ISOTOPES CORRECTION

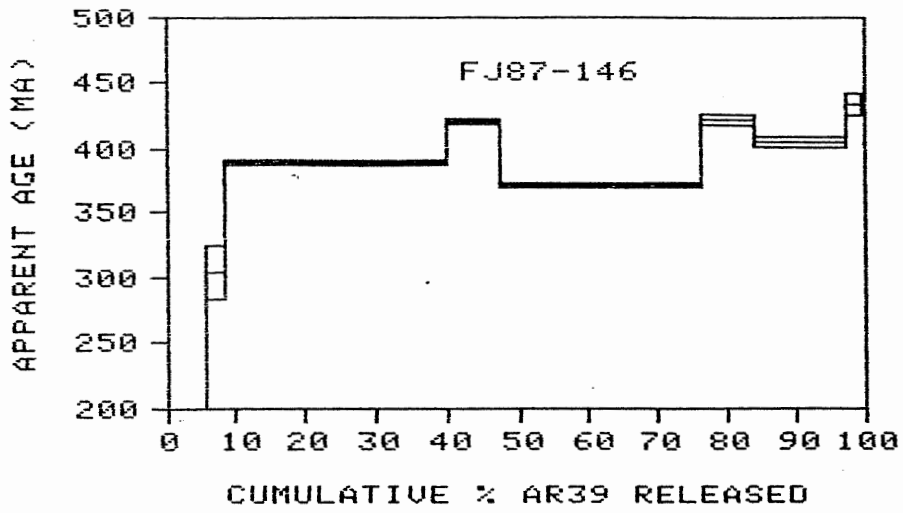
FJ87-146
APPARENT AGE (MA)
500
450
400
350
300
250
200
0 10 20 30 40 50 60 70 80 90 100
CUMULATIVE % AR39 RELEASED

REFERENCES

Balkwill HR (1978) Evolution of Sverdrup Basin, Arctic Canada. Amer Assoc Petroleum Geol Bull 62(6):1004-1028

Cameron BI (1989) Petrochemistry and origin of altered Permian basalts in the Sverdrup Basin, Arctic Canada. M.Sc. thesis, Dalhousie University, Halifax, Nova Scotia

Christie RL (1957) Geological reconnaissance of the north coast of Ellesmere Island, District of Franklin, Northwest Territories. Geol Surv Can Paper 56-9

Cox KG, Bell JD, Pankhurst RJ (1979) The interpretation of igneous rocks. Allen and Unwin, London

Deer WA, Howie RA, Zussman J (1966) An Introduction to the Rock Forming Minerals. Longman Group Limited, Essex, England

Embry AF, Osadetz KG (1988) Stratigraphy and tectonic significance of Cretaceous volcanism in the Queen Elizabeth Islands, Canadian Arctic Archipelago. Can J Earth Sci 25:1209-1219

Floyd PA, Winchester JA (1978) Identification and discrimination of altered and metamorphosed volcanic rocks using immobile elements. Chem Geol 21:291-306

Floyd PA, Winchester JA (1975) Magma type and tectonic setting discrimination using immobile elements. Earth Plan Sci Lett 27:211-218

Henderson P (1982) Inorganic Geochemistry. Pergamon Press, Oxford, England

Hess P (1989) Origins of Igneous Rocks. Harvard University Press, Cambridge, Massachusetts

Jager E, Hunziker JC (1979) Lectures in isotope geology. Springer-Verlag, Berlin

MacDonald GA, Katsura T (1964) Chemical composition of Hawaiian lavas. J Petrology 5(1):82-133

Mason R (1978) Petrology of the metamorphic rocks. George Allen and Unwin, London

McDougall I, Harrison MT (1988) Geochronology and thermochronology by the $^{40}Ar/^{39}Ar$ method. Oxford University Press, New York

Middlemost EAK (1985) Magmas and Magmatic Rocks, An Introduction to Igneous Petrology. Longman Group Limited, Essex, England

Nesse WD (1986) Introduction to Optical Mineralogy. Oxford University Press, New York

Nisbet EG, Pearce JA (1977) Clinopyroxene composition in mafic lavas from different tectonic settings. Contrib Mineral Petrol 63:149-160

Pearce JA, Cann JR (1973) Tectonic setting of basic volcanic rocks determined using trace element analyses. Earth Plan Sci Lett 19:290-300

Pearce JA, Norry MJ (1979) Petrogenic implications of Ti, Zr, and Nb variations in volcanic rocks. Contrib Mineral Petrol 69:33-47

Peary RE (1907) Nearest the pole. Doubleday, Page and Co., New York

Richard LR, Clarke DB (1990) AMPHIBOL: a program for calculating structural formulae and for classifying and plotting chemical analyses of amphiboles. Amer Min 75:421-423

Ritcey DH (1989) A geochemical study of the Carboniferous Audhild volcanics, northwestern Ellesmere Island, Arctic Canada: initial volcanism in the Sverdrup Basin. Ba thesis, Dalhousie University, Halifax, Nova Scotia

Schei P (1904) Preliminary account of the geological investigations made during the second Norwegian Polar expedition in the "Fram"; Appendix I. In: "New Land", vol. II. Sverdrup O (1904) Longmans, Green and Co., Bombay and London

Scotese CR, Bambach RK, Barton C, Van der Voo R, Ziegler AM (1979) Paleozoic base maps. J Geol 87(3):217-277

Sobczak LW, Mayr U, Sweeney JF (1986) Crustal section across the polar continent-ocean transition in Canada. Can J Earth Sci 23:608-621

Trettin HP (1989) The Arctic Islands. In: The Geology of North America Vol.A, The Geology of North America-An Overview. Bally AW, Palmer AR (eds) Geol Soc Amer 349-370

Trettin HP (1986) Pearya: a composite terrane with Caledonian affinities in northern Ellesmere Island. Can J Earth Sci 24:224-245

Trettin HP (1969) Pre-Mississippian geology of northern Axel Heiberg and northwestern Ellesmere Islands, Arctic Archipelago. Geol Surv Can Bull 171

Trettin HP, Balkwill HR (1979) Contributions to the tectonic history of the Innuitian Province, Arctic Canada. Can J Earth Sci 16:748-769

Trettin HP, Parish R, Loveridge WD (1987) U-Pb determinations on Proterozoic to Devonian rocks from northern Ellesmere Island, Arctic Canada. Can J Earth Sci 24:246-256

Wilkinson L (1987) SYSTAT: the sysyem for statistics. SYSTAT Inc., Evanston, IL

Williamson M-C (1988) The Cretaceous igneous province of the Sverdrup Basin, Canadian Arctic: Field relations and petrochemical studies. Ph.D thesis, Dalhousie University, Halifax, Nova Scotia

Wilson M (1989) Igneous petrogenesis: a global tectonic approach. Unwin Hyman, London, UK

Winchester JA, Floyd PA (1977) Geochemical discrimination of different magma series and their differentiation products using immobile elements. Chem Geol 20:325-343

Wood DA (1980) The application of a Th-Hf-Ta diagram to problems of tectonomagmatic classification and to establishing the nature of crustal contamination of basalt lavas of the British Tertiary volcanic province. Earth Planet Sci Lett 50:11-30

York D (1969) Least squares fitting of a straight line with correlated errors. Earth Planet Sci Lett 5:320-324

Ziegler PA (1988) Evolution of the Arctic-North Atlantic and the Western Tethys. Amer Assoc Petroleum Geol Mem 43, Tulsa Oklahoma